JAERI-Tech
99-013

ANALYSIS OF STEAM GENERATOR TUBE RUPTURE AS A SEVERE ACCIDENT USING MELCOR 1.8.4

March 1999

Hongrun YANG*, Akihide HIDAKA and Jun SUGIMOTO

日本原子力研究所
Japan Atomic Energy Research Institute

本レポートは、日本原子力研究所が不定期に公刊している研究報告書です。
入手の問合わせは、日本原子力研究所研究情報部研究情報課（〒319-1195　茨城県那珂郡東海村）あて、お申し越しください。なお、このほかに財団法人原子力弘済会資料センター（〒319-1195　茨城県那珂郡東海村日本原子力研究所内）で複写による実費頒布をおこなっております。

This report is issued irregularly.
Inquiries about availability of the reports should be addressed to Research Information Division, Department of Intellectual Resources, Japan Atomic Energy Research Institute, Tokai-mura, Naka-gun, Ibaraki-ken 319-1195, Japan.

編集兼発行　日本原子力研究所

Analysis of Steam Generator Tube Rupture as a Severe Accident Using MELCOR 1.8.4

Hongrun YANG*, Akihide HIDAKA, and Jun SUGIMOTO

Department of Reactor Safety Research
Nuclear Safety Research Center
Tokai Research Establishment
Japan Atomic Energy Research Institute
Tokai-mura, Naka-gun, Ibaraki-ken

(Received January 26, 1999)

This report presents the results from the MELCOR 1.8.4 calculations for Steam Generator Tube Rupture (SGTR) with stuck open of all the safety valves in faulted SG as a severe accident. The calculations are based on Surry nuclear power plant. After performed using the once-through primary system model alone by 1.0×10^5s, the calculations were conducted with both of the once-through and hot leg countercurrent natural circulation models. The results, including event sequences, processes and progressions of core degradation, radionuclides release from core and reactor cavity, and source terms to the environment are described in detail. It is concluded that the availability of High Pressure Safety Injection (HPSI) can significantly delay the progression of core heat-up and approximately 7% of cesium iodide (CsI) can be released to the environment directly through the stuck open safety valve. Comparisons between the results from the two models are also given in this report. The present analyses also showed that during SGTR accident, the hot leg countercurrent natural circulation flow cannot be established well and therefore it has little effect on the mitigation of the core degradation.

Keywords : Severe Accident, SGTR, MELCOR 1.8.4. Surry Plant, Safety Valve Stuck Open, Core Degradation, Hot Leg Countercurrent Natural Circulation, Source Term

---

* Nuclear Power Institute of China

MELCOR 1.8.4コードを用いたシビアアクシデント事象としての蒸気発生器伝熱管破損事故解析

日本原子力研究所東海研究所安全性試験研究センター原子炉安全工学部
Hongrun YANG*・日高　昭秀・杉本　　純

（１９９９年１月２６日受理）

本報告書は、シビアアクシデント事象として、2次側の安全弁の開固着を伴うSurry炉の蒸気発生器伝熱管破損事故（SGTR）に対するMELCOR 1.8.4コードの計算結果をまとめたものである。事故発生後1.0×10^5秒までは一次系のループ流れを模擬したonce-throughモデルを用い、それ以降は、ホットレグ水平対向自然循環モデル及びonce-throughモデルの両方を用いて計算を行った。得られた計算結果は、事故の進展（イベントシーケンス）、炉心の溶融進展、炉心及び原子炉キャビティからの放射性物質の放出、環境中に放出される放射性物質の量（ソースターム）の観点から詳細に記述した。主な結論としては、高圧注水系（HPSI）が利用できれば炉心の温度上昇が大幅に遅延すること、CsIは開固着した安全弁から格納容器をバイパスして7％程度環境中に放出されることが明らかになった。once-throughモデルとホットレグ水平対向自然循環モデルを用いた場合についても計算結果の比較検討を行い、SGTRではホットレグ水平対向自然循環流はあまり発達しないため、それが事故進展に与える影響は小さいことを明らかにした。

東海研究所：〒319-1195　茨城県那珂郡東海村白方白根 2-4
* 中国核研究設計院

Contents

目　　次

Preface

This present work entitled "Analysis of Steam Generator Tube Rupture as a Severe Accident Using MELCOR 1.8.4," was performed at Severe Accident Research Laboratory (SARL) in Japan Atomic Energy Research Institute (JAERI), from May 12 through October 8, 1998, by Yang Hongrun, who is from Nuclear Power Institute of China (NPIC), and supervised by Dr. J. Sugimoto and instructed by Dr. A. Hidaka. The work is one of the subjects in the project of Severe Accident Analysis and Countermeasures for the Qinshan NPP, sponsored by International Atomic Energy Agency (IAEA). The objectives of the Agency's project, numbered by CPR/9/020, are to provide assistance for China using the most advanced severe accident computer codes to perform safety analysis as well as accident management for the Qinshan Nuclear Power Plant, and to transfer the severe accident research methodology.

This is a blank page.

1. INTRODUCTION

1.1 Outlines of MELCOR Code

The MELCOR[1] code is a fully integrated, relatively fast-running code that models the progression of accidents in light water reactor nuclear power plants. An entire spectrum of accident phenomena is modeled in MELCOR. Characteristics of accident progression that can be treated with MELCOR include the thermal-hydraulic response in the reactor coolant system, reactor cavity, containment, and confinement buildings; core heatup and degradation; radionuclide release and transport; hydrogen production, transport, and combustion; melt ejection phenomena; core-concrete attack; heat structure response; and the impact of engineered safety features on thermal-hydraulic and radionuclide behavior. MELCOR may also be used to analyze experiments and non-nuclear facilities. MELCOR is being developed at Sandia National Laboratories for the US Nuclear Regulatory Commission (NRC) as the successor to the Source Term Code Package. JAERI has received the MELCOR code based on the CSARP (Cooperative Severe Accident Research Program) agreement between JAERI and USNRC.

The MELCOR code has been designed to facilitate sensitivity and uncertainty analyses through the use of sensitivity coefficients. Many parameters in correlations, which are hardwired constants in most codes, are implemented as sensitivity coefficients in MELCOR. However, in MELCOR the constants are coded as sensitivity coefficients that can be changed by the user to determine the sensitivity of the results to the heat transfer correlation.

1.2 Brief Description of Steam Generator Tube Rupture (SGTR)

In the pressurized water reactor (PWR), water in the reactor coolant system (RCS) is pressurized to prevent it from boiling. This high pressure water is circulated through the heat exchanger tubes in steam generators where heat is transferred to the lower pressure secondary coolant system (SCS), producing steam that is used to generate electrical power. The tubes constitute a very significant portion of the RCS pressure boundary, and rupture of these tubes can result in release of RCS coolant to environment through either the atmospheric dump valves or secondary Power Operated Relief Valves (PORVs), bypassing the containment.

In NUREG-1150[2], it is estimated that the core melt frequency resulted from Steam Generator Tube Rupture (SGTR) is about 10^{-6} per reactor-year (for Surry plant; 6.0×10^{-6} per reactor-year, for Sequoyah plant; 7.1×10^{-6} per reactor-year). It seems that SGTR can be neglected relative to other severe accidents. But, this event will lead to primary radioactive materials releasing to environment directly.

1.3 Outlines of Present Calculation

In the case of an SGTR accident initiated by the double-ended guillotine rupture of one steam generator (SG) tube, if the operators fail to depressurize the RCS in a timely manner in a short time, there is a high probability that the secondary coolant will be released through the PORVs which are located at the secondary side of the faulted SG. The probability that the PORVs fail to reclose under these conditions is estimated to be very high (close to 1.0)[2]. The failure to close of PORVs by a local or manual action will result in a non-isolable path from the RCS to the environment. After the entire content of refueling water storage tank are pumped through the broken tube, the core uncovery would occur. The onset of core degradation is thus not expected until 10 hours after the start of the accident. In order to understand the accident progressions and consequences for SGTR as a severe accident, some calculations were executed using MELCOR1.8.4 code and Surry-1 power station input deck prepared by USNRC.

2. ANALYTICAL METHODS

There are two different current models in the primary system according to the SGTR accident progression time; one is the once-through model, the other is the hot leg countercurrent natural circulation model. Thus, different nodalizations are used between the two models. In the present analyses, the once-through model is used by 100,000 s. After that, both the once-through and the natural circulation models are used.

2.1 Once-through Model

2.1.1 Brief Description of Once-through Model

A once-through model is used to simulate the process from SGTR start to 100,000 s and provides the basis of further analysis. This has been the traditional modeling approach for analyzing plant behavior. In this model, the fluid volumes modeled include the downcomer, lower head, lower plenum, core, core bypass, upper plenum, and upper head, respectively. The core bypass represents the fluid volume between the core barrel and baffle, and connects the lower and upper plena. Flow paths are modeled between the inlet annulus and the upper head and between the inlet and upper plenum. Flow between the upper plenum and upper head occurs only through the guide tube assemblies. Heat structures modeled include the reactor vessel walls, the core barrel and baffle, the thermal shield, the upper and lower core support plates, and structures in the lower and upper plena. Especially, in this case, once-through model can represent one direction coolant flow in hot leg and steam generator tubes, which is very different from the hot leg countercurrent natural circulation model. The steam generator model includes the tubes, downcomer, boiler, dome, steam

line, main and auxiliary feed water systems, main steam isolation valve, PORVs and SRVs. The primary coolant flows through hot leg, tubes, pump suction in sequence, then goes to cold leg C, which means 'through SG once time'.

2.1.2 Assumptions

The major assumptions for present SGTR analysis are as follows:

1) The prompt power was calculated with RELAP5/MOD2/36.04 under assumptions of 2 years full power operation, an actinide yield factor of 0.52, and the ANS 79-3 fission product data. Group power fractions of 0.51 U-238, and 0.42 Pu-239 were used. The thermal power was normalized to 2297.65 MW, the difference between 2441 MW (100 % rated power) and 143.35 MW (steady state decay heat power from MELCOR DCH package).
2) Steady state is calculated for 200 s before a tube rupture initiation.
3) At 0 s, a double guillotine break in one SG U-tube occurs in the steam generator in loop C.
4) Reactor scram occurs at low pressurizer pressure.
5) The scram signal closed the feed water valve, and tripped reactor coolant pumps and turbine.
6) Auxiliary Feed Water (AFW) begins at 5 s after the main feed water isolation.
7) High Pressure Safety Injection (HPSI) is activated depending on low pressurizer pressure signal, and initiated with 13 s delay. The HPSI is always available until Refueling Water Storage Tank (RWST) is depleted.
8) There are no operator's actions.
9) All the safety valves in faulted SG are stuck open.
10) Faulted SG PORV is opened or closed according to the pressure conditions, or if the Safety Relief Valve is stuck open or not.

2.1.3 Nodalization

Nodalization for MELCOR includes three basic parts, which are for control volumes (CV), for core (COR) and for heat structures (HS) respectively. The followings are the scheme of nodalization.

(1) CV Nodalization

Figure 2.1.1 shows the nodalization of control volumes as well as the connected paths. There are 36 control volumes for this SGTR analysis case:

1) CV001 ---ENVIRONMENT
2) CV005 --- BASEMENT
3) CV010 --- CAVITY
4) CV020 --- STG A/B/C CUBICL

5) CV041 --- PRESS CUBICLE
6) CV050 --- LOWER DOME
7) CV055 --- DOME
8) CV100 --- DOWNCOMER
9) CV110 --- LOWER PLENUM
10) CV120 --- CORE
11) CV130 --- CORE BYPASS
12) CV140 --- UPPER PLENUM
13) CV150 --- UPPER HEAD
14) CV290 --- FW SOURCE
15) CV291 --- AFW SOURCE
16) CV295 --- SG PRESSURE
17) CV296 --- AFW DEPRESS SINK
18) CV400 --- HOT LEG C
19) CV405 --- SG U-TUBE UP C
20) CV406 --- SG U-TUBE DN C
21) CV410 --- PRESSURIZER
22) CV420 --- PUMP SUNCTION C
23) CV440 --- COLD LEG C
24) CV450 --- SG DOWNCOMER C
25) CV460 --- SG BOILER C
26) CV465 --- SG DOME C
27) CV500 --- HOT LEG AB
28) CV505 --- SG U-TUBES UP AB
29) CV506 --- SG U-TUBES DN AB
30) CV520 --- PUMP SUCTION AB
31) CV540 --- COLD LEG AB
32) CV550 --- SG DOWNCOMER AB
33) CV560 --- SG BOILER AB
34) CV565 --- SG DOME AB
35) CV605 --- BROKEN U-TUBE UP
36) CV606 --- BROKEN U-TUBE DOWN

Here, CV001 is used for environment, CV005, 010, 020, 041, 050, and 055 are for reactor building, CV100, 110, 120, 130, 140, and 150 are for primary - core system, CV400, 405, 406, 420, 440, 500, 505, 506, 520, 540, 605, and 606 are for primary - coolant system, CV410 is for primary - pressurizer, CV290, 291 295, 296, 450, 460, 465, 550, 560, and 565 are for secondary coolant system. There are total 62 flow paths to connect these control volumes. Loop A and B have been combined to Loop AB to avoid much more expensive CPU time.

(2) Core Nodalization

In the core, 3 rings and 13 levels are nodalized for this case, where, the first two levels (from bottom to top) are for lower plenum, the third one is for the barrel base plate and the others are for active core. **Figures 2.1.2** and **2.1.3** give the nodalization of the core.

(3) Heat Structures Nodalization

In this case, there are about 140 heat structures nodalized as associated with control volumes, flow paths, core, etc., to simulate heat transferring, materials depositing and other processes.

2.1.4 Input Deck

This input deck was originally prepared for USNRC for the analysis of SGTR sequence of Surry nuclear power plant with MELCOR 1.8.3. However, the input deck was used for MELCOR 1.8.4 calculation in the present study.

2.2 Hot Leg Countercurrent Natural Circulation Model

2.2.1 Brief Description of Hot Leg Countercurrent Natural Circulation Model

Three natural circulation flow phenomena that can be important during severe accidents are in-vessel circulation, hot leg countercurrent flow, and flow through the coolant loops[4]. In the hot leg countercurrent flow, superheated vapor enters the top of the hot leg, displacing saturated vapor, which then flows back to the reactor vessel along the bottom of the hot leg. When the hotter vapor enters the steam generator inlet plenum, it will rise toward the steam generator tubes. Vapor enters some of the tubes, displacing the cooler steam that was in the tubes. The displaced vapor enters the outlet plenum, then reenters other steam generator tubes, forcing vapor into the inlet plenum. A density gradient is thus established between tubes. This density gradient then pulls more hot vapor into the tubes, displacing cooler steam. The process continues until a steady flow is established, with hot vapor flowing from the inlet plenum to the outlet plenum through some of the steam generator tubes, and cooler vapor returning to the inlet plenum through the remaining tubes.

In order to simulate the hot leg countercurrent flow, several modeling changes were made by BNL. The hot leg was divided into top and bottom halves. The return flow from the bottom half of the hot leg entered the hot leg nozzle connection. This approximated the elevation difference between the top and the bottom halves of the hot leg, so that the driving force for the natural circulation flow should be close to that of the actual situation. It also prevented the hot and cold steam flows from mixing immediately in the upper plenum. The steam generator inlet plenum was

divided into three volumes. A mixing volume in the middle connected to the flows entering and leaving both the hot leg and the steam generator tubes. The volumes on either side of the mixing volume passed the hot and cold vapors that did not mix with other fluid in the inlet plenum between the hot leg and steam generator tubes. The steam generator tubes were divided into two sets, hot flow tubes and cold flow tubes, which connected the inlet and outlet plena. The hot flow tubes represented 35 % of the flow and heat transfer area; the cold return flow tubes represented 65 % of the total flow and heat transfer area.[3] The reactor coolant pump suction piping was still connected to the steam generator outlet plenum, so that clearing of the liquid from the loop seals could occur if appropriate conditions existed.

For the in-vessel natural circulation, it can be calculated by fine-scaled control volume nodalization of core with the option of dT / dz model (which is used in MELCOR for temperature distribution calculation in core) being turned off, but currently the capability is seriously limited by the increased CPU time required (due to a substantially larger flow matrix and a reduced material Courant time step limit) and by calculational difficulties during core degradation (caused by control volumes completely filling up with debris).[2]

2.2.2 Assumptions

There were no other more assumptions (comparing with once-through model) except for those characterized by the hot leg countercurrent natural circulation model.

2.2.3 Nodalization

Figure 2.2.1 gives the nodalization of control volumes associated with hot leg countercurrent model (CV605, CV606 and Loop AB were not included in this figure). Due to the differences between the once-through and the natural circulation models, the nodalization for the natural circulation calculation is very different from once-through calculation. (See the description of natural circulation model above in 2.2.1). The changes and additions focus on the CV nodalization, heat structures and flow paths. The followings are the detailed schemes which are different from the once-through model:

(1) Hot Leg Nodalization

In once-through model, only two CVs were nodalized, which were, CV400 (hot leg c) and CV500 (hot leg ab). In natural circulation model, the hot leg nodalization is, CV401 (hl c top 1), CV402 (hl c top 2), CV421 (hlc bot 1), CV422 (hlc bot 2), CV501 (hlab top 1), CV502 (hlab top 2), CV521 (hlab bot 1), and CV522 (hlab bot 2).

(2) Steam Generator Nodalization (for Primary System)

In once-through model, there were 6 CVs, which were CV405, 406, 505, 506, 605 and 606 (See chapter 2.1.3 (1)).

In natural circulation model, the nodalization was including CV409, 411, 412 (sg c in hot, mix and cold, respectively), CV413 (sgc tubesup hot), 414 (sgc tubesdn hot), 416 (sgc tubesup cold), 417 (sgc tubesdn cold), 415 (sgc outlet), 509 (sg ab in hot), 511 (sg ab in mix), 512 (sg ab in cold), 513 (sgab tubesup hot), 514 (sgab tubesdn hot), 516 (sgab tubesup cold), 517 (sgab tubesdn cold), 515 (sgab outlet), 605 (broken u-tube up) and 606 (broken u-tube dn). Here, CV409, 411, 412, 413, and 417 were equivalent to CV405 in the once-through model, CV414, 416, and 415 were equivalent to CV406 in once-through model. The changes for SG AB were the same as those for SG C.

(3) Other Code Package Nodalization

The nodalizations for HS (heat structure) and FL (flow path) had been updated corresponding to the changes in CV (control volume) package nodalization. The core nodalization had no necessity to be modified.

2.2.4 Input Deck

The input deck for hot leg countercurrent flow natural circulation model was prepared by USNRC. It is noted that the initial condition of the input deck was determined based on the results from the once-through model calculation for 100,000 s from the start.

3. ANALYTICAL RESULTS AND DISCUSSIONS

3.1 Analytical Results of Once-through Model by First 100,000 s

3.1.1 Sequence of Predicted Events

The sequence of events and its timings of occurrence calculated using the once-through model are summarized in **Table 3.1.1**. Because of the high pressure safety injection (HPSI) operation, it can be seen that the accidental progression was very slow and the core was still intact till the time of 100,000 s from the accident initiation.

3.1.2 Discussions of Calculated Results

The followings are the discussions based on the results calculated from -200 to 100,000 s using the once-through model.

(1) Primary System Pressure

Figure 3.1.1 shows the primary system pressure. It can be seen that at the beginning of the accident, due to the main coolant pumps stop, primary circulation flow decreased, causing the heat removal decreasing and the temperature increasing accordingly, then primary system pressure went up (the initial pressure of primary system was 15.73 MPa). After that, because of the pressurizer adjustment and the SG U-tube break flow, energy loss made the pressure begin to drop. When the pressure of primary system reached the low pressure scram set point (13.0 MPa), reactor tripped, and the primary system pressure declined sharply and reached the set point for high pressure safety injection (HPSI) at about 9 s. After 13 s delay, the HPSI began operating and the primary pressure increased accordingly. Because the SG C PORV opened and closed cyclically, the pressure became oscillating at high values. But after the PORV was stuck open, an obvious depressurization could be observed. Then the pressure was controlled and adjusted by the pressurizer. When the liquid level in pressurizer crossed the heater trip set point, the heater would be turned on or off. During this period, after a series slight fluctuation, the pressure became stable and was almost kept at constant.

At about 58,000 s, the refueling water storage tank was exhausted by HPSI, the safety injection flow became zero, this caused the pressure drops sharply and deeply. This deep depressurization would also cause a flash vaporization occurring in the intact SG tube which would have an effect on the pressure in that SG boiler (see **Fig. 3.1.6**). When the pressure came to the set point of accumulator safety injection, the accumulators of all three loops would be first initiated, then, the depressurization would slow down but could not be halted because the operation status of accumulators was strongly depended on the pressure in the accumulators. With the primary pressure decreasing, the saturation temperature in core reduced, meantime, the core began to be heated up (see **Fig. 3.1.12 ~ Fig. 3.1.15**) and the liquid temperature became closer and closer to the saturation temperature (see **Fig. 3.1.2**). During this period, the pressure in the affected steam generator secondary side began to increase due to the temperature increasing (see the description in section (2)).

At about 70,000 s when accumulator injection stopped, steam began to be produced in the core (see **Fig. 3.1.3**), and the pressure in primary system was nearly equal to that in the affected SG secondary side and the break flow rate decreased considerably, these factors caused the primary system pressure stopped decreasing and even increased a little. At about 98,000 s, because the

volumes of affected steam generator tubes and boiler were full of steam, the condition for heat transfer was worsened abruptly, no energy would be transferred to the boiler pool and very little energy to the boiler atmosphere (see **Figs. 3.1.4** and **3.1.5**), this caused the pressure in primary system increased suddenly and that in affected SG boiler decreased sharply (also see section (2)).

(2) Secondary System Pressure

For steam generator secondary side, **Fig. 3.1.6** shows the pressures in the faulted steam generator (SG boiler C) and in the intact steam generator (SG boiler AB). In the faulted steam generator, as soon as the break occurred, due to the large amount of energy flow directly from the primary coolant system, the pressure went up; then, after the main coolant pumps tripped, the energy reduced and caused the faulted SG secondary pressure decreased. But immediately because of the turbine trip, the pressure rose again. When the pressure reached the set point of PORV of SG C, the PORV opened and closed cyclically according to the pressure, so the pressure appeared oscillating. At about 7,500 s (see 3.1.1), the PORV in this faulted SG was stuck open and failed to close forever, the pressure decreased quickly. When HPSI stopped, the core began to be heated up and more heat was transferred to this SG boiler, then the pressure in SG boiler C increased accordingly. In the affected SG, because the pressure on the primary side had decreased very deeply and had a very small value at that time, the saturation temperature in the primary system was not high enough to prevent the liquid temperature from reaching that saturation temperature (see **Fig. 3.1.7**), then steam was produced. At about 98,000 s, the heat transfer condition worsened abruptly due to change of break flow from liquid to gas phase and very little energy could be transferred to the SG secondary side (also see section (1)), so its pressure decreased sharply. Then, after the energy equilibrium between primary and secondary sides was developed, the pressure would increase again.

For the intact steam generator secondary side, it shows that the pressure had the similar trend to that in the faulted SG before the PORV of the faulted SG was stuck open. After the PORV of the faulted SG was stuck open, the pressure in the intact SG secondary side was also decreased because, at that time, the faulted steam generator removed most of energy produced in the primary side through tube heat transfer and the break flow, and the intact steam generator almost had no energy to be added or even had a reverse heat transfer from it to primary side (see **Fig. 3.1.8**, the temperature of SG C liquid was nearly equal to the core liquid temperature, shortly after the HPSI operation, the temperature of SG AB liquid would be higher than them), however, the decreasing speed was very slow compared with that for the affected SG. At the moment when HPSI stopped, there could be seen a sudden depressurization, this is because of a very high heat flux from SG AB boiler to tubes (see **Fig. 3.1.9**). After that, because the temperature of primary system coolant increased and the flashing in SG AB tubes made the heat transfer efficiency reduced, the heat transfer from SG AB to primary side became much less than before and the pressure in the intact

SG secondary side decreased slowly. At about 98,000 s, while the heat transfer condition in the faulted SG worsened abruptly, contrary to the sharp depressurization of faulted SG secondary side, the pressure in the intact SG secondary side increased rapidly, because the primary temperature rose quickly and was high enough to match the temperature in SG AB and there was no longer any heat transfer from secondary to primary but from the primary to secondary.

(3) Containment Pressure and Temperature

The containment pressure is shown in **Fig. 3.1.10**. During the whole period from the steady state -200 s to 100,000 s, though an SGTR occurred, the containment vessel was never failed, so the containment pressure was only slightly affected by the pressurizer cubicle. The temperature of the containment atmosphere is shown in **Fig. 3.1.11**. The trend of curve is slightly different from the pressure curve. Since the vessel did not fail, there was no unsafety trail in the containment.

(4) Fuel Temperature

Figures 3.1.12 through **3.1.15** are the temperatures of fuel. The third ring of the core was not listed here. A detailed figure (from -200 to 600 s) for level 13, ring 1 of the core was drawn to explain the process in this period (see **Fig. 3.1.16**). At the time when the tube break occurred, because of the break flow which brought more energy out of the core, the fuel temperature declined. When the reactor scrammed, due to the heat source loss, the temperature decreased suddenly to a very low level. Then, after HPSI operation, the temperature continued decreasing slowly. From **Figs. 3.1.12** through **3.1.15**, it can be found that the temperatures would increase at the time of HPSI stopped. After that, the core began to be heated up. From **Figs. 3.1.13** and **3.1.15**, it can be seen that the temperature of fuel in level 12 and 13 began to increase, this indicated that the top of the core may begin to uncover. **Figure 3.1.17** shows the temperature trend of the cladding in Ring 1, level 13 which was similar to the fuel after reactor scram. At the time of 100,000 s, it was still far from the cladding failure temperature of 1173 K.

(5) Collapsed Water Level in Core

Figure 3.1.18 shows the collapsed water level in the core, lower plenum and the core bypass. From the curve of core collapsed level (the top of the fuel rod was 6.722 m high and the lowest was 3.064 m high from the bottom head), it was seen that the level would decrease sharply at the moment of break occurring due to the break flow. After the high pressure safety injection system was activated, the level recovered to normal, but after the refueling water storage tank was emptied and the accumulator stopped injecting, the collapsed level decreased again. Then, because the core was heated up and the water in core swelled, the collapsed level increased slightly; but

quickly, because of the break flow and the steam being produced in the core, the level decreased sharply again. At about 80,000 s, because the increased pressure in the core (see (1)) raised the core saturation temperature and made the steam production reduced (see **Fig. 3.1.3**) and also because the break flow decreasing, the collapsed level in core was elevated accordingly. After that, since temperature in core became higher and higher and steam production became more and more, the level had to decrease again. Near 97,000 - 98,000 s, due to the sudden increase of pressure in the core, there also could be seen an elevated level. Finally, the collapsed level would be lower and lower. It did not reach the lowest location of the core till this calculation terminated.

For the bypass collapsed level, it also decreased when the core level did so, but the decreasing speed was much lower than that of core because the temperature in the bypass water was always lower than that in the core.

(6) Steam Generator Tube Temperature

Figure 3.1.19 shows the steam generator tube temperature. At the break beginning, the broken tube temperature rose quickly at an increment of about 25 K. Then, after the coolant pump tripped, the heat removed from the core to the steam generator decreased and this caused the tube temperature dropped sharply. At this time, the temperature of other tubes in the affected steam generator dropped also and were nearly equal to the broken tube, then their curves showed almost the same tendency. When the high pressure injection system began to be activated, with the increase of the energy transferred from the core and the increase of the faulted SG boiler pressure and temperature, the tubes' temperature increased to nearly the normal temperature relatively to the initial state. But after the PORV in the faulted SG was stuck open, due to the large quantity heat removed by the steam release through the PORV, the tubes' temperature decreased suddenly and deeply by 140 K. While the HPSI stopped, the temperature increased again, because at this time, the energy produced in the core could not be removed effectively from the affected SG due to the loss of coolant and accordingly, would be added to the tubes. Then, with the decreasing of the pressure in primary system and the increasing of the pressure in the faulted SG secondary side (see sections (1) and (2)), the pressure difference began to smaller and smaller and this caused the break flow so small that the temperatures in both sides of the SG tube would increase and made the tubes' temperature increased also but not quickly. At about 98,000 s, since the pool in the faulted SG boiler vaporized completely, the steam temperature increased quickly and that caused the quick increase of tube temperature.

For the temperature of the intact SG tubes, the temperature tendency was something like that of the faulted SG not-broken tubes before the PORV in faulted SG was stuck open. After that, the temperature also decreased but not as fast as that of the affected tubes. Then because almost no energy was added to the intact SG and very little heat was transferred through the tubes, the

temperature almost kept a constant with very slow decreasing. At the time of HPSI stopped, due to the sudden and deep depressurization in the tubes, the pool in the tubes flashed and that caused the tube temperature had a fast drop. After that, the temperature curve became flat. Also at the time of 98,000 s, because the heat transfer condition worsened quickly and the core was heated up, the tube temperature increased quickly accordingly.

(7) Hot Leg and Pressurizer Surge Line Temperatures

Figures 3.1.20 and **3.1.21** present the trends of the hot leg temperature and the pressurizer surge line temperature, respectively. What should be concerned about these temperatures are whether they have reached the creep failure temperature or not. From the two figures, it could be seen that at the end of this calculation, the temperatures were still below their initial temperatures and far lower than the failure temperatures.

(8) Coolant Mass Flow Rates

Figures 3.1.22 through **3.1.24** present the flow rates of the core, high pressure safety injection (HPSI) and the accumulator velocity.

(9) Radionuclide Releases

During this calculation, the fuel cladding was not heated up to the cladding burst or failure temperature and therefore quite small amount of radionuclides was released from the core.

3.2 Analytical Results of Once-through Model from 100,000 to 150,000 s

This calculation was performed to compare the once-through model with the hot leg countercurrent natural circulation model and to evaluate the effect of hot leg countercurrent on the progression of this SGTR severe accident. In this calculation, the nodalizations of control volumes, flow paths and heat structures are identical to the calculation from - 200 to 100,000 s.

3.2.1 Sequence of Predicted Events

The sequence of events and its timings of occurrence calculated after 100,000 s using the once-through model are summarized in **Table 3.2.1**. From this table, the cladding oxidation began at about 108.3 min (the time after first 100,000 s calculation, the followings are the same as above). After its temperature reached 1173 K, the cladding was failed and caused the fission gas products in the fuel-cladding gap released. First release occurred in the radial ring 1 at 112.92 min

followed by rings 2 and 3 at 117.58 and 131.70 min, respectively. At about 135.0 min, the first relocation occurred. After the core uncovery completed at 193.3 min, the collapsed liquid level in lower plenum began to drop and caused the heat up of the core support plate. At 232.80 min, the core support plate failure first occurred in radial ring 3 and closely followed by the failure in radial rings 2 and 1 at the time of 236.73 min and 239.20 min, respectively. About 9 min later, the lower head penetration in radial ring 2 failed, the initial diameter of the hole was about 0.267 m. Also at this time, the cavity woke up and the debris began to eject into the reactor cavity from the vessel. The liquid level in the lower plenum decreased sharply to zero accordingly. A second accumulator delivery of accumulators remaining inventory in all loops was predicted between 250.60 and 251.38 min. After the inventories exhausted, no operation was assumed to mitigate the accident.

3.2.2 Discussions of Calculation Results

The followings are the results as well as its based discussions calculated after 100,000 s using the once-through model.

(1) Primary System Pressure and Temperature

Figure 3.2.1 shows the primary system pressure. It can be seen that from the beginning of this calculation, the primary system pressure continued to increase slowly due to the core heatup and degradation. At about 1.081×10^5 s (135.0 min) when the relocation first occurred (**Fig. 3.2.2**), the pressure began to increase and reached a peak of about 5.8 MPa at about 1.090×10^5 s, with also the reason that the oxidation rate had a very sharp increase (**Fig. 3.2.3**). Then, the pressure decreased because the heat in the vapor generated by the relocation was removed from the core by the break flow. Similar processes would occur at any time when the melt relocated axially, with differences of the melt mass and energy from each other. At the time 1.116×10^5 s (193.3 min) when the core completely uncovered (**Fig. 3.2.4**), all the water in core control volume was changed to vapor and this caused a large amount of vapor generation and a relatively maximum pressure value in the core. This maximum value was about 6.2 MPa. Then, the pressure decreased again to about 4.5 MPa at 1.128×10^5 s (215.0 min). From this time to 1.133×10^5 s (216.7 min), the pressure increased quickly to another pressure peak, about 5.6 MPa. During this time, a large melt relocated from the core to lower plenum and caused to a lot vapor generation (**Fig. 3.2.5**). Then the pressure decreased again to about 4.0 MPa. After the core support plate failure in all radial rings, the pressure had a sudden rise to 5.2 MPa. At the time of 1.1488×10^5 s (248.0 min), the lower head penetration in radial ring 2 failed, and the pressure in core fell down to the containment pressure immediately and would never increase.

Figure 3.2.6 gives the liquid and gas temperatures in the core control volume. The pool temperature was mostly kept at a constant of 540 K (saturated temperature at the pressure at that

time) till the core completely uncovered, then the pool in the core disappeared with its temperature rising quickly. The atmosphere temperature began to increase because the core had begun to heat up. At about 1.04×10^5 s (66.7 min), because the void fraction of core outflow rose quickly and the heat removal through this flow decreased, also because the oxidation began at 1.067×10^5 s and the enthalpy released, the atmosphere temperature increased sharply up to about 2100 K at 1.081×10^5 s when the first relocation occurred. The relocation would cause the vaporization and the colder vapor would decrease the whole atmosphere temperature. Then the temperature rose again, followed by the oscillation due to other relocation processes.

At 1.116×10^5 s when the core uncovery completed, the temperature slightly decreased. After that, the temperature curve can be seen a very steep drop at 1.133×10^5 s (221.7 min), this was because at that time, a large core debris melt fell into the lower plenum (**Fig. 3.2.5** and also discussed above in pressure analysis) and agitated up the cold water and steam which could cool the hotter vapor in the core atmosphere. After that, the speed of core heat-up and degradation was accelerated due to oxidation reaction and the temperature quickly rose to the maximum value, 2700 K. Then, at 1.1504×10^5 s (250.6 min), the second accumulator ejection occurred and made the core atmosphere temperature rapidly decrease to the saturated temperature. After the accumulator inventory exhausted, the temperature bounced back to about 1230 K, then from this point, after a little reduction, the temperature began to increase slowly again and was influenced by the hydrogen deflagration at 142 and 145 min, respectively. At the end of the calculation, the temperature was about 1450 K.

(2) Secondary System Pressure

Figure 3.2.7 shows the pressures in the secondary side of the faulted SG and the intact SGs. Before the relocation occurred in the core, the pressure in Boiler AB followed the same trend as the primary system and then it would almost keep a constant of 5 MPa. For Boiler C, because the PORV had been stuck open, the pressure had decreased to 0.6～0.7 MPa and would fall down to the same level as the primary system fall to at the time when the lower head penetration failed.

(3) Containment Pressure and Temperature

Figures 3.2.8 and **3.2.9** present the pressures and atmosphere temperatures of basement, cavity and dome in containment. In **Fig. 3.2.8**, the pressure trends of the basement, cavity and dome have no differences. Before the lower head penetration failure, the pressure was kept at almost a constant with very little increase. Then, because of the penetration failure with the mass and energy input to the containment, the pressure rose sharply followed by a little decrease due to the accumulator inventory ejection. After that, the pressure was elevated by the decay power and the enthalpy released from the interaction between the core melt or debris and the concrete or other

materials consisted in the containment. At the end of this calculation, the pressure in containment was about 1.16 kPa with several pulses due to the processes of repeated hydrogen deflagration.

From **Fig. 3.2.9**, it can be seen that the atmosphere temperature curves of the basement and dome are almost same, which climb very slowly in almost a constant speed. For the cavity, the cavity atmosphere temperature had a sharp increase st the time of the lower head penetration failure and then dropped due to the accumulator inventory ejection. After the time 1.2699×10^5 s (449.90 min) when the first deflagration occurred, the temperature always showed very unstable and frequent oscillations with large amplitudes because of the violent processes between the debris and the concrete in the cavity. The maximum value involved in these oscillations was about 2230 K. At the end of this calculation, the average atmosphere temperature in cavity was about 1900 K.

(4) Fuel Temperatures and Core Degradation

Figures 3.2.10 through **3.2.15** show the fuel temperatures at various levels in the different radial rings during the core damage period. The drop on each curve from the top to zero directly mean the fuel at that level and in that ring collapsed. It is indicated that all fuel temperatures kept almost constants at the beginning. The features in outer two rings are very similar with slightly differences from the timings, all the axial levels in each ring would collapse at the same time which was 1.143×10^5 s for the second ring and 1.141×10^5 s for the third ring. For the first ring, the behavior can be also said similar to the outer two rings, but the collapsing timings were quite different between each level, which were, 1.133×10^5 s for the top level to the tenth level, 1.140×10^5 s for the ninth level and 1.144×10^5 s for the others. There were two significant heat-up processes observed, especially in the upper half part of each ring, one was the heat-up when the specific level uncovered and another was that when the oxidation began. After the fuel temperature had reached a very high value, it increased slowly and even appeared some little oscillations till the fuel collapsed. The reason is that the Zr-water reaction stopped due to exhaustion of unoxidized metal.

At 1.13968×10^5 s (232.80 min), 1.14204×10^5 s (236.73 min) and 1.14352×10^5 s (239.20 min), the core support plate failure occurred in third, second and first radial rings, respectively. It is noted that the first failure occurred in the third ring, instead of the first ring where the power density was higher. This may be explained from **Fig. 3.2.5**, in which the mass relocated to the axial level 3 in ring 3 was heavier than that in other two rings and the energy was much enough to heat the support plate to the failure temperature.

At 1.1488×10^5 s (248.0 min), the lower head penetration in the second ring failed. This probably because at that time, the mass distributed to the bottom of lower plenum (the top of lower head) in the second ring reached a very high value (5.3×10^4 kg, about three times than other two

rings, see **Fig. 3.2.16**) and the enthalpy brought by the mass heat the penetration enough (1273 K) to fail. After the penetration failed here, the melt would fall through the hole and temperatures of penetrations would decrease quickly, the other two penetrations had no opportunities to fail.

Figure 3.2.17 shows the total masses of core materials (zircaloy, zirconium dioxide, steel and steel oxide) remaining in the vessel during this SGTR case calculation. As in the figure, most of the unoxidized zircaloy (about 95 %) and all the oxides were transferred to the cavity. For the steel and steel oxide, about 60 % of steel and all the oxides left the core. It can also be seen from this figure that about 60 % of zircaloy and very little steel were oxidized.

(5) Collapsed Liquid Level

Figure 3.2.4 gives the collapsed liquid levels of the core, lower plenum and pressurizer. At about 1.04×10^5 s (66.7 min), because the void fraction of core outflow rose quickly and the heat removal through this flow decreased, the core was heated rapidly and the core level collapsing speed increased. At about 1.116×10^5 s (175.0 min), the core collapsed level decreased to 3.064 m high from the vessel bottom, which was the lowest location of the core, and the core uncovery completed. After that, the level of lower plenum began to reduce. This collapsed level decreased almost in a same speed, except for that at two time points. One was at 1.133×10^5 s (221.7 min), when a large core debris melt fell into the lower plenum (**Figs. 3.2.5** and **3.2.11**) and vaporized the cold water to steam and caused a sharp drop. Another exception was at the time before the lower head penetration failed, because all the core support plate failed and many core debris entered the lower plenum, the virtual volume increased suddenly and the level had a sudden rise accordingly. Then, after the lower head penetration failed at 1.1488×10^5 s (248.0 min), the lower plenum collapsed level fell to zero immediately. At 1.1504×10^5 s (256.6 min), due to the accumulators injection which also caused the level in core had a small level pulse, the collapsed level in lower plenum recovered to about 1.2 m, and then, after the accumulator inventory exhausted, the level would changed to and kept on zero. During the whole calculation, collapsed liquid level in pressurizer was kept at 8 m high from the RPV bottom head which means no liquid in pressurizer.

(6) Coolant Mass Flow Rates

Figure 3.2.18 presents the mass flow rates to and from the core. With the core heating-up and degradation, the flow rate from the core to upper plenum decreased from 80 kg/s to 3 kg/s at 1.035×10^5 s, then, it continued decreasing slowly with several small oscillations due to relocations and other processes such as vaporization, condensation, oxidation, etc. Three relative large oscillations occurred at the times when the core completely uncovered and when the lower head penetration failed and the following accumulator inventory injected. After the accumulator inventory

exhausted, the outlet flow rate was kept at zero. For the inlet mass flow rate to core from the lower plenum, the same sharp drop occurred at the beginning of this calculation. Because of the core heating-up and degradation, after this flow rate fell down to about 10 kg/s, it was always in the frequent oscillations and the vibration amplitudes varied from -12 kg/s to 33 kg/s (the negative value meant the flow was from the core to lower plenum). After the penetration failed and the accumulator inventory exhausted, the inlet flow rate also became zero and kept on it.

Figure 3.2.19 gives the steam generator break flow rate from the broken tube to the boiler in Loop C. The figure is similar to that of the primary system pressure because the break flow and its direction were determined by the pressure difference between the primary and secondary systems, and the secondary system was mostly kept at a constant during the core degradation. Another dominating factor was the coolant mass flow rate from the core to the hot leg. That was the reason why the figure was not completely the same as that of primary pressure. After the core had begun melting and relocation, the highest flow rate value out of broken tube was about 2.65 kg/s (1.45 kg/s for BK DN plus 1.20 kg/s for BK UP) occurring at 1.116×10^5 s (175.0 min) when the core uncovery completed. These trends could be referred to the discussion of primary pressure. As soon as the lower head penetration failed, the break flow rate dropped to zero.

Figure 3.2.20 shows the accumulators deliveries. A second accumulators injection was predicted in this calculation beginning at 1.1504×10^5 s (250.60 min) and ending at 1.1508×10^5 s (251.38 min) and 58.77 m^3 of inventory was delivered.

Figure 3.2.21 presents the vapor release rate from the power operated relief valve (PORV) in SG C. Radionuclides released from the core would enter the environment directly through this valve and bypass the containment. After the gap release occurred in the core, the release rate through PORV varied from 1.9 to 2.5 kg/s until the time when vessel failed and the release rate changed to zero.

Figure 3.2.22 gives the mass flow rates from the hot leg to steam generator with a reference to the flow rates from the broken tube to boiler. The flow rate from hot leg C to SG C ranged from 0.5 to 2.5 kg/s and was mostly more than 1.5 kg/s. For the flow rate from hot leg AB to SG AB, it could be divided into two parts, one part was before 1.07×10^5 s by which the flow rate was above zero and around 1 kg/s, the other part was after 1.07×10^5 s from which the flow rate was below zero with instantaneous rebounding above zero to high values for three times.

Figure 3.2.23 shows the enthalpy flow rates from the core to boiler through hot legs and steam generators. It can be seen that the break flow has the ability to remove about 8 MW of heat.

(7) Hot Leg and Surge Line Pipe Temperatures

Figure 3.2.24 presents the temperatures of hot legs and surge line pipes. Since most of superheated steam was transported through hot leg C to the break point and very small amount of superheated steam passed the hot leg AB and surge line, only the hot leg C pipe was heated up to approximate 1300 K (no hot leg failure predicted in the present calculation) while the temperatures of other two pipes rose slowly to about 613 K at the end of this calculation.

(8) Hydrogen Production and Deflagration

Figure 3.2.25 presents the hydrogen productions in the core and cavity. The hydrogen production first occurred at 1.065×10^5 s when the oxidation (the reaction between zircaloy and water) began. With the progression of oxidation, the hydrogen production increased rapidly to about 425 kg at 1.1488×10^5 s (248.00 min) when the lower head penetration failed and the processes in the core stopped. Then, the main location of hydrogen production was changed to the reactor cavity where the oxidation of metals by the concrete decomposition gases such as H_2O and CO_2 was predicted, meantime, another reluctant carbon monoxide (CO) could also be predicted. At the end of this calculation, the hydrogen produced in cavity reached 225 kg. At 1.2699×10^5 s (449.9 min), when the concentrations of H_2 and / or CO reached a critical value, the deflagration first occurred in the cavity followed by the occurrences whenever the criterion was satisfied.

(9) Radionuclide Releases

Since the MELCOR code has been developed as a tool for Probabilistic Risk Assessment (PRA), the code can consider the release and transport of radioactive fission products and for the release to the environment (source term). As a source term code, MELCOR especially deals with the fission products (and daughters) released during an accident, which are particularly important for determining consequences and risks. MELCOR treats fission products in molecular forms, not only the radioactive fission products elements themselves, but also the nonradioactive elements with which fission products may interact. Furthermore, MELCOR combines elements into material classes, groups of elements with similar chemical behavior. The initial radionuclide inventories for each class are generally based on whole-core inventories calculated using the ORIGEN[5],[6] code, and distribution may be specified for fuel in the core, the fuel-cladding gap, and initial cavity debris, and the atmosphere and pool of any control volume. Release of radionuclides can occur from the fuel-cladding gap by exceeding a failure temperature criterion of losing intact geometry, from material in the core using the various CORSOR[7],[8] empirical release correlations based on fuel temperatures and during core-concrete interactions in the reactor cavity using the VANESA[9] release model.

In this calculation, 15 material classes were considered as the default, which meant Cs and I were released separately, instead of combination into CsI. **Table 3.2.2** gives the radionuclide fractional distributions (by total released class-dependent masses) in the primary, containment, environment and steam generator and gives the total released masses and gives the total released masses at the end of the MELCOR analysis, 1.5×10^5 s, together with the initial inventory calculated by ORIGEN code from **Ref.10**. **Figures 3.2.26** through **3.2.37** show the radionuclide masses, according to the fission product species class defined by the input, released from the fuel in the in- and ex-vessel portions of the accident, accompanied by a trace showing the sum of the two. Though the containment was kept intact, the releases to environment through SG power operated relief valve (PORV) was predicted.

The gap release began at 1.06775×10^5 s (112.92 min) when the cladding in radial ring 1 failed. At the time of 1.1488×10^5 s (248.00) when the lower head penetration failed, ex-vessel releases were initiated, however, for noble gases (Xe), alkali metals (Cs), platinoids (Ru) and early transition elements (Mo), ex-vessel release stage ended at once, and, for other classes, ex-vessel release would continue to contribute to source term.

It can be seen from **Table 3.2.2** that almost all of Xenon, Cesium and Iodine class materials were released from the fuel in this calculation. **Figures 3.2.26, 3.2.27** and **3.2.29** show that almost all (about 95 %) of those releases occurred in-vessel, with the remaining 5% released in ex-vessel stage in the reactor cavity. It should be noted that, in **Table 3.2.2**, the total distribution fraction (Primary + Containment + Environment + SG) was more than 1.0.

The reason for large release fraction of Cesium and Iodine into environment can be explained as follows. In the once-through model calculation, Cesium and Iodine were separately treated and Cesium Iodide (CsI) which is considered to be most probable form during severe accidents from a thermochemical theory was not formed since the input deck obtained from USNRC was used without any modifications. Therefore, the deposition mass of Cesium and Iodine in both RCS and containment became small because most of them were in vapor form. As a result, their release fractions into environment became large. If the formation of CsI was taken into account in the calculation, large amount of CsI aerosol might have deposited onto RCS or containment due to natural deposition processes and therefore the release fractions of Cesium and Iodine might have decreased as in the calculation with the hot leg countercurrent natural circulation model.

The release behavior predicted by MELCOR in this calculation can be grouped into several subdivisions. For Class 1 (Xe), Class 2 (Cs) and Class 4 (Iodine), $\sim$100% of initial radionuclide inventories were released, about 95 % / 5 % releases occurred at in- and ex-vessels, respectively. The next major release fractions are of Class 5 (Te), Class 11 (Cd) and Class 12 (Sn) which were predicted to be 76.54 %, 78.09 % and 78.02 %, respectively. Following them, 46.33 % of Class 3

(Ba), 25.21% of Class 7 (Mo) and 2.49 % of Class 6 (Ru) was predicted to be released. Finally, quite small fraction of Class 8 (Ce), Class 9 (La) and Class 10 (U) were released in this calculation and the fractions were 0.092 %, 0.202 % and 0.202 %, respectively.

The release patterns varied depending on the RN class also, however, the variations in this case were not significant. For Xe, Cs and Iodine, about 95 % / 5 % of releases occurred at in- and ex-vessels, respectively. For Te and Ce, 54.15 % and 58.92 % of releases were predicted at in-vessel. The in-vessel releases of other classes was more than 98% of the total, and especially, all of the Class 6 (Ru) and 7 (Mo) releases occurred in vessel.

The released radionuclide distributions can be also grouped into a few subdivisions. More than 90 % of the noble gases (Class 1) and iodine (Class 4) were released to environment by the end of this simulation, while most (65～85 %) of Ba, Ru, Mo, La, U, Cd and Sn still remained in primary system with about 5 % of the amounts released to the environment. For Te and Ce, about halves of the releases were distributed in the containment with about 34 % and 44 % in RCS and about 10 % and 3 % were released into environment, respectively. For Cs, more than a half was retained in RCS while 15 % was released to the environment. Since this calculation was performed for SGTR analysis, steam generator acquired some fractions from the releases accordingly. About 20 % of Cs and 5 ～10 % of all other classes retained at the SG except for Xe and Iodine.

The total masses of fission products released from the fuel are shown in **Fig. 3.2.38**. Almost of all the releases occurred during the stages of in-vessel core damage and the melt ejection, and only very little release occurred during the ex-vessel stage. About 57 % of fission products released were deposited on heat structures while 43 % were found in the control volumes of pool or atmosphere, and about 90 % of fission products in the control volumes was vapor form rather than aerosol form because most of aerosol was immediately deposited onto the heat structures.

3.3 Analytical Results of Hot Leg Countercurrent Natural Circulation Model from 100,000 to 150,000 s

3.3.1 Sequence of Predicted Events

The sequence of events and its timings of occurrence calculated after 100,000 s using the hot leg countercurrent natural-circulation model are summarized in **Table 3.3.1**. It can be seen that zircaloy of cladding began to be oxidized at about 86.7 min (after first 100,000 s calculation) before the cladding failure (at axial level 13). At 93.85 min, the cladding of radial ring 1 failed and the gap release began, then followed by the radial rings 2 and 3. The first relocation occurred at about 113.3 min. After the core uncovered completely at about 170 min, at 211.12 min, the core support

plate first failure occurred in radial ring 2, then, 6 min later, the ring 1 core support plate was also failed. At the time of 246.10 min, the lower head penetration in radial ring 2 failed, the initial diameter of the hole was about 0.267 m which corresponds to the size of electrical penetrations in radial ring 2. This caused the beginning of debris ejection to the cavity and waking up various processes in the cavity. The collapsed level of lower plenum decreased sharply and deeply. A second accumulator delivery of accumulators remaining inventory in all loops was predicted between 247.73 min and 248.67 min and could cause the sudden increase of the lower plenum collapsed level. But after the accumulators inventories exhausted, the level of lower plenum would be decreased to zero. At 249.85 min, the ring 3 core support plate failed. When time reached 1.3863×10^5 s (643.90 min), a first deflagration started in the cavity and ended at 1.3864×10^5 s (644.03 min). At 1.387×10^5 s (645.23 min), the lower head penetration in radial ring 1 failed. The initial diameter of the hole was 0.127 m which corresponds to the size of electrical penetrations in radial ring 3.

3.3.2 Discussions of Calculated Results

The followings are the results as well as its based discussions calculated after 100,000 s using the hot leg countercurrent natural circulation model.

(1) Primary System Pressure and Temperature

Figure 3.3.1 shows the primary system pressure. It can be seen that from the beginning of this calculation, the primary system pressure continued to increase slowly due to the core heatup and degradation. After the time of about 1.068×10^5 s (113.3 min), when the first melt relocation occurred, the speed of the pressure increasing became more and more rapidly, with several little oscillations due to the relocation. The pressure rose abruptly and formed a pressure spike of 7.5 MPa at about 1.078×10^5 s (130. min). The reason is that, from 116 min to 130 min, the axial top level to level 7 of all the radial rings in the core melted and relocated and this resulted in a large vapor generation through the debris/coolant heat transfer and produced a large RCS pressure increase. Accordingly, with the significant reduction of the steam generation and the heat removal out of the core, the primary pressure ran down sharply to 5.3 MPa.

At the time of about 1.102×10^6 s (170 min), as the core was completely uncovered (**Fig. 3.3.3**), the pressure rose back a little. After that, the pressure continued to decrease. At about 1.115×10^5 s (191.7 min), a second pressure spike of about 6.0 MPa occurred, this phenomenon was caused by the relocation of a large mass of hot debris from the core region to the lower plenum. It can be seen from **Fig. 3.3.4** that all the masses of UO_2 and Zr in the axial level 3 (core plate), increased from zeroes to the maximum values. The transient heat transfer rates should be sufficient enough to quench the hot debris and generate a large steam pressure increase. After that,

nothing could avoid the primary system from depressurization except the water injection of accumulators from 247.73 min initiated by low pressure signal to 248.67 min ended by exhaustion. At 1.15×10^5 s (249.9 min), all the support plates failure occurred followed by the lower head failure. Accordingly, the primary system pressure decreased at the moment to the deepest value and was kept at a constant to fit the containment pressure.

Figure 3.3.5 gives the core control volume material (Liquid and Atmosphere) temperatures. The liquid temperature in the pool of this control volume almost kept a constant value of 540 K until the complete core uncovery. The atmosphere temperature began to increase as the core began to heat up due to cladding oxidation. The total cumulative oxidation energy is shown in **Fig. 3.3.2**. The increasing rate was improved with the heat-up rate increase in the core. At the time of 1.068×10^5 s (113.3 min) when the first relocation occurred, because the debris quenching generated much relatively colder vapor, the atmosphere temperature decreased rapidly after it reached 2000 K. Then the temperature increased again. This process would repeat at any time when relocation occurred and lower temperature vapor generated, only had the difference in the magnitude of increment or reduction resulted from the difference of the mass and energy of melt relocated and vapor generated. At about 1.102×10^5 s (170.0 min) when the core uncovery completed finally, all the liquid was changed to steam and this resulted in the decrease of atmosphere temperature to 1200 K because no more colder steam could be added in. After that, the temperature increased quickly again and reached 2200 K in a very short time.

At about 1.115×10^5 s (191.7 min), a massive core melt slumped to the support plate and agitated up much water in the lower plenum. As a result, the core temperature decreased to nearly the saturated temperature. Then, the temperature shot up again to reach the maximum value at the time of 1.1302×10^5 s (217.03 min) before the support plate failure at radial ring 1. After that, the temperature decreased again. At 1.1486×10^5 s (247.73 min), after the lower head penetration failed, because of the accumulators injection, the temperature of atmosphere in the core fell suddenly to the minimum value of 500 K. After that, the temperature had an obvious bounce then rose again, but the heat-up rate became smaller and smaller. At the time of 1.387×10^5 s, when the lower head penetration failure occurred in the first radial ring, the temperature oscillated and then continued to rise slowly again. At the end of this calculation, the temperature was about 1550 K.

(2) Secondary System Pressure

Figure 3.3.6 shows the secondary system pressure. The secondary system pressure of SG AB (boiler) gradually increased. On the other hand, the secondary system pressure of SG C (boiler) was kept at low level due to PORV stuck open and decreased again at the time of lower head failure at 1.1486×10^5 s (247.73 min).

(3) Containment Pressure and Temperature

In this SGTR analysis, the containment was divided into six control volumes which were basement, reactor cavity, SG A/B/C cubicle, press cubicle, lower dome and main dome as shown in **Fig. 2.1.1**. **Figures 3.3.7** and **3.3.8** give the pressures and atmosphere temperatures of basement, cavity and dome as representatives in containment. From **Fig. 3.3.7**, it can be seen that the pressure curves display almost the same trends. However, at the moment of 1.148×10^5 s (246.1 min) when the lower head penetration in radial ring 2 was failed, the cavity pressure rose quickly from 70 kPa to a much higher value (about 84 kPa) but immediately reduced to a very low value (66.8 kPa) due to the accumulator injection, then after the accumulators were exhausted, the pressure of cavity bounced to 91 kPa and was equal to those of basement and dome again. This result was because the cavity was directly influenced by the injection, but not for the basement and dome. After the transient heat transfer passed, all the pressures had to go down sharply to 83 kPa, then began to increase again due to the decay heat of fission products. After the pressures reached 110 kPa at about 1.3×10^5 s, the curves were observed to become flat, that meant those factors (decay power, reaction heat, etc.) which elevated the pressure had been mitigated and could only keep on the present pressure or improve a little. At the time of 1.387×10^5 s, when the lower head penetration failed in the first radial ring, a pulse of pressures occurred. At the end of this calculation, the pressures was about 125 kPa.

From **Fig. 3.3.8**, it can be seen that the features of the basement, cavity and dome temperatures were almost the same, however, the temperature of the cavity is of course greater than those of basement and dome. These temperatures kept almost constants before the lower head penetration failure. At the time of the penetration failure, the temperatures increased in an instant. Then because of the accumulator injection, the temperatures decreased again to some new relatively low and stable values and then slowly increased. For the temperatures of the basement and the dome, it can be seen that the curves were almost straight lines, except a pulse when the penetration in the first radial ring failed, and the slopes of the lines were also very small. At the end of this calculation, the temperatures of the basement and dome were about 360 K. But for the cavity temperature, the case was much more complicated. Many large oscillations could be observed on the cavity temperature curve because the violent reaction between the debris and the concrete in the debris pool in cavity. When the oscillations occurred, the maximum temperature could reach 2200 K. At the end of this calculation, the average temperature of cavity atmosphere was about 1800 K.

(4) Fuel Temperatures and Core degradation

Figures 3.3.9 through **3.3.14** show the fuel temperatures at various levels in the different radial rings during the core damage period. The behavior in all three rings was very similar, only delayed in time in the outer two rings due to lower power densities. At the beginning

of this calculation, all temperatures increased slowly because the coolant in the core could receive some decay heat from the core and vaporize, then remove the heat through the vapor flow. With the core level decreasing and the uncovery continuing, the temperatures rose quickly in the order from higher axial level to the lower and from inner radial ring to outer. It can be seen obviously that fuel temperatures in the highest axial level could get the maximum values much more earlier than the lowest. At about 1.03×10^5 s (50 min), an abrupt heat-up rate increase occurred at the highest level because the highest level had uncovered at that time. At 1.068×10^5 s (113.3 min), the first relocation occurred at the highest axial level (13th) in the first radial ring and almost in the meantime, the level collapsed. Similar observations on other levels and in other rings can also be available.

At 1.127×10^5 s (211.1 min), 1.130×10^5 s (217.0 min) and 1.150×10^5 s (249.9 min), after all the fuel had failed, the core support plates of the second, the first and the third rings failed in turn, respectively. It seems unreasonable that the core support plate failure first occurred in the radial ring 2, instead of the ring 3 or ring 1. However, since MELCOR predicted not only the axial debris relocation but also the radial relocation, it was possible for support plate failure occurred first at any ring. In this case, maybe because of a more melt relocation from ring 1 to ring 2 but a less melt relocation even a reverse relocation from ring 2 to ring 3 or a lot heat transfer from ring 3 to the surrounded heat structures, the plate failure consequently occurred first in the second ring and resulted in failure of the lower head penetration in ring 2. This phenomenon can be demonstrated by the material (such as ZrO_2) masses relocated to the support plate in each ring (see **Fig. 3.3.15**). In **Fig. 3.3.15**, it can be seen that at the time of a massive core melt slumped to the support plate, the mass of ZrO_2 in ring 2, level 3 (core support plate) was much more than those in ring 1 and ring 3 in same level. The earlier failure of ring 2 penetration resulted in the delay of the support plate failure in ring 3. Though the radial ring 2 penetration failed and some of the core melt and debris had entered the cavity, the process in core had not yet stopped and the degradation continued because there were still some masses remained on the axial level 1 (see **Fig. 3.3.16**). At 1.3871×10^5 s, the lower head penetration in radial ring 1 failed and all the mass relocated at the axial level 1 fell down to the reactor cavity (see **Fig. 3.3.16**).

Figure 3.3.17 shows the total masses of some core materials (zircaloy, zirconium dioxide, steel and steel oxide) remaining in the vessel during this SGTR accident. Most of the unoxidized zircaloy and the oxides (both about 80 %) were transferred to the cavity after penetration 2 and 1 failed. However, much of the structural steel in the lower plenum and core support plate was predicted to remain unmelted and in place even after the vessel breach. It can also be seen from this figure that more than half of initial zircaloy and very little steel were oxidized.

(5) Collapsed Liquid Level

Figure 3.3.3 shows the collapsed liquid levels in the core, lower plenum and pressurizer. In this calculation, the pressurizer and surge line were modeled separately to simulate the natural circulation. Therefore, here the pressurizer collapsed level referred to that of surge line to keep consistence with other calculations. From the figure, it can be seen that the core collapsed level decreased continuously with the core heating-up and degrading. At about 1.078×10^5 s (130 min), there was a sudden decreasing and then sudden increasing on the curve. This was because at this time, the oxidation reaction released a large quantities of heat and made the vaporization rate increase rapidly. At 1.102×10^5 s (170 min), the core collapsed level decreased to 3.064 m, which was the lowest point of the core, and the core uncovery completed. After that, the level of lower plenum began to decrease. This collapsed level decreased almost according to the same rate, except for that at two time points. One was at 1.115×10^5 s (249.9 min), when the core slumped a massive debris to the lower plenum, so the water in the lower plenum had to quench the hot debris and a lot of steam was generated, as a result, the collapsed level decreased sharply.

Just before the lower head penetration failure, the collapsed level increased suddenly and even surpass the initial level of the lower plenum. This can be explained by **Fig. 3.3.18** which shows the virtual volumes of the core and lower plenum. It can be seen that at this time, the virtual volume of lower plenum increased abruptly to a very high value and would cause the total volume of lower plenum increase accordingly. That was the reason why the level increased unexpectedly, in fact, the level should not be considered as a real collapsed level. Then, after the lower head penetration in radial ring 2 was failed at 1.148×10^5 s (246.10 min), all the water went into the cavity and the collapsed level of lower plenum decreased to zero at this moment. At the time 1.149×10^5 s (247.73 min), due to the accumulators injection, the collapsed level appeared about 1.2 meters increase, and then, after the accumulators exhausted, the level fell to zero again.

(6) Coolant Mass Flow Rates

In this SGTR case calculation, to simulate the hot leg countercurrent flow, the hot legs had been divided into top and bottom parts. The superheated vapor would enter the top of the hot legs, the steam generators inlets, tubes, outlets and then from the outlets flowed back to the reactor vessel along the bottom of the hot leg. **Figures 3.3.19** and **3.3.20** show the mass flow rates of hot legs in loops AB and C, respectively. From **Fig. 3.3.19**, it can be seen that a stable natural circulation flow in the AB loop hot leg had been established during the core heat-up, except a little oscillation around zero flow rate in the time between 1.02×10^5 s and 1.03×10^5 s. The flow rate was not so large, generally below 5 kg/s. However, the stable hot leg countercurrent was never observed in the loop C from **Fig. 3.3.20**. This result was probably because the steam generator tube rupture, which caused the circulation interrupted at the broken point, occurred in loop C.

These flow rates can be considered as the indicators of the core temperature increase. While steam generation and / or pressure changed in the core, the flow rates would change accordingly, this can be expressed on the curves. To evaluate the heat removal efficiency of the hot leg countercurrent, **Fig. 3.3.21** which gives the temperatures of the vapor in the top and the bottom of hot leg AB was prepared. From this figure, the temperature of the vapor flow out of the core through the upper plenum to the top of the hot leg was higher and sometimes much higher than that from the bottom of hot leg to the upper plenum. This can, to some extent, shows that heat removal occurred at steam generators due to the hot leg countercurrent flow.

Figures 3.3.22 and **3.3.23** present the mass flow rates to and from the core, respectively. With the progression of core heat-up and degradation, the coolant flow rate at the core outlet began to decrease to zero. From the time of about 1.068×10^5 s, when the first core melt relocation occurred, to the time of about 1.078×10^5 s, when a very high oxidization power generated, the flow rates oscillated in a very large range, especially the flow from the lower plenum to the core (120 $\sim$ -270 kg/s). After that, the flow rates almost kept on the zero line until the core uncovery completed at 1.102×10^5 s (170.0 min) when there was another oscillation on the curve. As followed, the flow rates recovered to zero again. But from **Fig. 3.3.23**, a high flow rate spike of 140 kg/s was observed at about 1.115×10^5 s, this was because a massive core melt relocated to the lower plenum and accordingly, the core pressure increased at this moment. At the time of 1.1477×10^5 s (246.10 min), when the lower head penetration failure occurred, there was a reverse flow from the upper plenum to the core then to the lower plenum. Then, no flow would pass through the core.

Figure 3.3.24 gives the steam generator break flow rate from the broken tube to the boiler (secondary system) in loop C. The feature of the figure is very similar to that of the primary system pressure. This is reasonable, because the break flow rate should be determined by the pressure difference between primary system and the boiler and the pressure in the boiler almost kept a constant during this case calculation. There are two flow rate spikes on the curve, the maximum is about 1.95 kg/s, occurring at 1.078×10^5 s; another is 1.42 kg/s, occurring at 1.115×10^5 s. After the lower head penetration failure, the primary system pressure decreased and then the break flow rate decreased to zero at once.

Figure 3.3.25 shows the accumulators deliveries. Surry has three accumulators, each of them has the initial water volume of 29.385 m^3. Before the core uncovery, the accumulators had delivered 29.385 m^3 during 5.86×10^4 s to 6.64×10^4 s in the first calculation stage. MELCOR predicted another accumulators injection at 1.1486×10^5 s (247.73 min) and 1 minute later, the accumulators inventory were exhausted after the remaining of 58.77 m^3 was delivered.

(7) Hot Leg and Surge Line Pipe Temperature

Figures 3.3.26 and **3.3.27** give the pipes temperatures of hot legs in AB and C loops, respectively. **Figure 3.3.28** gives the temperature of surge line. As indicated in these figures, all the temperatures were not higher than the failure temperature (1273 K). That means that the natural circulation was modeled while the superheated vapor could not heat the hot legs and surge line up to their failure temperatures. However, it can not be concluded that the pipe temperature would never exceed the failure temperature because the present calculation was stopped at 1.500×10^5 s due to the limit of calculation time.

(8) Hydrogen Production and Deflagration

Figure 3.3.29 presents the hydrogen productions in the core and cavity. As indicated in the figure, the hydrogen production first occurred at 1.052×10^5 s when the oxidation (the reaction between zircaloy and water or vapor) began. With the progression of oxidizing, the hydrogen production increased rapidly to about 325 kg at about 1.13×10^5 s after the core support plate had failed in radial rings 1 and 2. When the lower head penetration failed and the core debris ejected into the cavity, the hydrogen production began to occur in the cavity. In cavity, the hydrogen was produced from the oxidation of metals by H_2O and another product carbon monoxide (CO) was produced from the reaction between metals and CO_2 (CO_2 was from concrete decomposition). At the time of 1.387×10^5 s, the penetration in the first radial ring failed and caused a little production increase of H_2 in core and a rapid increase rate in the reactor cavity. By the end of this calculation, the hydrogen production was 535 kg (335 kg in core and 200 kg in cavity). At 1.386×10^5 s, when the concentrations of H_2 and / or CO reached a critical value, the first deflagration occurred in the cavity and would be followed by other occurrences whenever the criterion was satisfied.

(9) Radionuclide Releases

As the default, MELCOR considers 15 material classes, however, in this present calculation, cesium class was combined with iodine class, that is, the 16th class named by CsI was added. **Table 3.3.2** gives the radionuclide fractional distributions in the primary, containment, environment, and steam generator and gives the total released masses at the end of the MELCOR analysis, 1.5×10^5 s. Though the containment was not predicted to fail, releases to the environment could occur through the fault steam generator power operated relief valve. **Figures 3.3.30** through **3.3.42** show the radionuclides masses released from the fuel in the in- and ex-vessel portions during the accident.

The gap release began to occur at the time of 1.056×10^5 s when the cladding in radial ring 1 failed. Significant radionuclide releases from the fuel occurred at the onset of core melt, about

1.068×10^5 s (113.3 min) followed by the release from molten debris at the reactor cavity. Transportation to the containment for the more volatile radionuclide classes was rapid, while the less volatile classes showed significant release from the fuel after it had relocated to the cavity, especially for tetravalents (Ce), almost had no in-vessel release. For noble gases (Xe) and alkali metals (Cs) releases to the containment were mostly finished by 1.148×10^5 s (246.10), as soon as the lower head penetration in the second radial ring failed, and all finished after the penetration in the first ring failed. For platinoids (Ru), the release was finished at the first penetration failure. However, for chalcogens (Te), uranium (U) and main group elements (Cd, Sn), the releases had not completed even after the end of calculation.

Table 3.3.2 shows that almost all of the Class of Xenon and Cesium (if ~ 10 kg Cesium in CsI included) volatiles were released from the fuel in this calculation. **Figures 3.3.28** and **3.3.29** show that about 90 % of those releases occurred at in-vessel, with the remaining 10 % released at ex-vessel in the cavity. It is noted that **Fig. 3.3.31** shows very little release for Class 4 (I) and no release in the cavity. In this calculation, iodine was assumed to be combined with cesium into CsI as soon as it released from fuel, this is also the reason why cesium released totally only 1.25×10^2 kg, while the total production of cesium in the core was 1.36×10^2 kg. Additionally, VANESA, which is used to calculate the ex-vessel release within MELCOR, considers iodine to be released as CsI, so no iodine release occurred in cavity. Based upon physical insight, the Class 4 (I) should assemble closely Xe and Cs results.

From **Fig. 3.3.36** and **Figs. 3.3.39 ~ 3.3.41**, a very strange phenomenon is observed, which is, at about 1.49×10^5 s, abrupt releases for these classes (Mo, U, Cd and Sn) occurred. Since no enough messages were given by present MELCOR prediction, it is difficult to explain what had happened at that time. Maybe VENESA predicted a large vaporization here.

The release behavior predicted by MELCOR in this calculation can be grouped into several subdivisions. For Class 1 (Xe), Class 2 (Cs) and Class 16 (CsI, according to the masses released for Cs and I), almost all of initial radionuclide inventories were released, about 90 % / 10 % in-vessel and ex-vessel. The next major release fractions were of Class 5 (Te), Class 7 (Mo), Class 11 (Cd) and Class 12 (Sn) which were predicted more than 98 %. Following them, 52 % of Class 3 (Ba), 6.4 % of Class 8 (Ce) and 1.6 % of Class 6 (Ru) were predicted. Finally, only very little Class 9 (La) and Class 10 (U) were released in this calculation and the fractions were about 0.21 % and 0.13 % respectively.

The release pattern also varied depending on the RN class. Almost all of Ru release occurred in-vessel while nothing of Cs was released from in-vessel portion. For Xe, Cs and I (indicated by CsI), about 90 % and 10 % releases occurred in-vessel and ex-vessel, respectively. For Ba, Cd and Sn, about 70 % of releases were predicted at in-vessel. The in-vessel releases of other classes were

about 58% for U, 32 % for Te, 33 % for La and 22 % for Mo.

The released radionuclide distributions could be also grouped into a few subdivisions. The most important contributor to the environment was noble gases (Class 1), while others contributed a little. For CsI, more than 70% of the release retained in the primary system instead of release to the environment. It seems that many kind of radionuclides were deposited a lot at the primary system, such as CsI, Ru (93 %), Cs (73 %), CsI (72 %), Cd (62 %), Sn (62 %), Ba (57 %) and U (55 %). On the other hand, most of Xe and other RN class were distributed into the containment. The largest fraction at containment was from Ce (98 %), followed by Mo (77 %), Te (67 %), La (65 %) and U (42 %). For steam generator, 10% of CsI was released to it. Other relative large fractions were from Cs (8.8 %), Mo (7.6 %), Cd (4.2 %), Ba (3.7 %) and Sn (3.5 %).

The total mass of fission products released from the fuel is shown in **Fig. 3.3.43**. Except for the abrupt release in cavity at 1.49×10^5 s, it can be seen that most of the release occurred during core degradation with a little during cavity process. But at 1.49×10^5 s, that abrupt release contributed a lot to the vapor fraction and to the total release accordingly. Including the large vaporization, about 50.7 % of the fission products released were found in atmosphere of control volumes, in which 63.2 % was aerosol and 36.8 % was vapor. Remaining a little less than 50 % was deposited on heat structures.

3.4 Comparisons of Analytical Results between Once-through and Hot Leg Countercurrent Natural Circulation Models

In this SGTR analysis, the calculations after 100,000 s were performed using both the once-through and hot leg countercurrent natural-circulation models parallelly. The essential results from the two models were mostly the same each other. The effects of reactor coolant system natural circulation on the response of the Surry nuclear power plant during a station blackout transient were investigated with the SCDAP/RELAP5 code in NUREG/CR-5214[4]. Moreover, the effect of hot leg countercurrent natural circulation on the potential for HPME in Surry NPP was evaluated through the comparison with that of the once-through flow in NUREG/CR-5949[11], also using SCDAP/RELAP5. Both conclusions indicate that the natural circulation provides an effective mechanism for the transfer of core decay heat to the ex-vessel piping and this transfer will accordingly induce the accelerating increase in the temperatures of hot leg, surge line and steam generator tubes. However, in the present SGTR calculations, significant differences were not found in the results between the two models. The probable explanations are due to the characteristic of SGTR and the processing in MELCOR code. Followings are the comparisons between the results from the two models as well as some discussions.

From **Tables 3.2.1** and **3.3.1**, it can be seen that the progression of core damage predicted using the hot leg countercurrent natural circulation model was mostly the same as that using the once-through model. Generally, the natural circulation can be benefit to the mitigation of the core heat-up, but for SGTR, because PORVs had been stuck open and the secondary side of the fault steam generator had developed a direct connection to the environment, and this would result a continuous flow from the primary side (core) to the secondary side through the tube break. Accordingly the development of the natural circulation flow in the faulted loop would be impeded, it can be demonstrated from **Fig. 3.3.18**. The natural circulation did not exist until the hot legs were voided and superheated vapor was available to provide the required driving potential.

The difference in enthalpy transport rate between the flow from upper plenum to hot leg and that from hot leg to upper plenum in the intact loop can be observed from the calculation using the natural circulation model as shown in **Fig. 3.4.1**. It can be seen that these two enthalpy transport rates were almost the same, which meant there was no or very little heat removal through the intact loop even if the natural circulation was taken into account. Therefore, almost of all the heat removal is considered to have been attributed to the break flow in the faulted loop.

Although the predicted accident progression between the two models was almost the same, some small differences were found. In the case of the natural circulation model, the core support plate failure firstly occurred in radial ring 2, while it firstly occurred in radial ring 3 if using the once-through model. This is because the melt mass and energy relocated to the support plate in each ring was slightly different between the two models due to the difference in flow pattern in the core.

Another difference was found in the behavior of molten materials at the lower core level. In the case with the natural circulation model, the lower head penetration in the second radial ring was firstly failed at 1.127×10^5 s. According to **Fig. 3.3.16** based on the natural circulation model, it can be seen that just after the relocation of molten materials from higher level to axial level 1, most of all the molten materials was moved to the lower plenum and ejected into the reactor cavity due to the second penetration failure. This is because large amount of molten materials was moved to the axial level 1 during a short time and therefore the support plate was heated rapidly and failed. On the other hand, in the case with the once-through model, the molten materials was gradually relocated into the axial level 1 as shown in **Fig. 3.2.16** and all the relocated materials could stay on that level for some time up to the core support failure. After that, the materials were moved to the lower plenum and ejected to the reactor cavity during a very short time. It is considered that this difference in the behavior of molten materials at the lower core level between the two models was not caused only by the difference in the primary system modeling but also by some uncertainties in the relocation model.

The results from calculation using the once-through model showed that almost of all the axial levels in each radial ring was collapsed at the same time, whereas the collapsing occurred in the order of the level of core cell from higher to lower in the case with the hot leg countercurrent natural circulation model. This can be attributed to be the difference in coolant flow pattern in the core between the cases with and without the natural circulation at hot leg.

The total mass of material remained in core was quite different between the two calculations. In the calculation using the once-through model, 60 % of steel in core was moved into the reactor cavity, however, in the case of the natural circulation model, almost of all the steel in core was ejected into the reactor cavity. That is because the lower head penetrations of radial rings 1 and 2 were failed in the natural circulation model while only the radial ring 2 penetration was failed in the case with the once-through model.

The differences in "source term" were investigated between the two models. The release of Cs and Iodine was quite different between the two calculations because in the case with the natural circulation model, chemical form of CsI was treated while Cs and Iodine were dealt with separately in the case with the once-through model. For the total release from fuel, comparing **Table 3.2.2** with **Table 3.3.2**, it can be found that the most significant difference existed in the Class 7 (Mo) and Class 8 (Ce). The results from both the models on Mo are very close to each other except for the abrupt release at 1.49×10^5 s in the case with the natural circulation model. On the other hand, for the release of Ce, a very large release from the reactor cavity was predicted just after the first lower head penetration failure in the case with the natural circulation model. This is because the temperature of debris in the reactor cavity increased more due to steel oxidation in the case with the natural circulation model than the case with the once-through model. For the radionuclides distributions, overall tendencies were almost the same between the two model calculations.

4. CONCLUSIONS

Analyses of Steam Generator Tube Rupture (SGTR) of Surry nuclear power plant with one SG safety valve stuck open as a severe accident were performed using the MELCOR1.8.4 code. The once-through primary system model was used up to 1.0×10^5 s and after that, both the hot leg countercurrent natural circulation and once-through models were used to investigate the effect of primary coolant flow pattern on the accident progression .

(1) If the high pressure safety injection could be available during SGTR, the progression of core heat-up would be delayed considerably.

(2) If a steam generator secondary-side Power Operated Relief Valve (PORV) was stuck open, the hot leg countercurrent natural circulation flow would not be developed apparently and could not remove a lot of heat from the degrading core. As a result, it has little effect on the mitigation of the core degradation.

(3) Depending on the progression of core heat-up and degradation, the support plate between the activated core and the lower plenum would firstly fail at different place in radial direction. The process of core melt relocation and collapsing would probably define where is the first place at which support plate failure occurs.

(4) In case of SGTR with one PORV stuck open, although the containment has not failed yet, the radionuclide produced in the core can be also released to the environment through the direct path of the PORV bypassing the containment. Approximately 7 % of cesium iodide (CsI) can be released to the environment directly through the stuck open safety valve.

(5) Overall tendencies predicted by the cases with and without the hot leg countercurrent natural circulation were almost the same. However, the behavior of molten material at lower core level was partly sensitive to the primary system modeling even if the status and process parameters are the same. Moreover, there was a difference in the release fractions of Cs and iodine into environment between the analytical assumption of individual elements and CsI compound.

(6) A full plant calculation with the MELCOR code typically involves 15 to 25 control volumes and 100 to 200 heat structures. However, in the present calculation, many control volumes (totally 36 volumes for the once-through model and 57 ones for the natural circulation model) were used. The fine nodalization significantly decreased the time step less than 10^{-2} s and increased the CPU time as well as numerical instability. Here, only one calculation with the natural circulation model spent 2.56×10^6 s using the SUN Ultra Sparc. This may be a kind of lesson obtained by using the MELCOR code.

ACKNOWLEDGMENT

The authors would like to express their sincere appreciation to Mr. C. Ader of the Office of Nuclear Regulatory Research, USNRC, for providing opportunity to use MELCOR1.8.4 and the Surry input deck for analysis of Steam Generator Tube Rupture sequence.

REFERENCES

[1] R. M. Summers, R. K. Cole, Jr., R. C. Smith, D. S. Stuart, S. L. Thompson, S. A. Hodge, C. R. Hyman and R. L. Sanders, "MELCOR Computer Code Manuals, Primer and User's Guides, Version 1.8.3," NUREG/CR-6119, SAND93-2185 (1994).

[2] USNRC, "Severe Accident Risks: An Assessment for Five U.S. Nuclear Power Plants," NUREG-1150 (1990).

[3] W. A. Stewart, A. T. Pieczynski and V. Srinivas, "Experiments on Natural Circulation Flows in Steam Generators During Severe Accidents," Proc. of the International ANS/ENS Topical Meeting on Thermal Reactor Safety, San Diego, CA, February 2-6, 1986.

[4] P. D. Bayless, "Analysis of Natural Circulation During a Surry Station Blackout Using SCDAP/RELAP5," NUREG/CR-5214, EGG-2547, 1988.

[5] D. E. Bennett, "SANDIA-ORIGEN User's Manual," NUREG/CR-0987, SAND79-0299, Sandia National Laboratories, Albuquerque, NM (October 1979).

[6] Ostmeyer, R. M., "An Approach Treating Radionuclide Decay Heating for Use in the MELCOR Code System," SAND84-1404, NUREG/CR-4169, May 1985.

[7] Kuhlman, M. R., D. J. Lehmicke and R. O. Meyer, "CORSOR User's Manual," BMI-2122, NUREG/CR-4173, March 1985.

[8] M. Ramamurthi and M. R. Kuhlman, "Final Report on Refinement of CORSOR - An Empirical In-Vessel Fission Product Release Model," Battelle Memorial Institute, October 31, 1990.

[9] Powers, D. A., J. E. Brockmann and A. W. Shiver (1985), "VANESA: A Mechanistic Model of Radionuclide Release and Aerosol Generation During Core Debris Interactions with Concrete," SAND85-1370, NUREG/CR-4308, September 1985 Draft.

[10] L. Kmetyk/SNL and L. Smith/GCI, "Summary of MELCOR 1.8.2 Calculations for Three LOCA Sequences (AG, S_2D, and S_3D) at the Surry Plant," NUREG/CR-6107, SAND93-2042, March 1994.

[11] D. L. Knudson and C. A. Dobbe, "Assessment of the Potential for High-Pressure Melt Ejection Resulting from a Surry Station Blackout Transient," NUREG/CR-5949, EGG-2689, Idaho National Engineering Laboratory, November 1993.

Table 3.1.1 Sequence of Events for Once-through Model

Events	Time (s)**
Double guillotine break in one SG U-tube	0.0
Reactor scram on low pressurizer pressure	3.534×10^2 (5.890)
Main feed terminates - All loops	3.535×10^2 (5.892)
Reactor coolant pump trip - All loops	3.536×10^2 (5.893)
AFW initialization in intact loops	3.585×10^2 (5.975)
AFW initialization in faulted loops	3.586×10^2 (5.977)
HPSI signal on low pressurizer pressure	3.626×10^2 (6.043)
High Pressure Safety Injection operation	3.757×10^2 (6.262)
Faulted loop - SG C PORV first* open	3.567×10^3 (59.45)
Faulted loop - SG C PORV stuck open	7.467×10^3 (124.5)
Refueling Water Storage Tank (RWST) depleted by HPSI	5.827×10^4 (971.2)
Accumulators in all loops first* operation	5.859×10^4 (976.5)
First accumulator delivery in all loops stopped	6.642×10^4 (1107)
Initial Core Uncovery Beginning	$\sim 7.0 \times 10^4$ (1167)
Core still intact at the end of this calculation	1.000×10^5 (1667)

*: 'first' means that the status of the described system or component operation would be then 'off', 'on', ..., according to the set point for it.

**: The data in the parenthese are the timings in minutes.

Table 3.2.1 Sequence of Events Predicted by Once-through Model after 100,000s

Events	Time (s)*
Cladding Oxidation Beginning	~ 1.065 x 10^5 (1775.0)
Gap Release in Radial Ring 1	1.06775 x 10^5 (1779.6)
Gap Release in Radial Ring 2	1.07055 x 10^5 (1784.3)
Gap Release in Radial Ring 3	1.07902 x 10^5 (1798.4)
First Relocation Occurred	~ 1.081 x 10^5 (1801.7)
Core Uncovery Completed	~ 1.116 x 10^5 (1860.0)
Core Support Plate Failure in Radial Ring 3	1.13968 x 10^5 (1899.5)
Core Support Plate Failure in Radial Ring 2	1.14204 x 10^5 (1903.4)
Core Support Plate Failure in Radial Ring 1	1.14352 x 10^5 (1905.9)
Lower Head Penetration in Radial Ring 2 Failure	1.14880 x 10^5 (1914.7)
Loop AB and C Accumulators Operation	1.15036 x 10^5 (1917.3)
Loop AB and C Accumulators Inventory Exhausted	1.15083 x 10^5 (1918.1)
Deflagration First Started in Cavity	1.26994 x 10^5 (2116.57)
First Deflagration Ended in Cavity	1.26997 x 10^5 (2116.62)
End of Calculation	1.50000 x 10^5 (2500.0)

* The data in the parenthese are the timings in minutes.

Table 3.2.2 Radionuclide Releases Predicted by Once-through Model

RN Material Class and Representive Element	Primary Fraction (%)	Containment Fraction (%)	SG Fraction (%)	Environment Fraction (%)	Total Released (kg)	Initial Inventory[10] (kg)
Noble Gases, Xe	0.0114	9.71	0.00374	90.22	2.4464×10^{2}	2.4483×10^{2}
Alkali Metals, Cs	55.80	8.16	20.36	15.15	1.3626×10^{2}	1.3645×10^{2}
Alkaline Earths, Ba	77.19	6.64	9.02	6.81	4.9767×10^{1}	1.0740×10^{2}
Halogens, I	0.0123	9.47	0.00411	93.10	1.0503×10^{1}	1.0545×10^{1}
Chalcogens, Te	33.93	49.41	9.84	6.32	1.6441×10^{1}	2.1481×10^{1}
Platinoides, Ru	70.97	18.13	5.88	4.72	3.7603	1.5110×10^{2}
Transition Metals, Mo	74.97	14.76	5.42	4.59	4.4915×10^{1}	1.7819×10^{2}
Tetravalents, Ce	43.92	48.25	3.86	3.10	2.8865×10^{-1}	3.1440×10^{2}
Trivalents, La	67.95	20.57	6.34	4.87	5.8827×10^{-1}	2.9170×10^{2}
Uranium, U	67.32	21.73	5.97	4.61	1.2337×10^{2}	6.1025×10^{4}
More Volatile Main Group Metals, Cd	81.55	4.29	7.90	5.90	5.5715×10^{-1}	7.1350×10^{-1}
Less Volatile Main Group Metals, Sn	83.04	4.46	6.53	5.49	3.1613	4.0521

Table 3.3.1 Sequence of Events Predicted by Hot Leg Natural Circulation Model after 100,000s

Events	Time (s)*
Cladding Oxidation Beginning	~ 1.052 x 10^5 (1753.3)
Gap Release in Radial Ring 1	1.05631 x 10^5 (1760.5)
Gap Release in Radial Ring 2	1.05906 x 10^5 (1765.1)
Gap Release in Radial Ring 3	1.06741 x 10^5 (1779.0)
First Relocation occured	~ 1.068 x 10^5 (1780.0)
Core Uncovery Completed	~ 1.102 x 10^5 (1836.7)
Core Support Plate Failure in Radial Ring 2	1.12667 x 10^5 (1877.8)
Core Support Plate Failure in Radial Ring 1	1.13022 x 10^5 (1883.7)
Lower Head Penetration in Radial Ring 2 Failure	1.14766 x 10^5 (1912.8)
Loop AB and C Accumulators Injection	1.14864 x 10^5 (1914.4)
Loop AB and C Accumulators Inventory Exhausted	1.14920 x 10^5 (1915.3)
Core Support Plate Failure in Radial Ring 3	1.14991 x 10^5 (1916.5)
Deflagration First Started in Cavity	1.38634 x 10^5 (2310.6)
First Deflagration Ended in Cavity	1.38642 x 10^5 (2310.7)
Lower Head Penetration in Radial Ring 1 Failure	1.38714 x 10^5 (2311.9)
End of Calculation	1.50000 x 10^5 (2500.0)

* The data in the parenthese are the timings in minutes.

Table 3.3.2 Radionuclide Releases Predicted by Hot Leg Natural Circulation Model

RN Material Class and Representive Element	Primary Fraction (%)	Containment Fraction (%)	SG Fraction (%)	Environment Fraction (%)	Total Released (kg)	Initial Inventory[10] (kg)
Noble Gases, Xe	0.0362	13.41	0.0216	86.55	2.4423×10^{2}	2.4483×10^{2}
Alkali Metals, Cs	72.98	11.39	8.80	6.40	1.2511×10^{2}	1.3645×10^{2}
Alkaline Earths, Ba	56.95	34.61	3.72	3.91	5.5946×10^{1}	1.0740×10^{2}
Halogens, I	see CsI	see CsI	see CsI	see CsI	1.4755×10^{-9}	1.0545×10^{1}
Chalcogens, Te	26.73	67.35	2.50	2.45	2.1388×10^{1}	2.1481×10^{1}
Platinoides, Ru	92.55	1.21	2.94	3.25	2.4615	1.5110×10^{2}
Transition Metals, Mo	21.04	77.35	7.59	0.813	1.7744×10^{2}	1.7819×10^{2}
Tetravalents, Ce	0.635	97.47	0.0251	0.024	1.9999×10^{1}	3.1440×10^{2}
Trivalents, La	31.24	65.27	1.13	1.20	6.1591×10^{-1}	2.9170×10^{2}
Uranium, U	54.68	41.66	0.164	1.81	8.1835×10^{1}	6.1025×10^{4}
More Volatile Main Group Metals, Cd	62.09	28.97	4.22	4.27	7.0558×10^{-1}	7.1350×10^{-1}
Less Volatile Main Group Metals, Sn	62.21	30.04	3.49	3.76	4.0328	4.0521
Cesium Iodine, CsI	72.09	10.58	10.28	6.67	2.1319×10^{1}	No Data

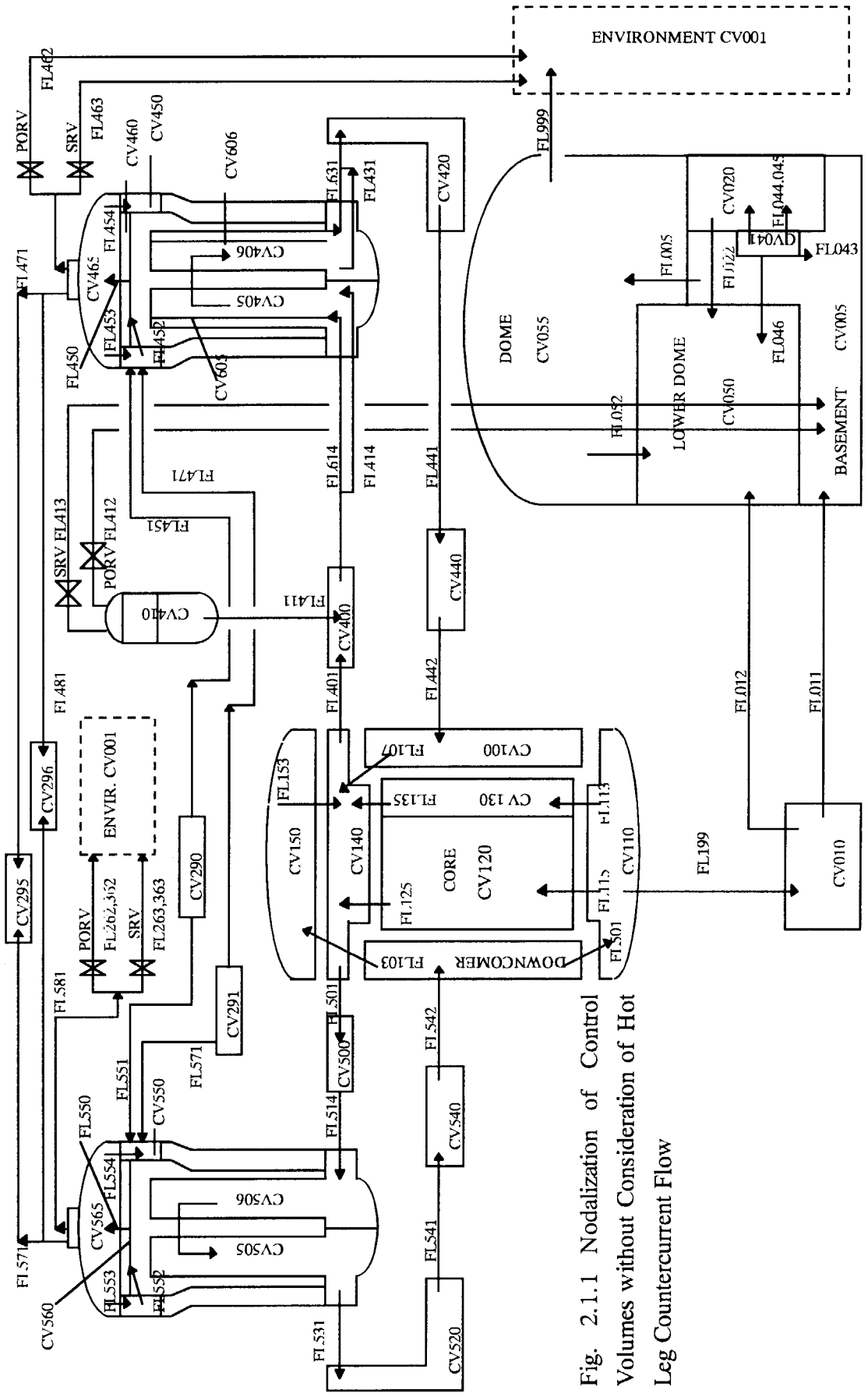

Fig. 2.1.1 Nodalization of Control Volumes without Consideration of Hot Leg Countercurrent Flow

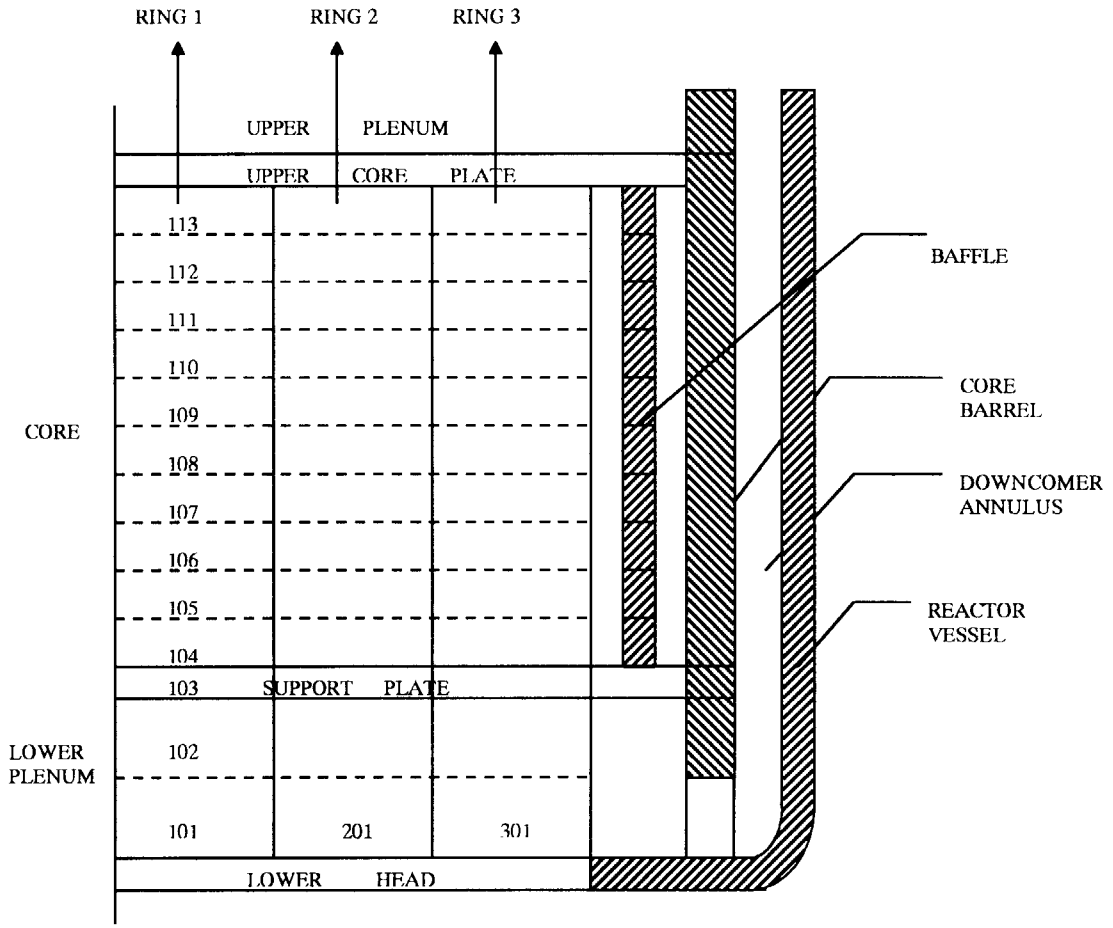

Fig. 2.1.2 Core Nodalization (1)

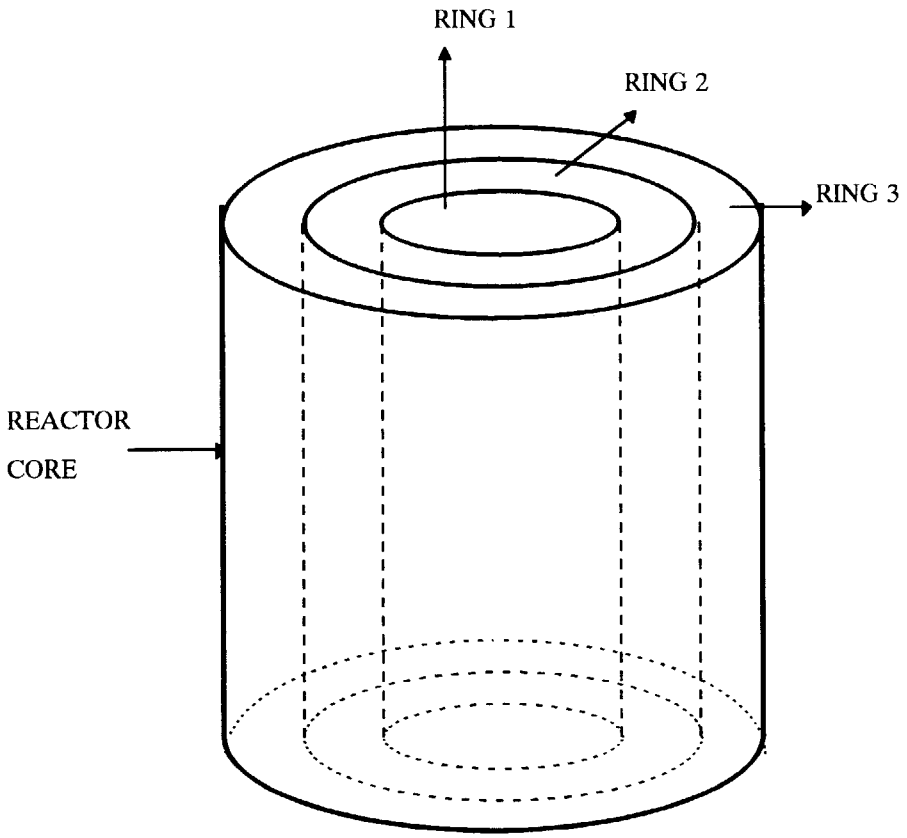

Fig. 2.1.3 Core Nodalization (2)

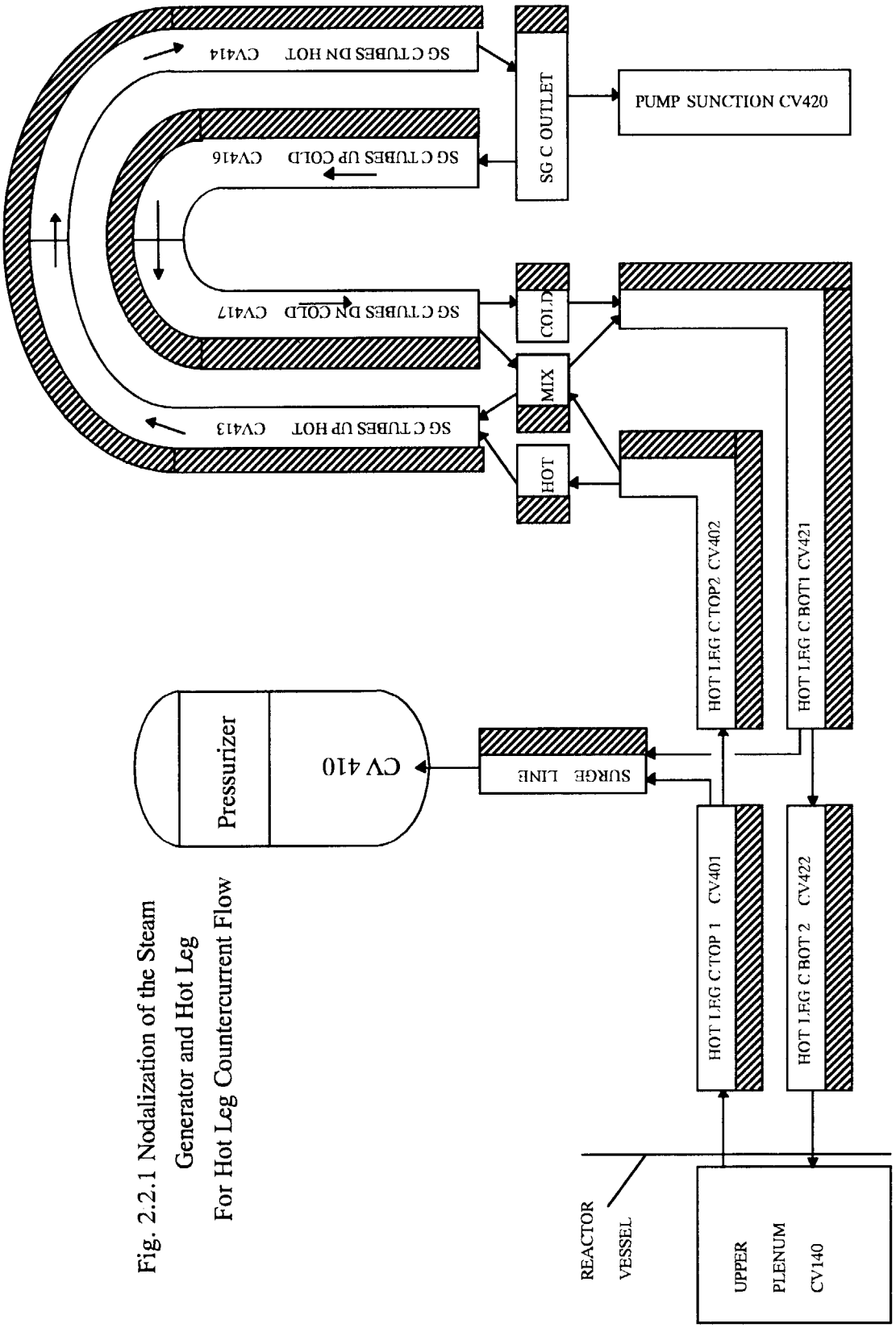

Fig. 2.2.1 Nodalization of the Steam Generator and Hot Leg For Hot Leg Countercurrent Flow

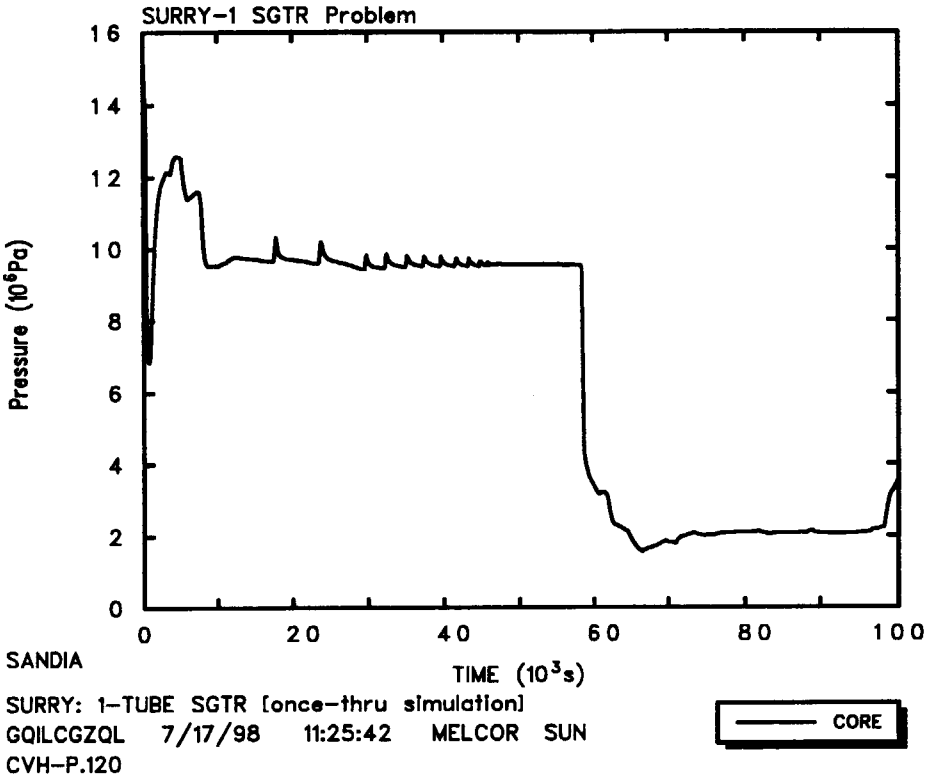

Fig. 3.1.1 Initial Results from Once-through Model -- Primary System Pressure

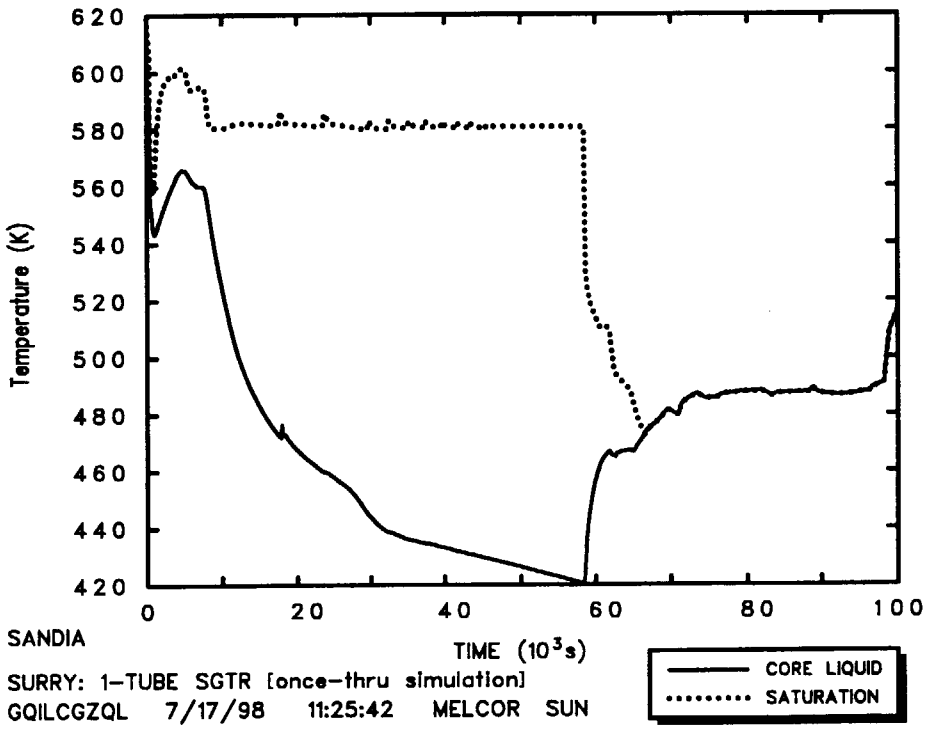

Fig. 3.1.2 Initial Results from Once-through Model -- Liquid and Saturation Temperature in Core

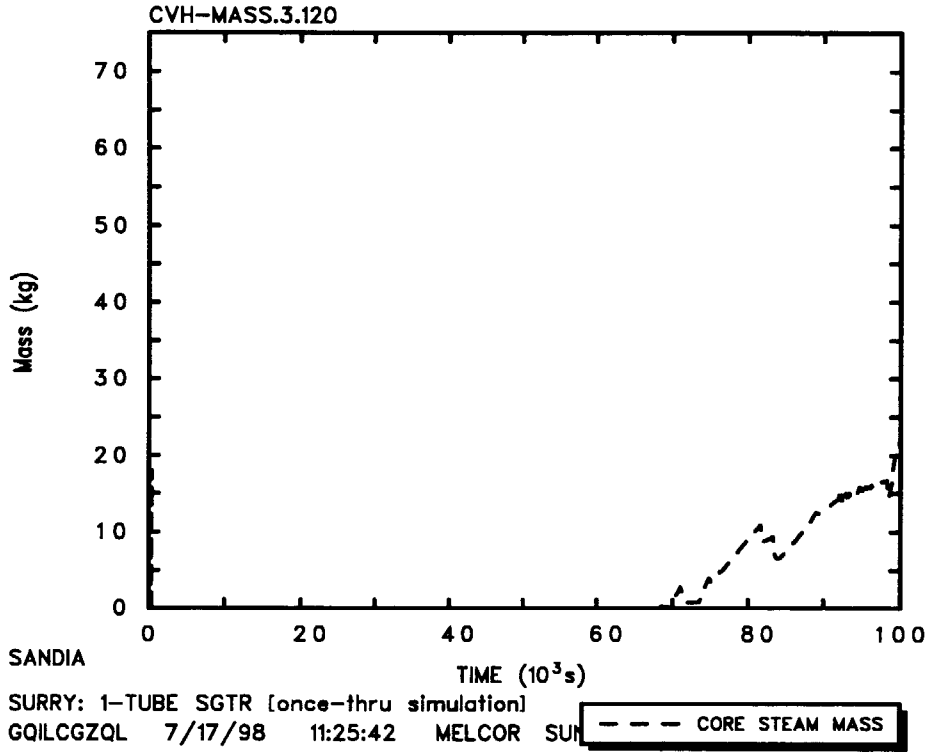

Fig. 3.1.3 Initial Results from Once-through Model -- Steam Mass in Core

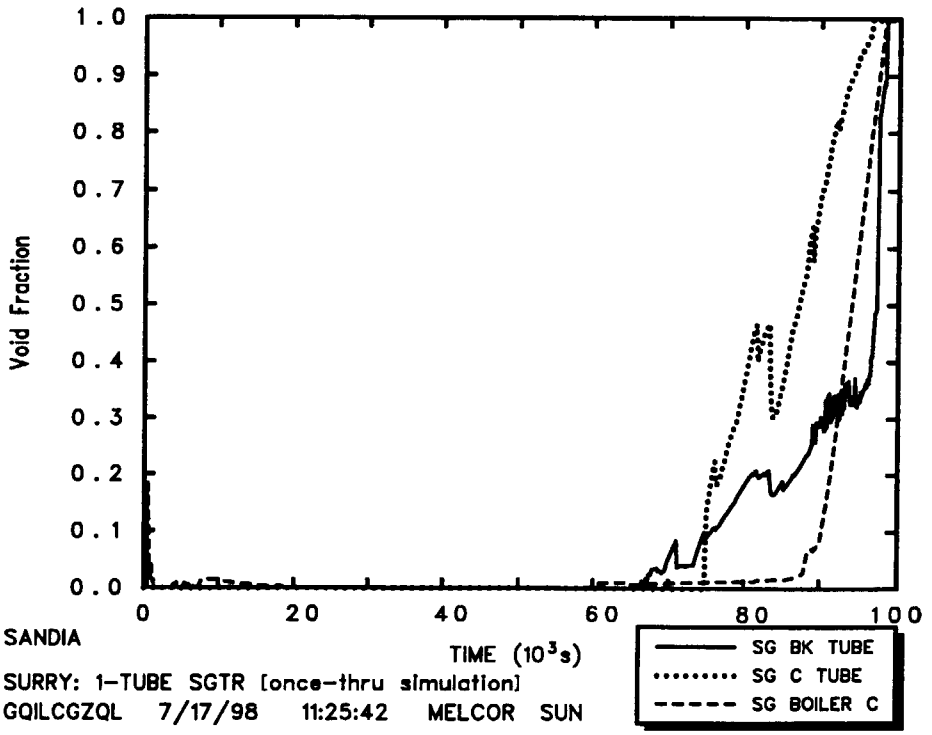

Fig. 3.1.4 Initial Results from Once-through Model -- SG C Void Fraction

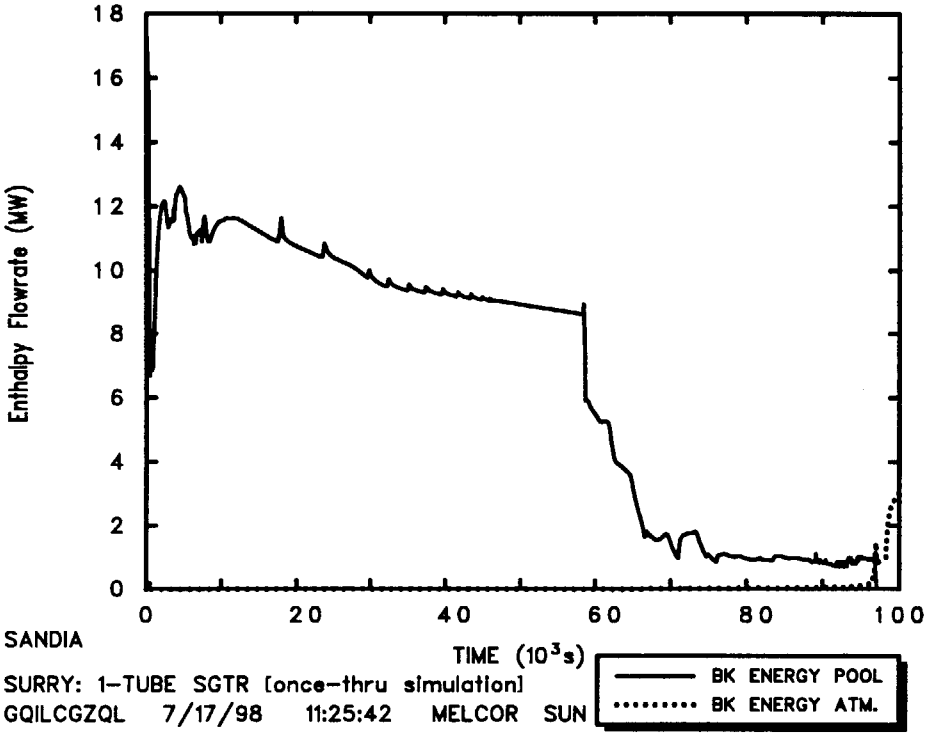

Fig. 3.1.5 Initial Results from Once-through Model -- SG Break Energy Flowrate

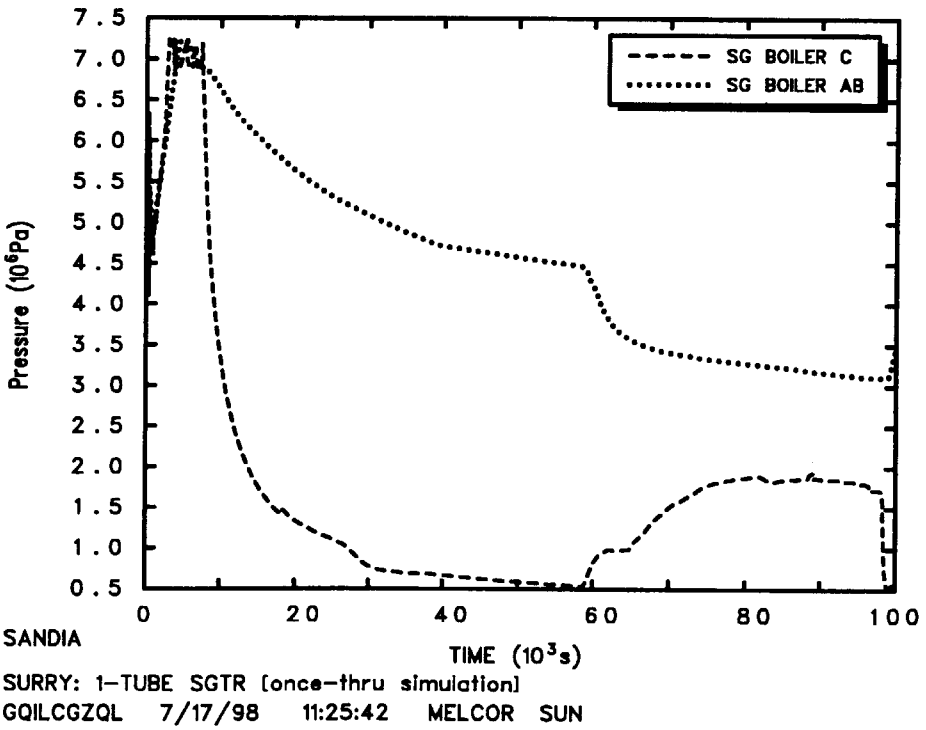

Fig. 3.1.6 Initial Results from Once-through Model -- Secondary System Pressure

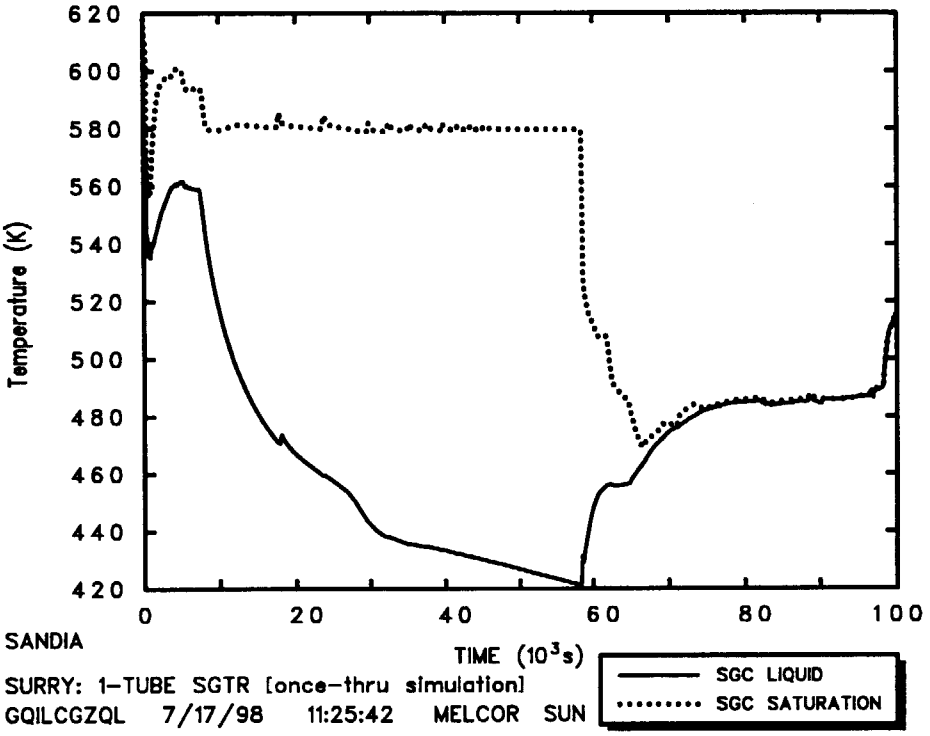

Fig. 3.1.7 Initial Results from Once-through Model -- SG C Liquid Temperature

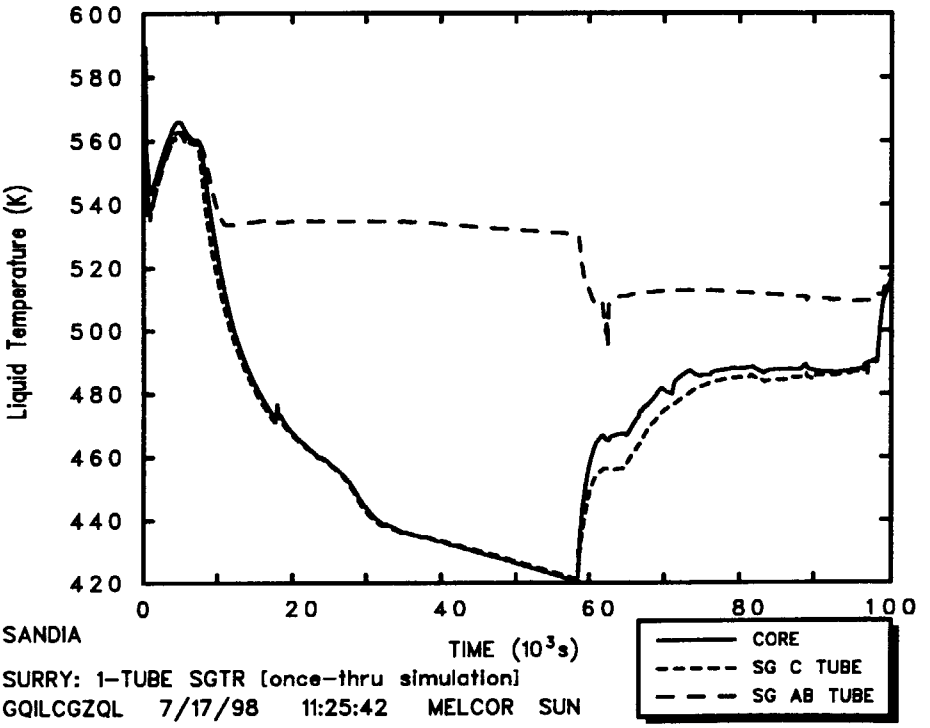

Fig. 3.1.8 Initial Results from Once-through Model -- Liquid Temperature Comparison among Core, SG C and SG AB

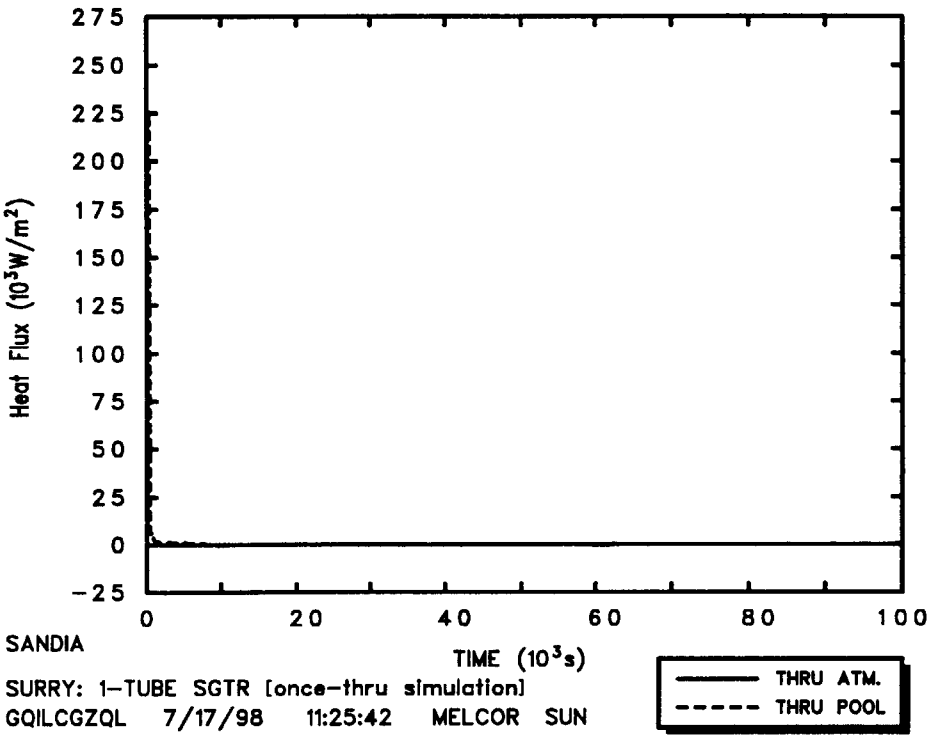

Fig. 3.1.9 Initial Results from Once-through Model -- Heat Flux from SG AB Tube to Boiler

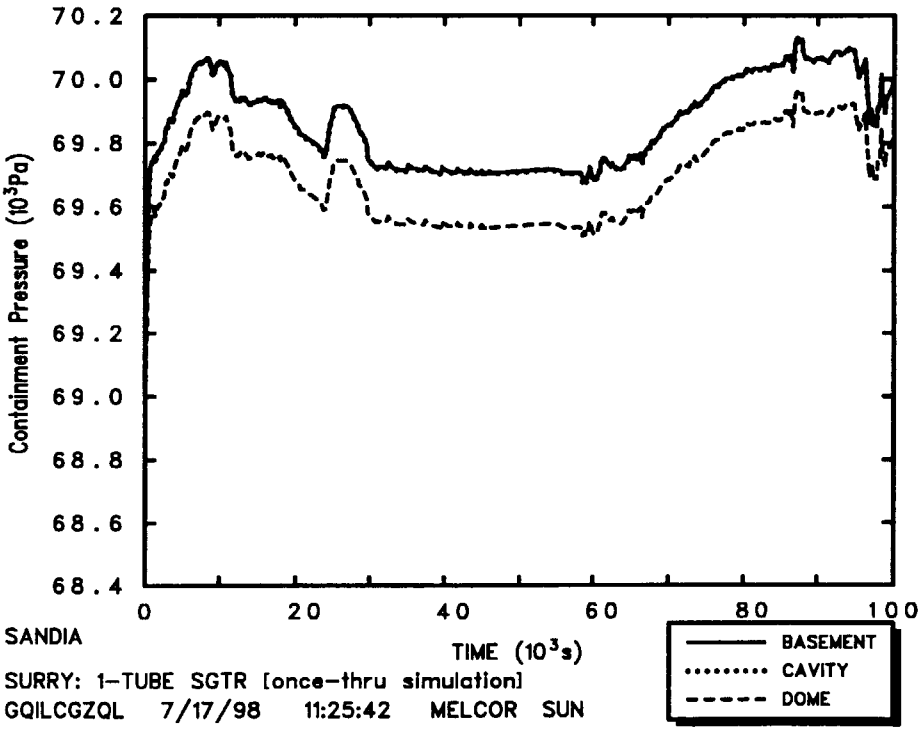

Fig. 3.1.10 Initial Results from Once-through Model -- Containment Pressure

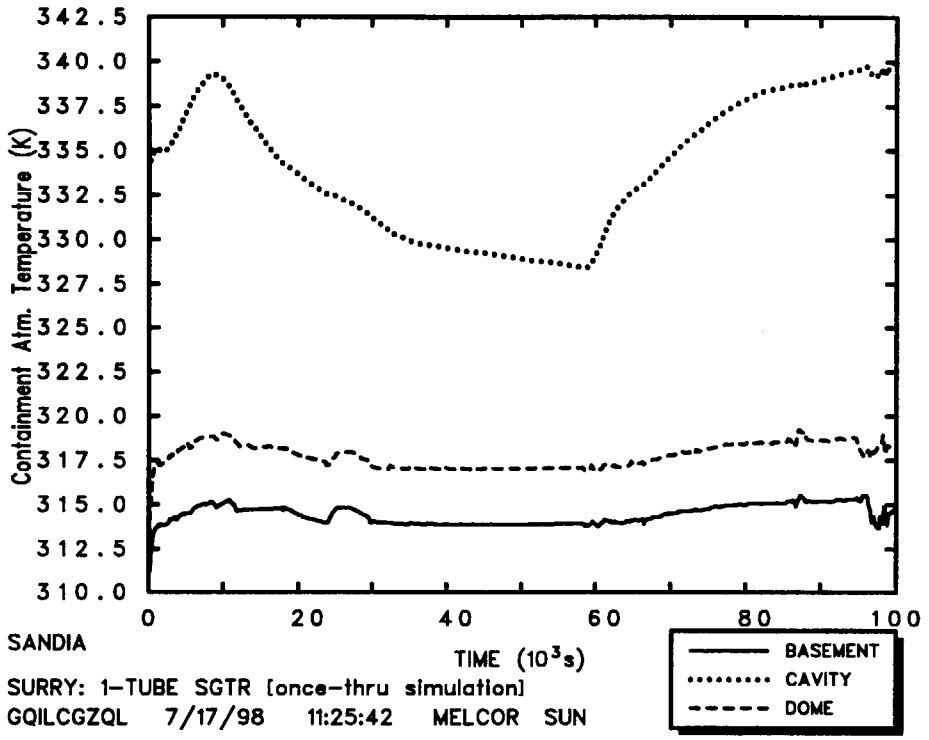

Fig. 3.1.11 Initial Results from Once-through Model -- Containment Atmosphere Temperature

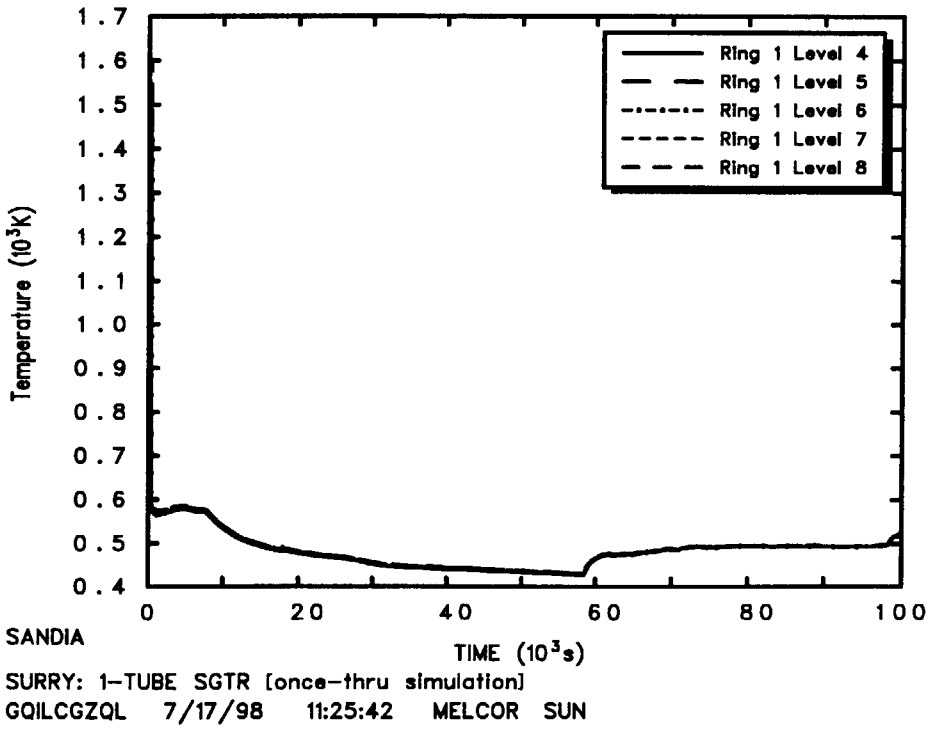

Fig. 3.1.12 Initial Results from Once-through Model -- Fuel Temperatures in Ring 1 Core Cells at Level 4 ~ Level 8

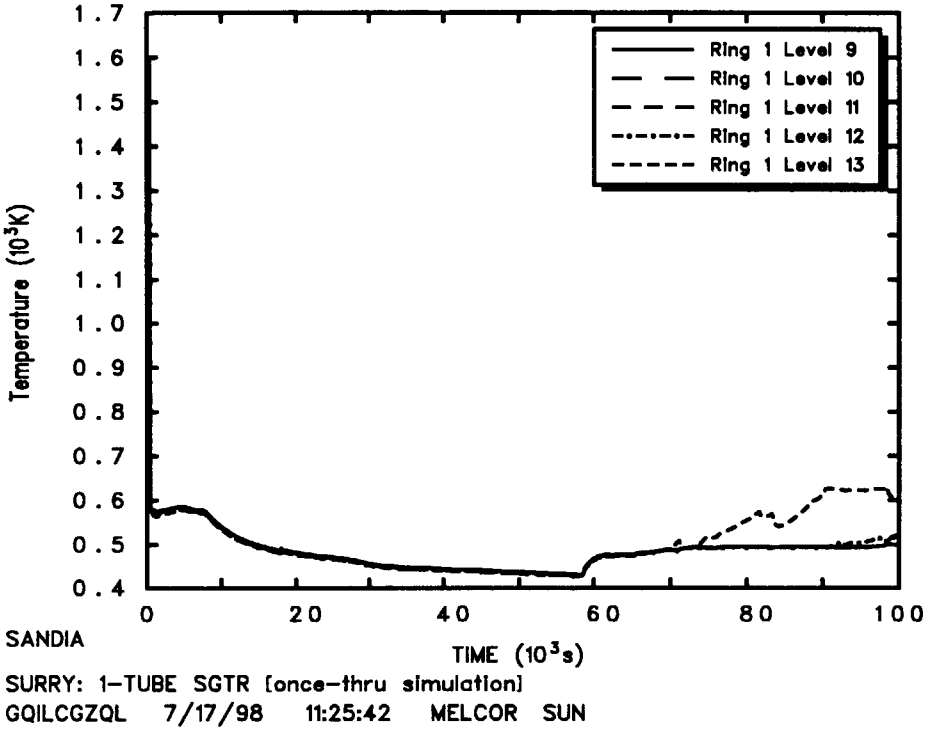

Fig. 3.1.13 Initial Results from Once-through Model --
Fuel Temperatures in Ring 1 Core Cells at Level 9 ~ Level 13

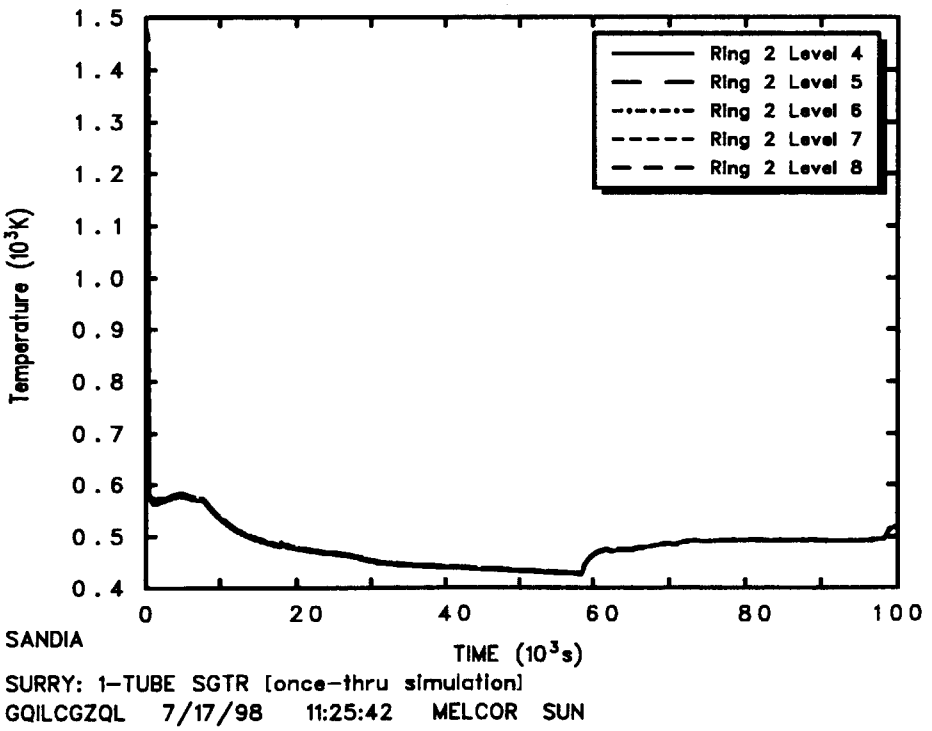

Fig. 3.1.14 Initial Results from Once-through Model --
Fuel Temperatures in Ring 2 Core Cells at Level 4 ~ Level 8

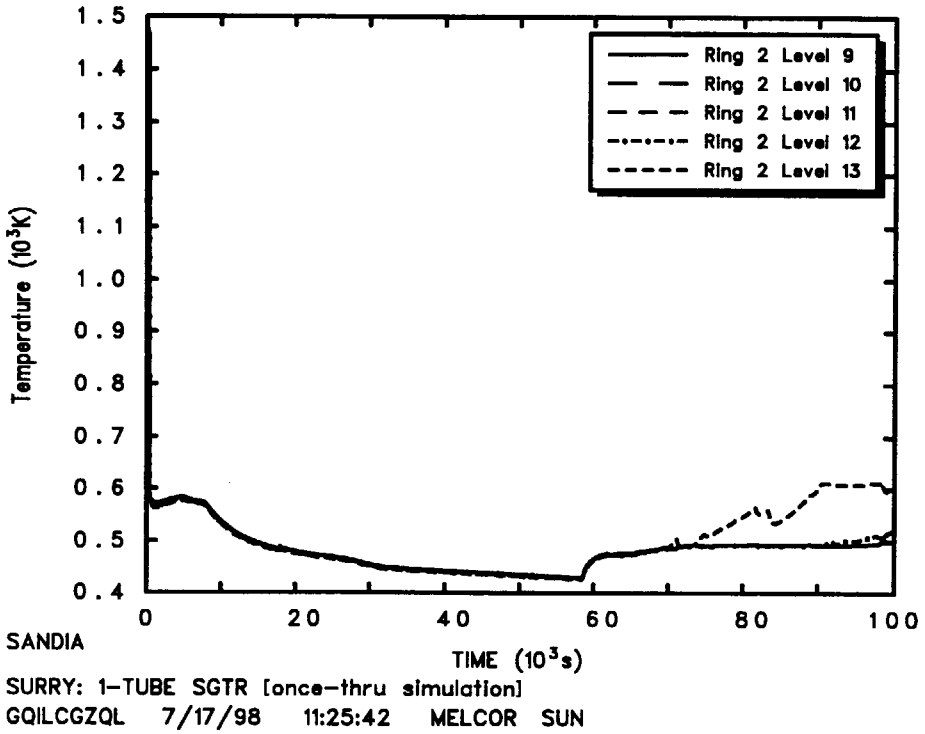

Fig. 3.1.15 Initial Results from Once-through Model --
Fuel Temperatures in Ring 2 Core Cells at Level 9 ~ Level 13

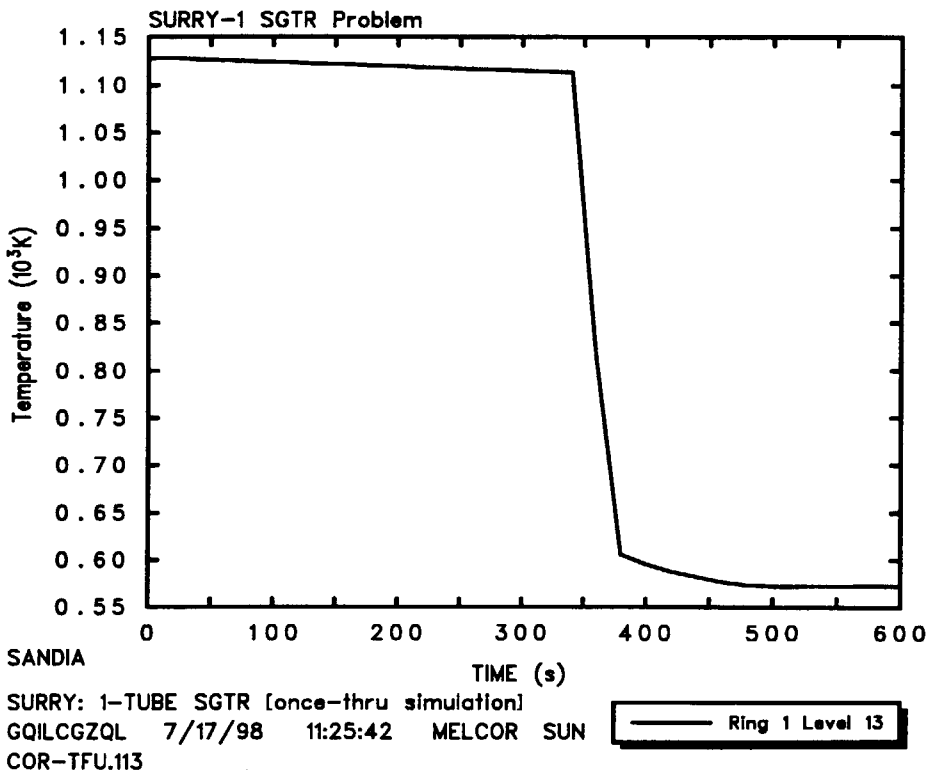

Fig. 3.1.16 Initial Results from Once-through Model --
Fuel Temperatures in Ring 1 & Level 13 Core Cell (Detailed)

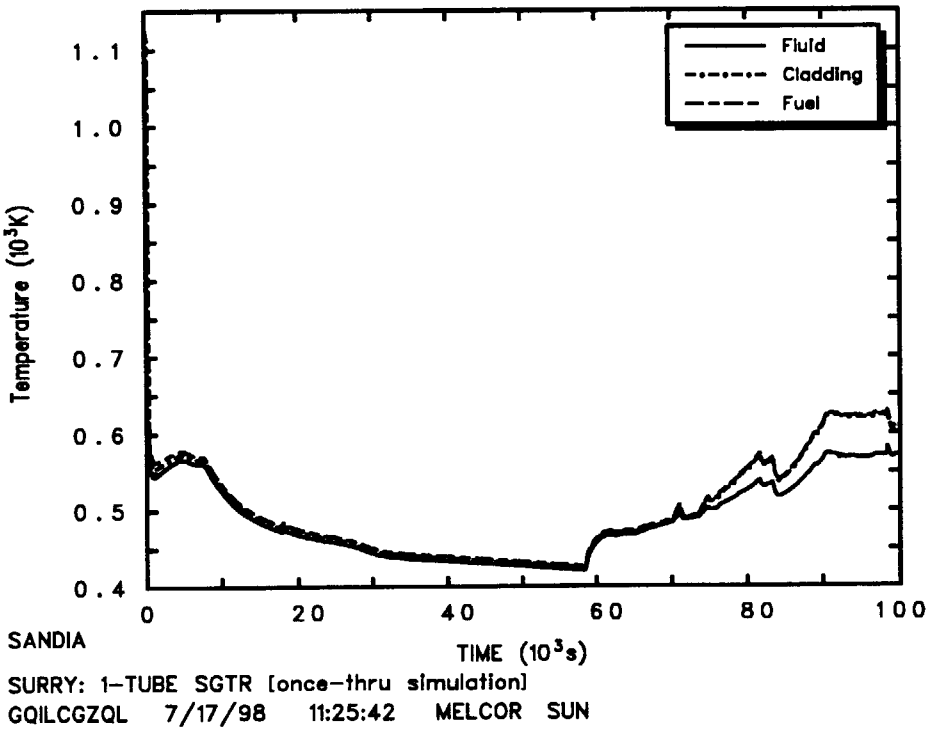

Fig. 3.1.17 Initial Results from Once-through Model -- Temperatures in Ring 1 Level 13 Cell

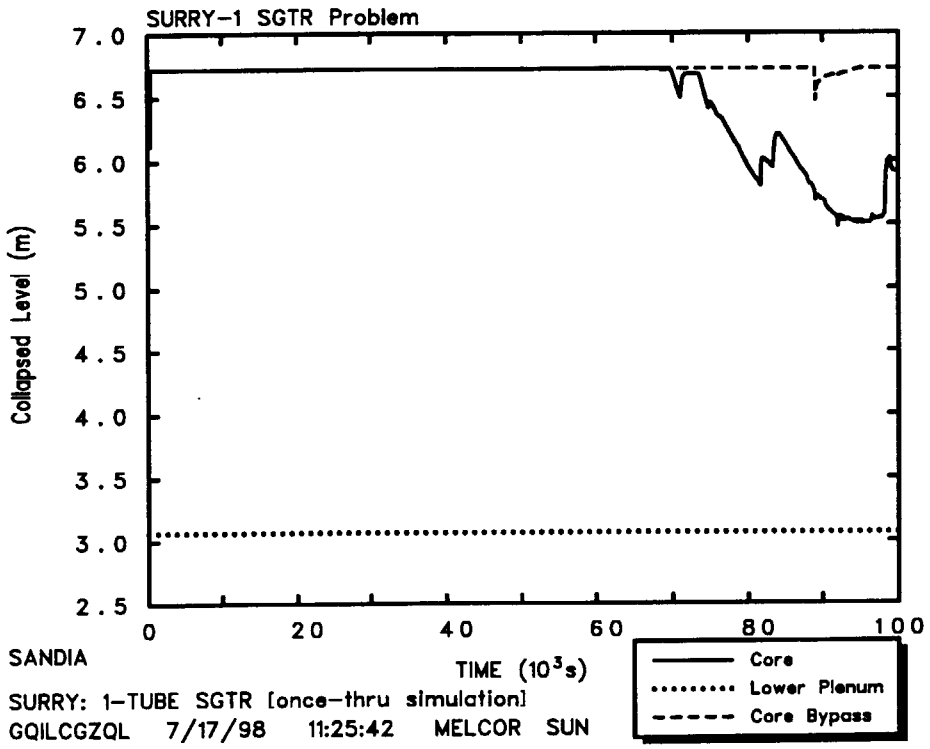

Fig. 3.1.18 Initial Results from Once-through Model -- Collapsed Level of Core, Lower Plenum, and Core Bypass

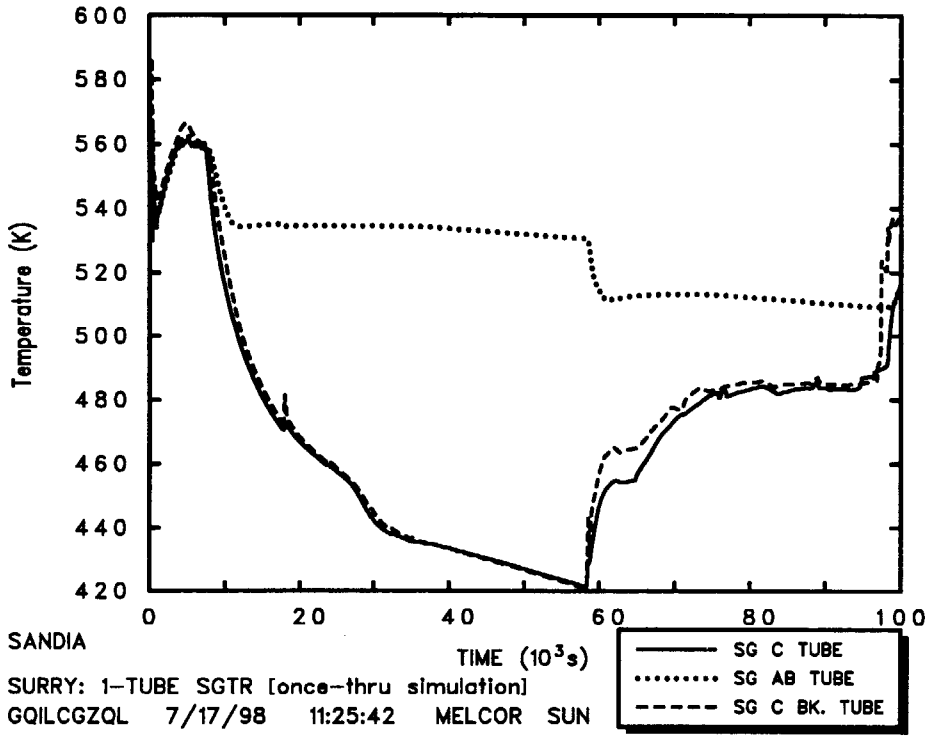

Fig. 3.1.19 Initial Results from Once-through Model -- SG Tube Temperatures

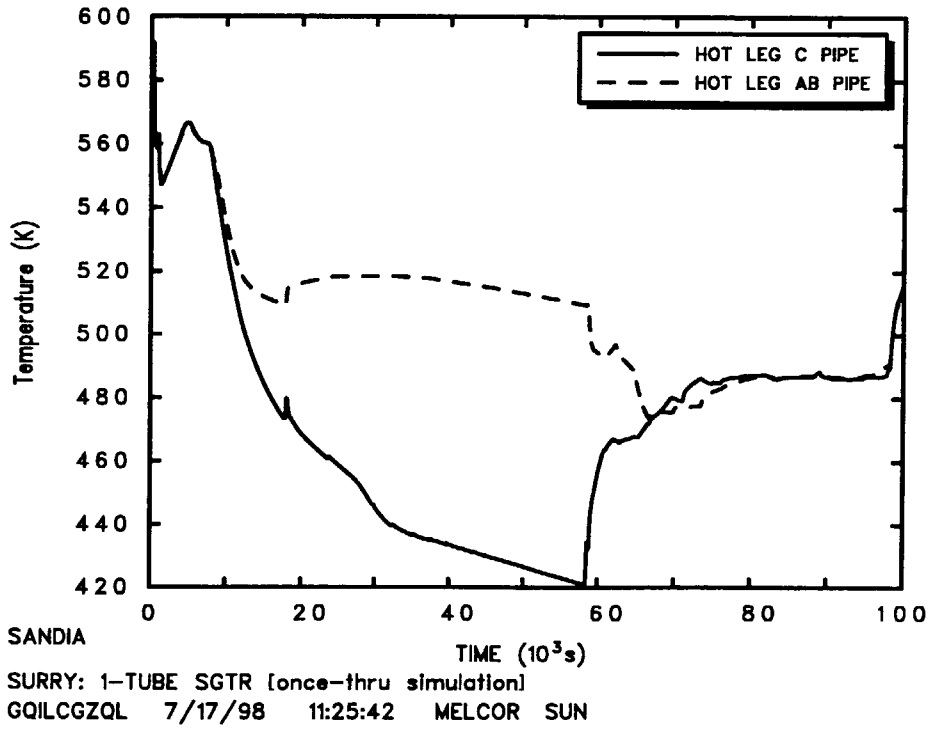

Fig. 3.1.20 Initial Results from Once-through Model -- Hot Leg Pipe Temperatures

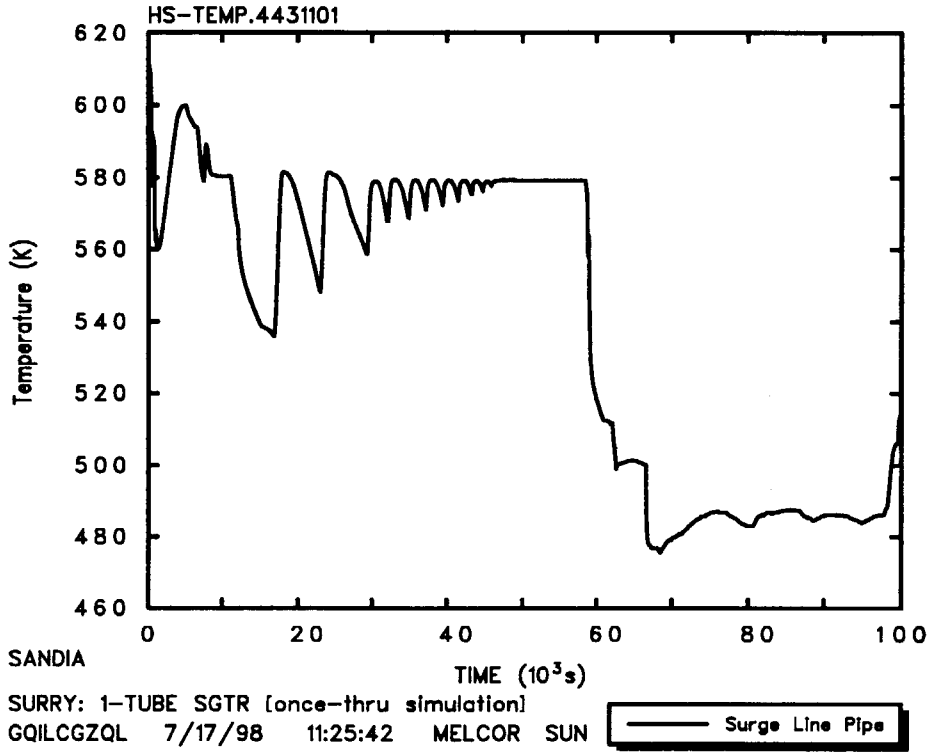

Fig. 3.1.21 Initial Results from Once-through Model -- Surge Line Pipe Temperatures

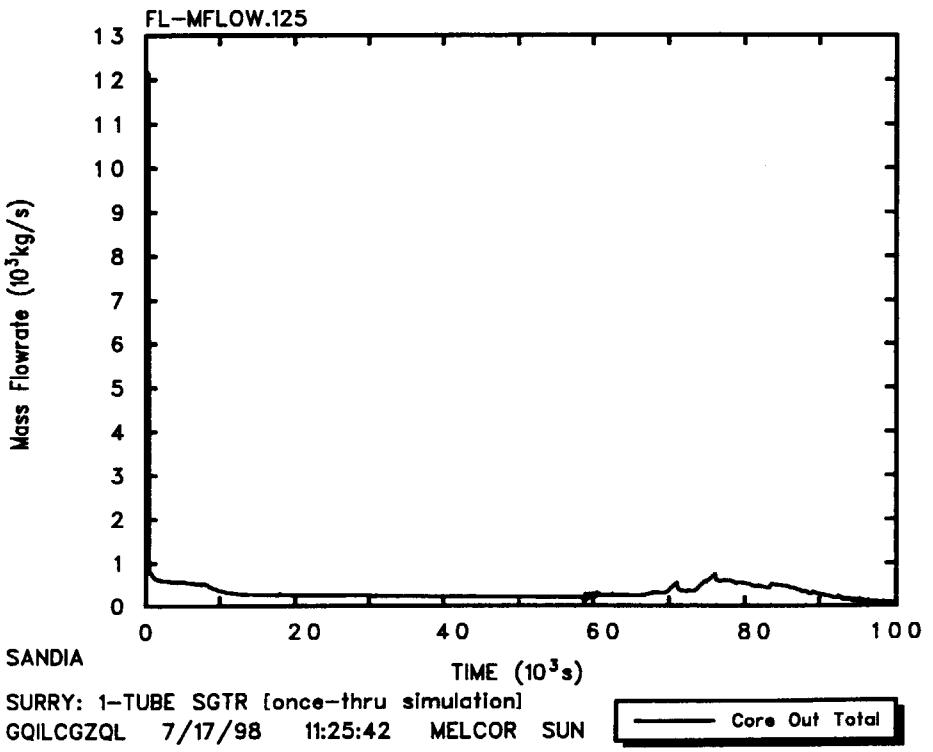

Fig. 3.1.22 Initial Results from Once-through Model -- Core Outlet Total (Pool & Atmosphere) Mass Flowrate

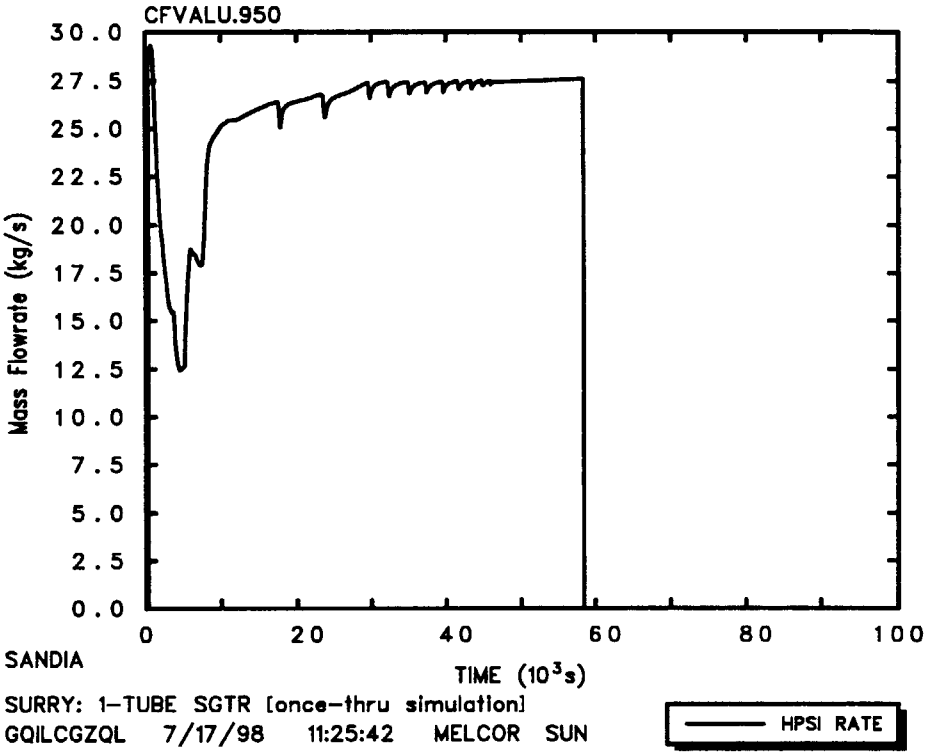

Fig. 3.1.23 Initial Results from Once-through Model -- HPSI Flowrate

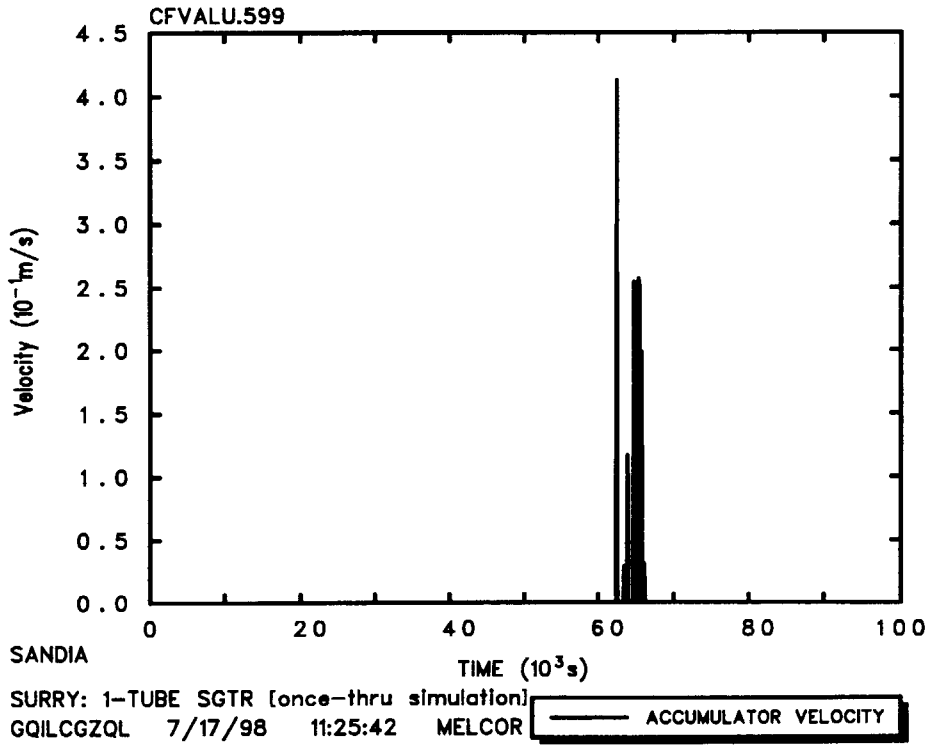

Fig. 3.1.24 Initial Results from Once-through Model -- Accumulator Velocity

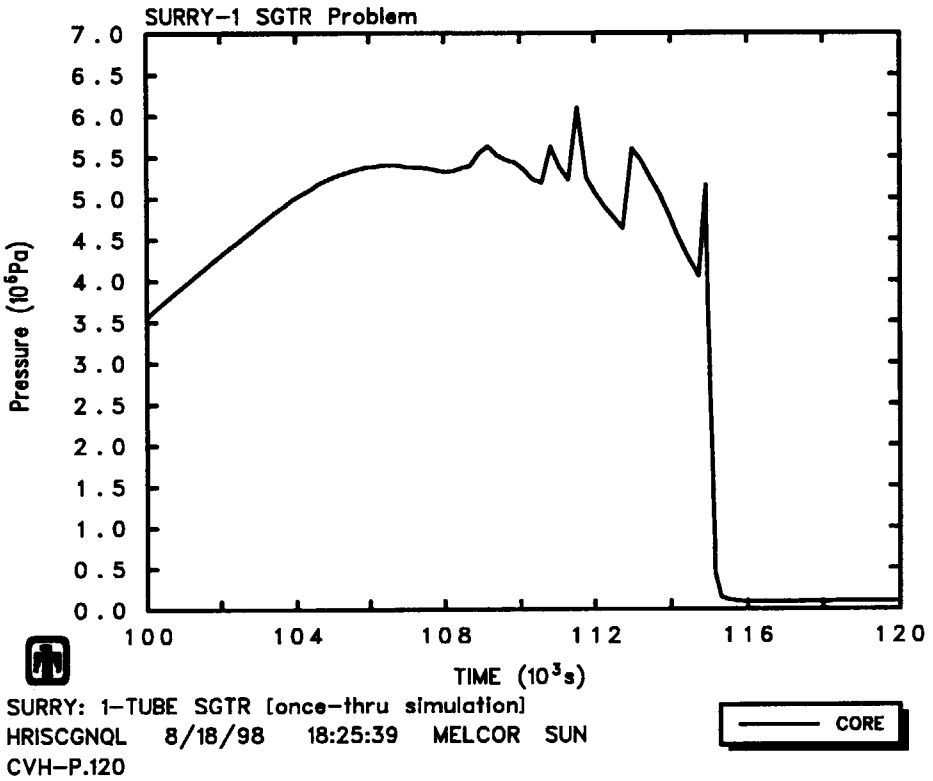

Fig. 3.2.1 Final Results from Once-through Model -- Primary System Pressure

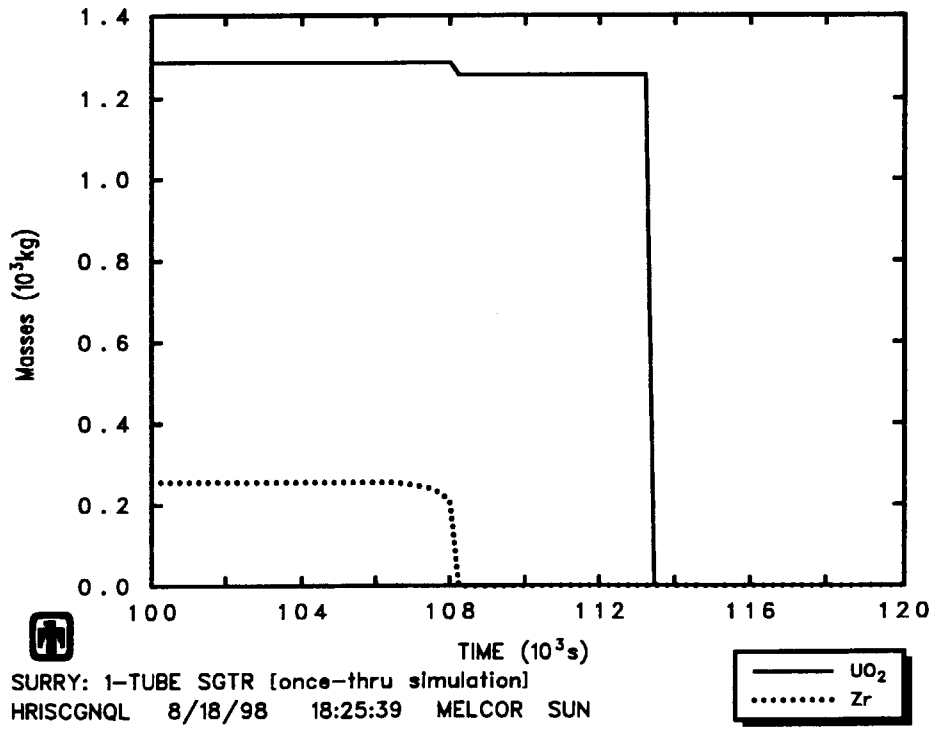

Fig. 3.2.2 Final Results from Once-through Model -- the Masses of UO_2 and Zr at Level 13 Core Cell

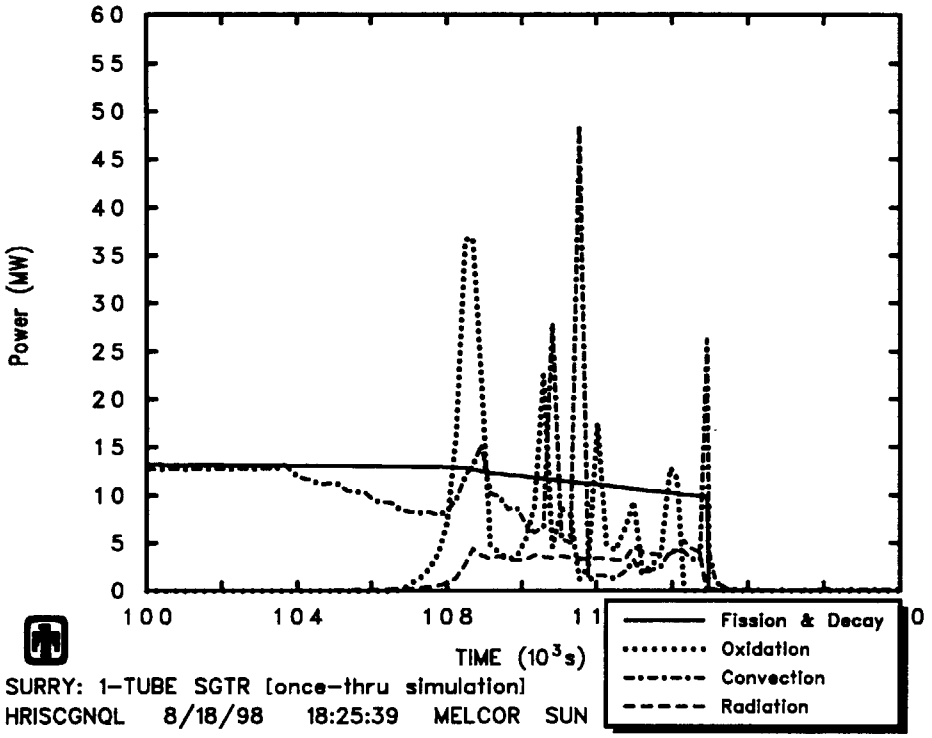

Fig. 3.2.3 Final Results from Once-through Model --
Power Rate of Decay, Oxidation, Convection and Radiation

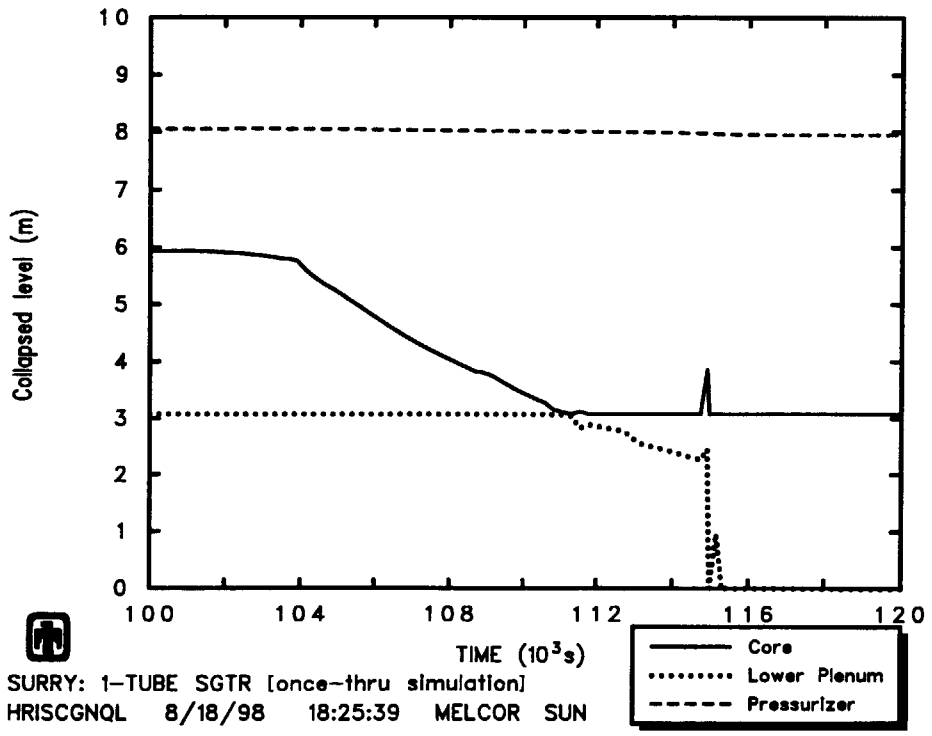

Fig. 3.2.4 Final Results from Once-through Model --
Collapsed Level of Core, Lower Plenum and Pressurizer

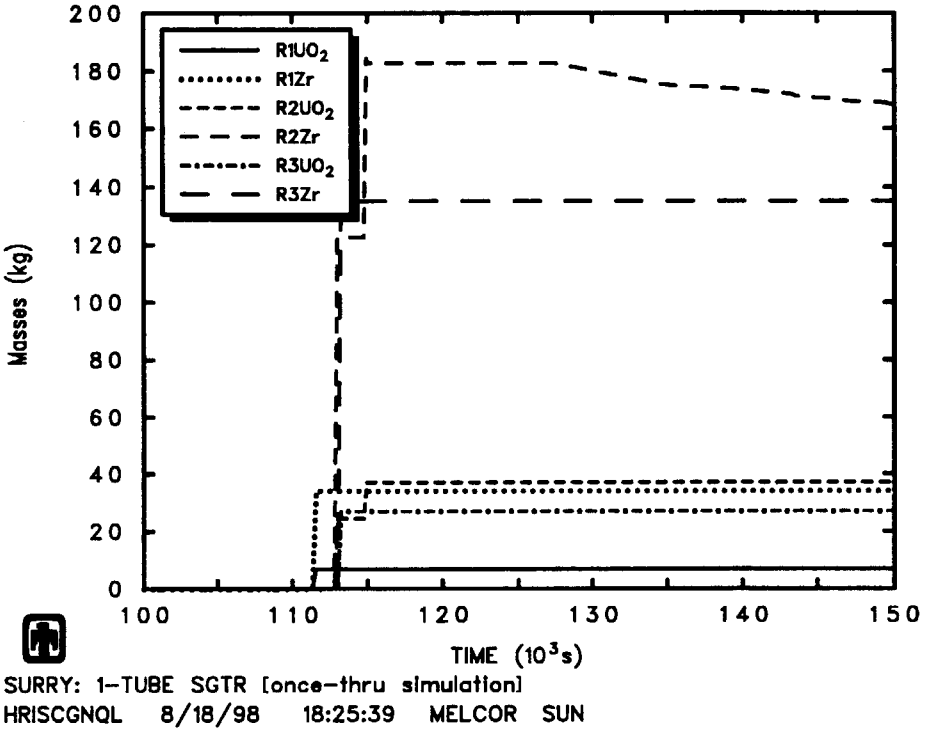

Fig. 3.2.5 Final Results from Once-through Model -- the Masses of UO_2 and Zr at Level 3 Core Cells

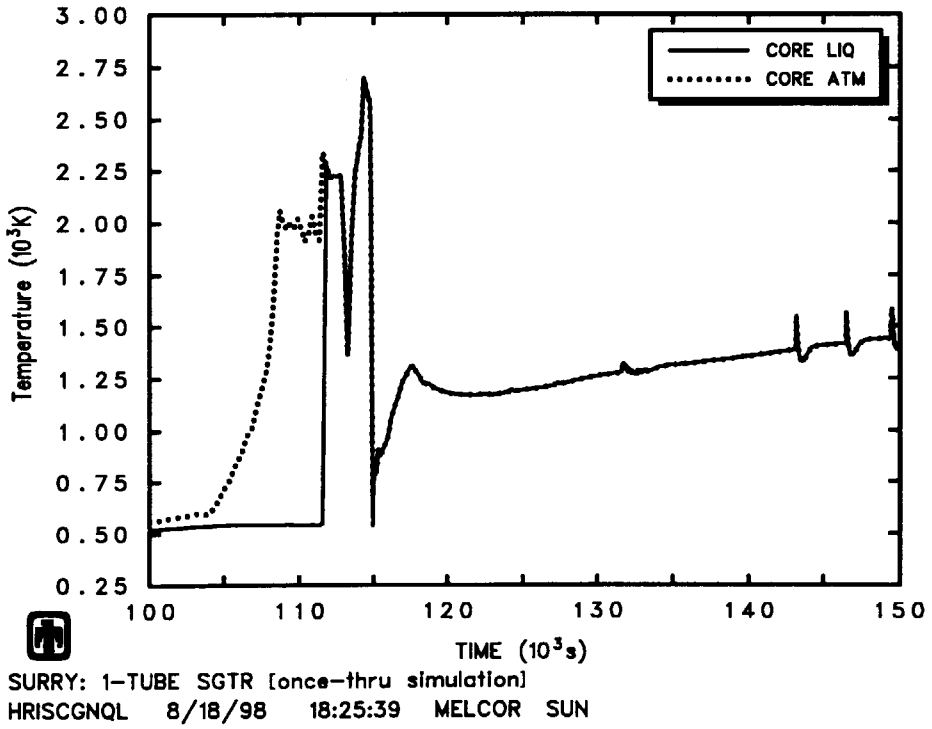

Fig. 3.2.6 Final Results from Once-through Model -- Core Temperature

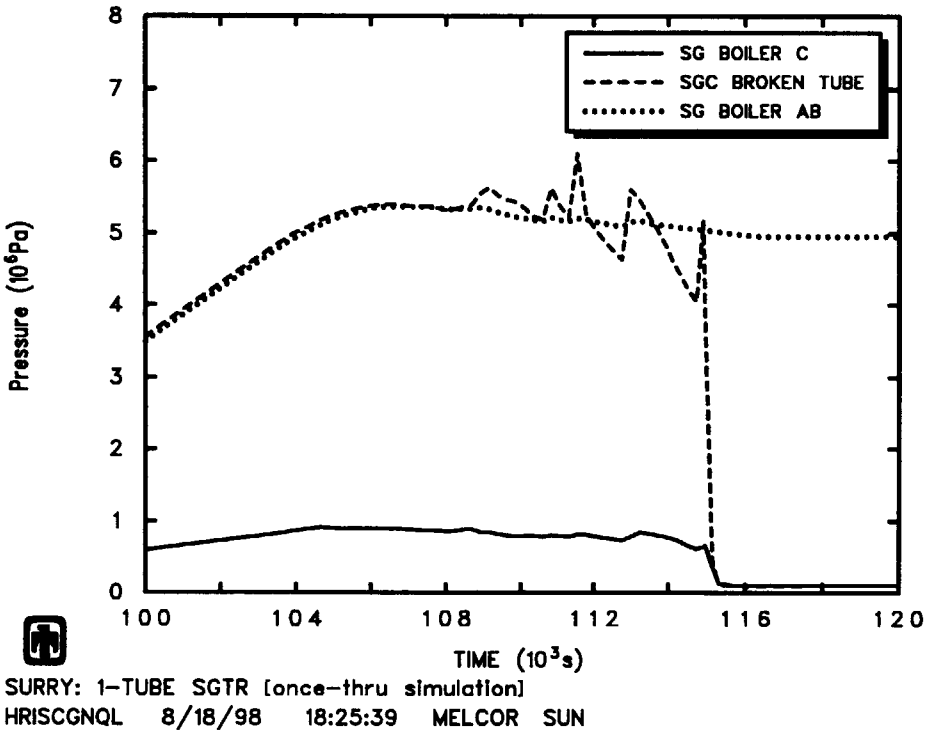

Fig. 3.2.7 Final Results from Once-through Model -- Secondary System Pressure

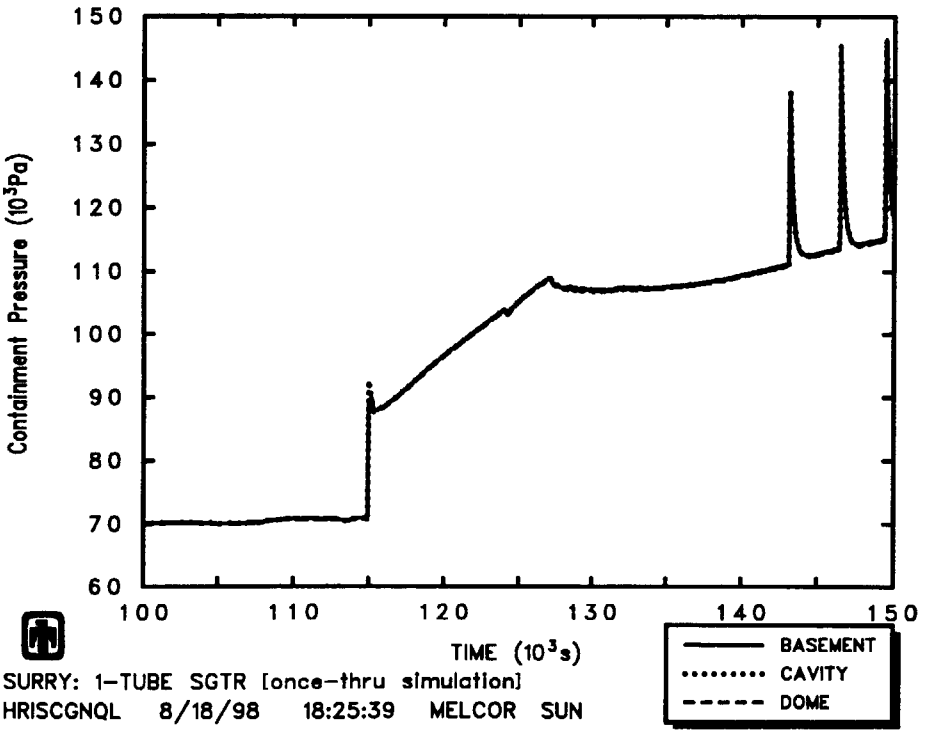

Fig. 3.2.8 Final Results from Once-through Model -- Containment Pressure

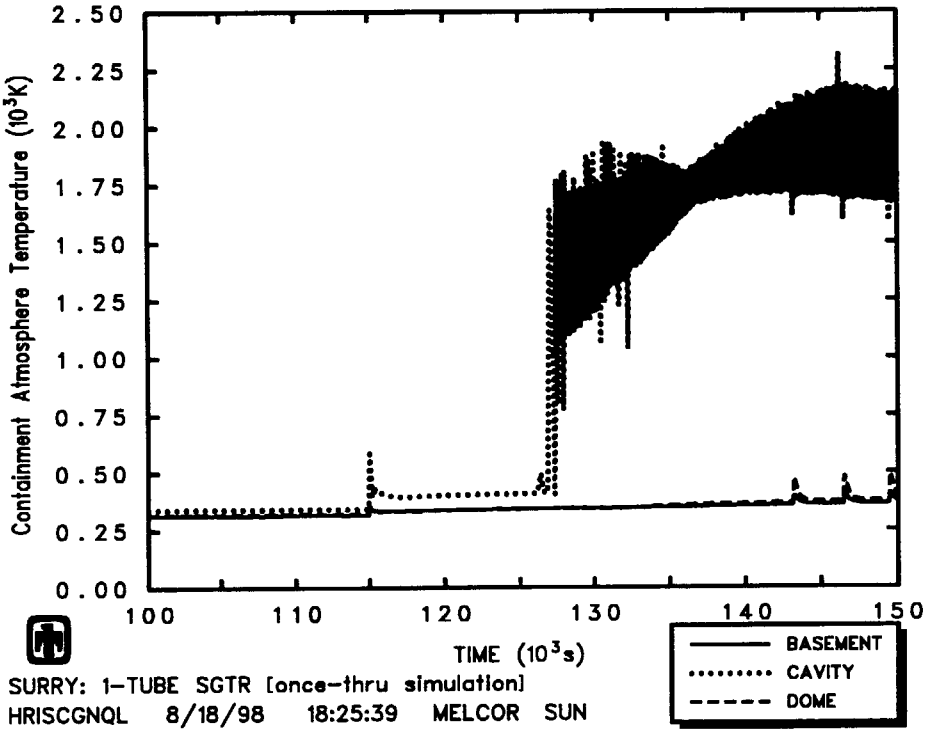

Fig. 3.2.9 Final Results from Once-through Model -- Containment Atmosphere Temperature

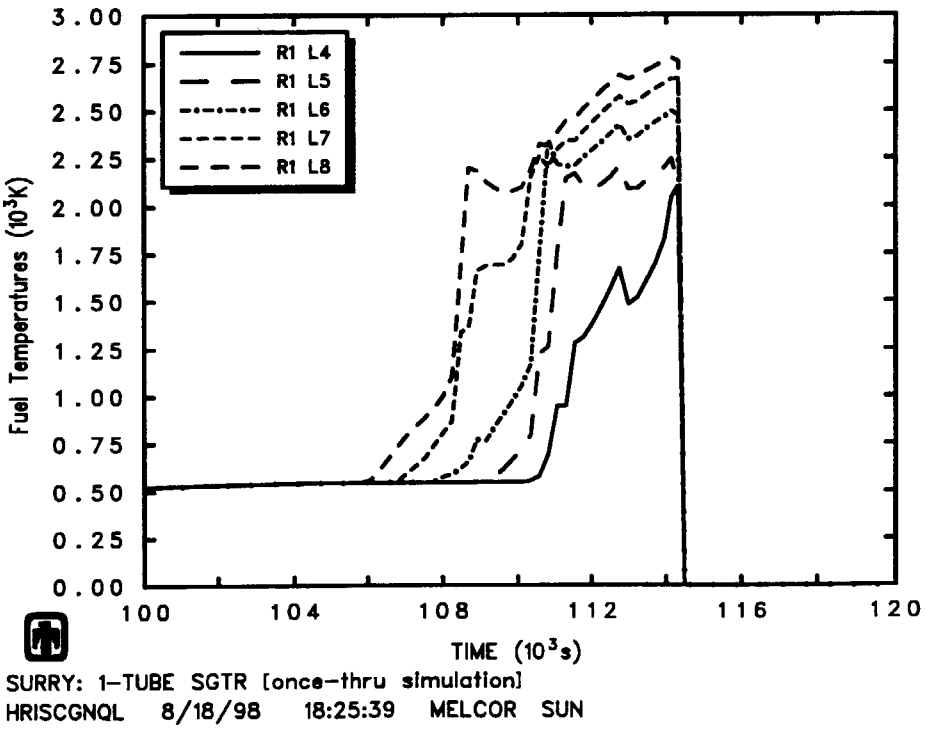

Fig. 3.2.10 Final Results from Once-through Model -- Fuel Temperatures in Ring 1 Core Cells at Level 4 ~ Level 8

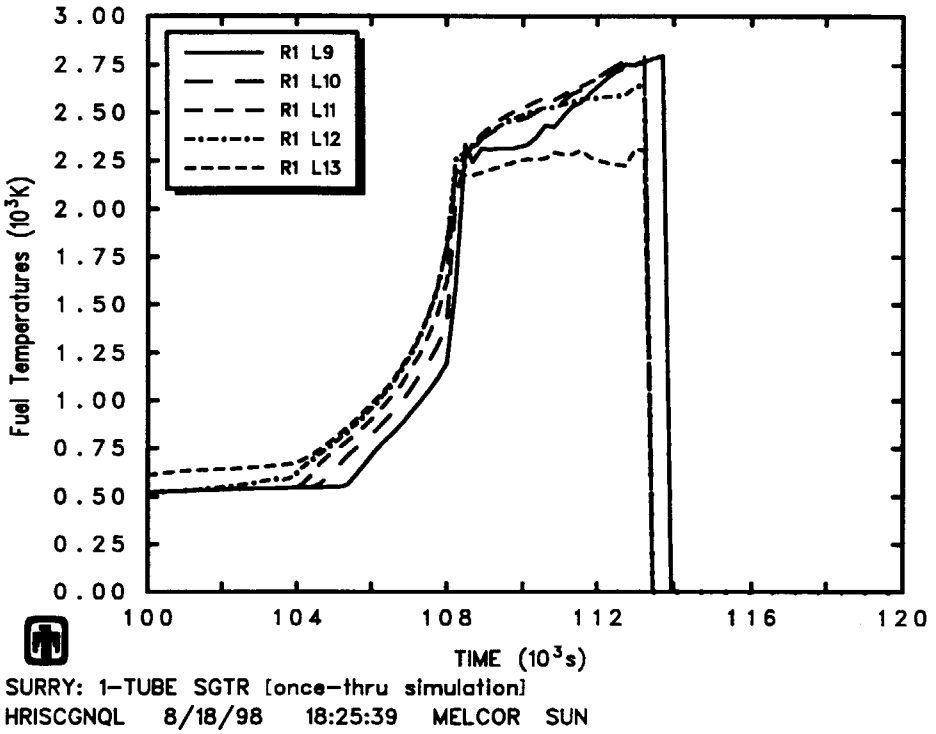

Fig. 3.2.11 Final Results from Once-through Model --
Fuel Temperatures in Ring 1 Core Cells at Level 9 ~ Level 13

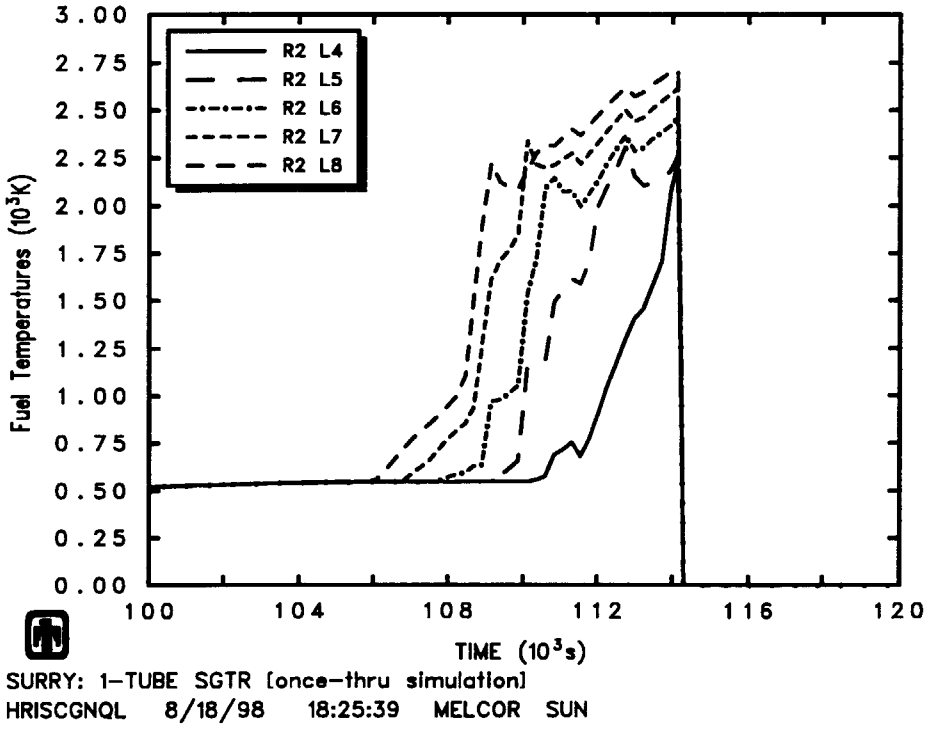

Fig. 3.2.12 Final Results from Once-through Model --
Fuel Temperatures in Ring 2 Core Cells at Level 4 ~ Level 8

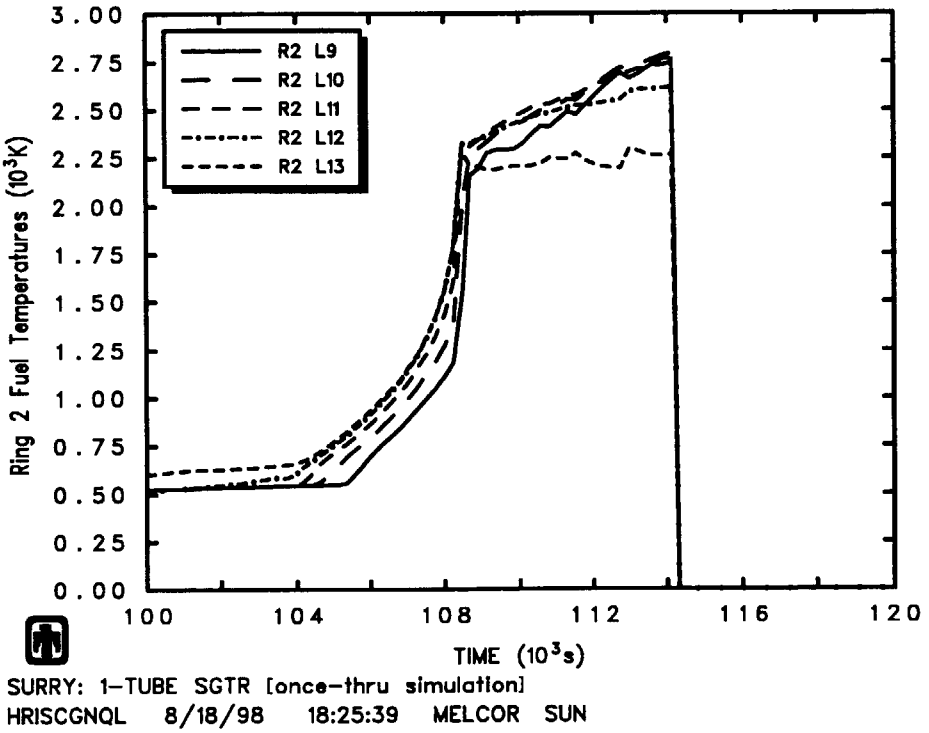

Fig. 3.2.13 Final Results from Once-through Model --
Fuel Temperatures in Ring 2 Core Cells at Level 9 ~ Level 13

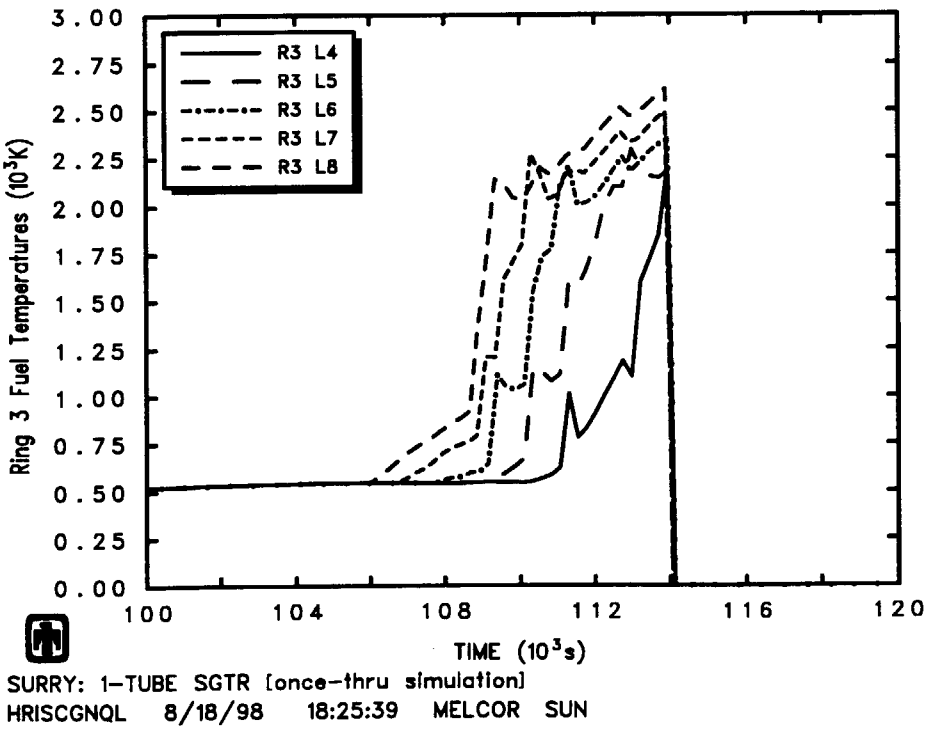

Fig. 3.2.14 Final Results from Once-through Model --
Fuel Temperatures in Ring 3 Core Cells at Level 4 ~ Level 8

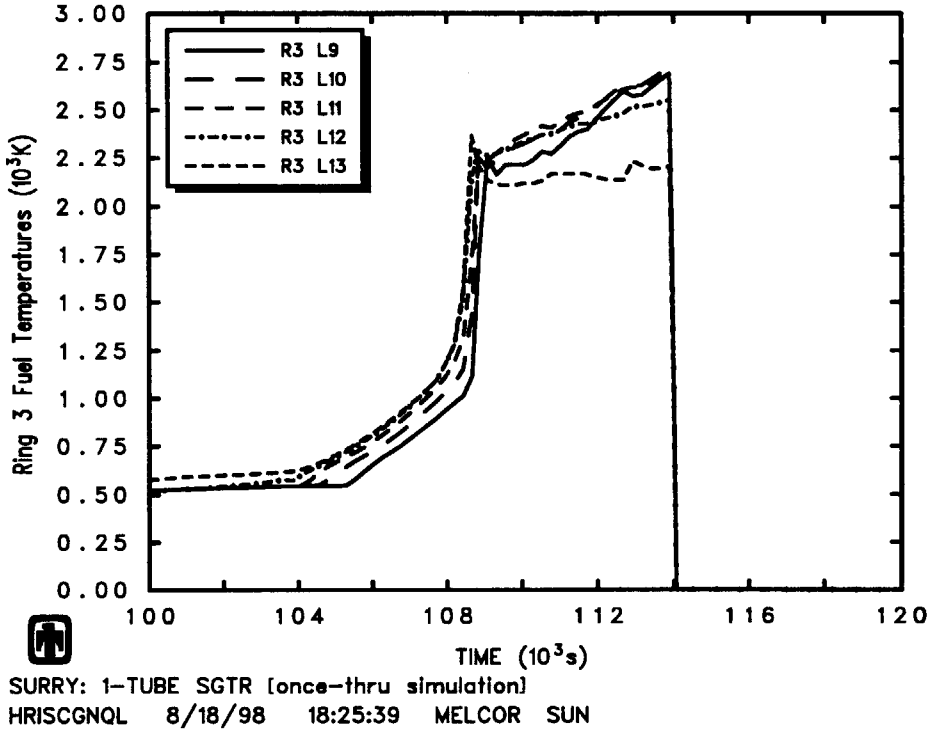

Fig. 3.2.15 Final Results from Once-through Model --
Fuel Temperatures in Ring 3 Core Cells at Level 9 ~ Level 13

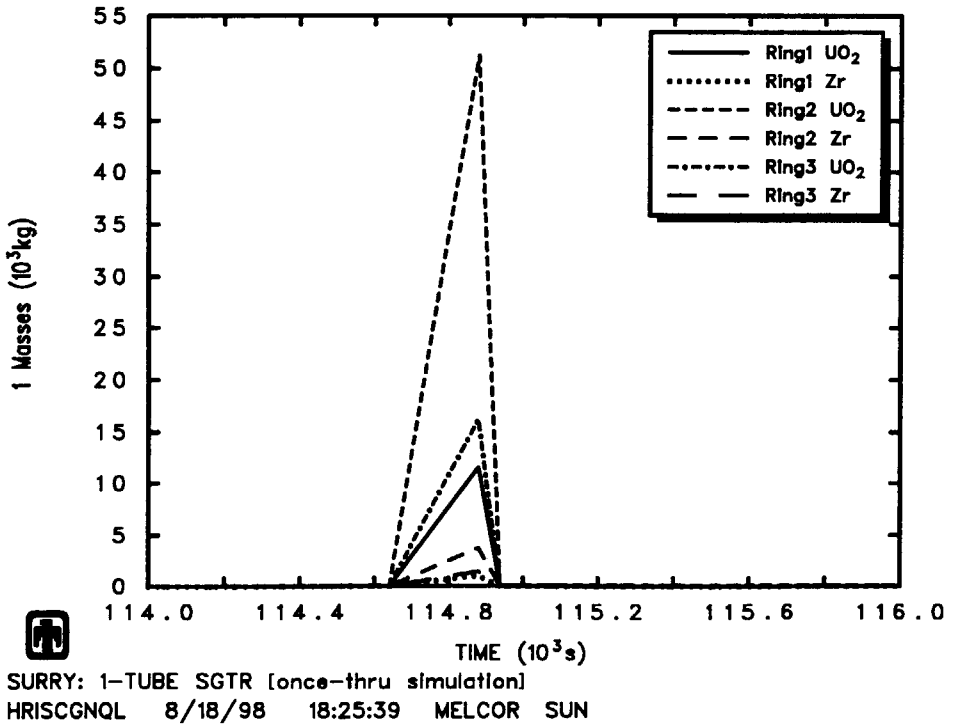

Fig. 3.2.16 Final Results from Once-through Model --
UO_2 & Zr Masses at Level 1 Core Cells

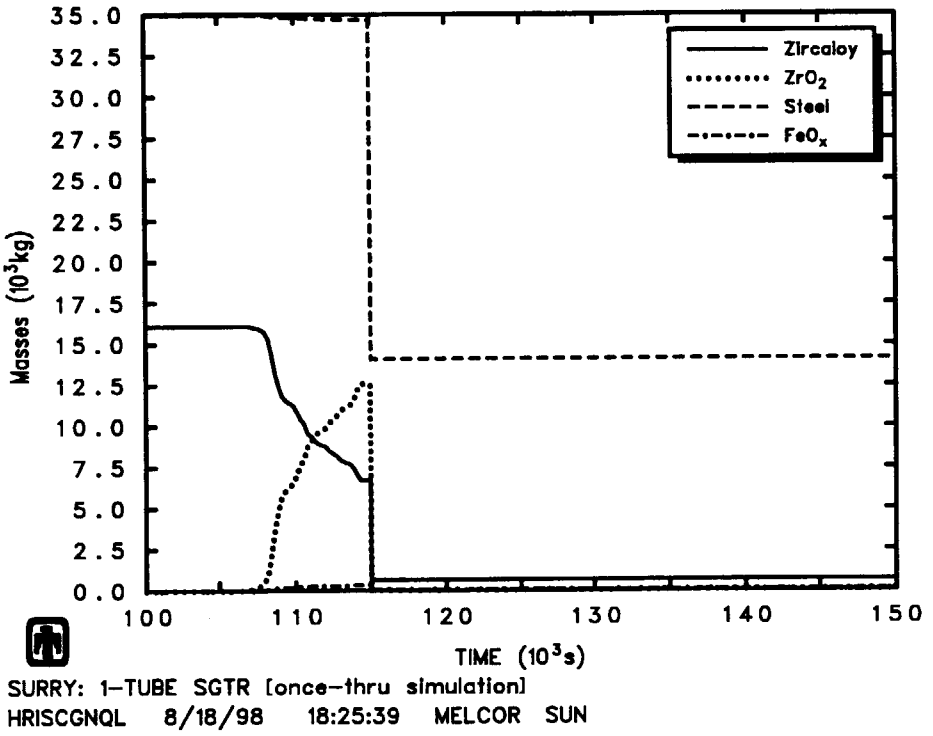

Fig. 3.2.17 Final Results from Once-through Model -- Total Metal Material Masses in Core

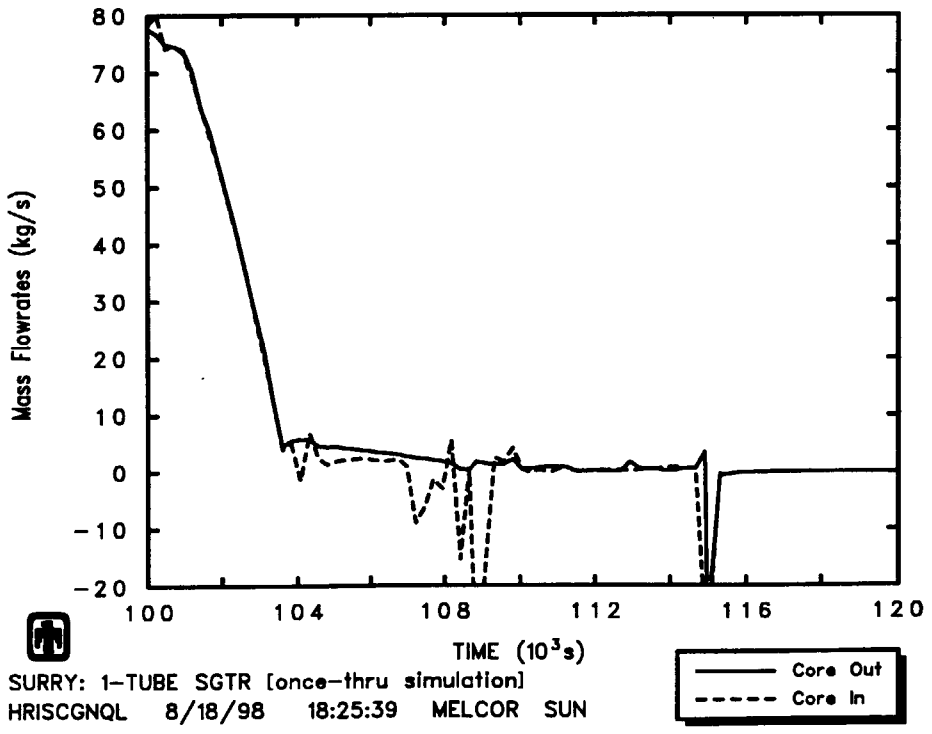

Fig. 3.2.18 Final Results from Once-through Model -- Core Mass Flowrates

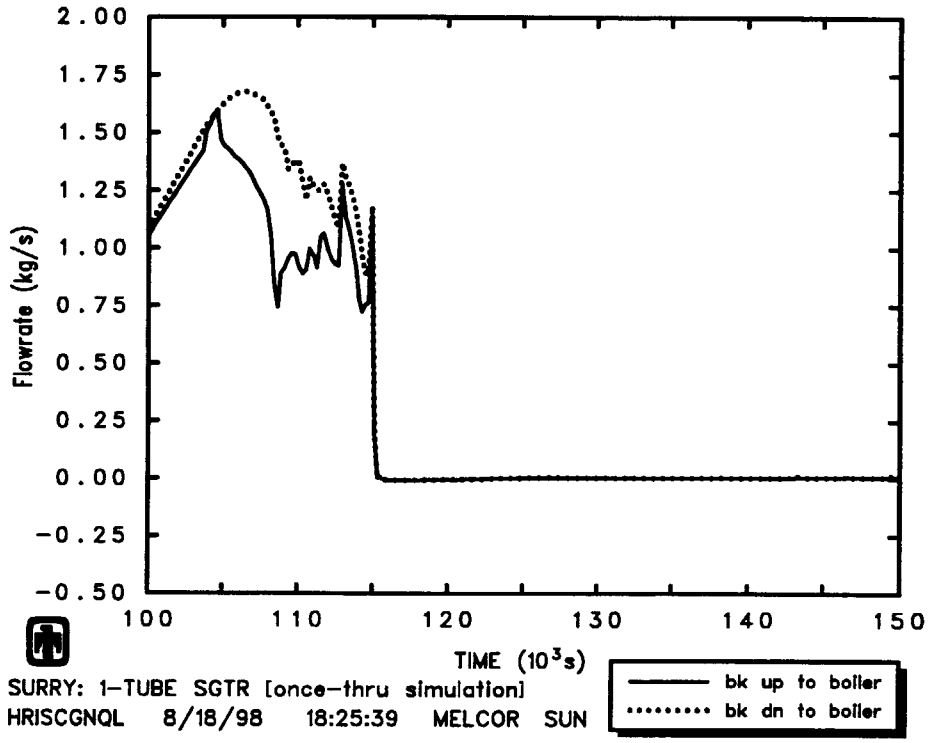

Fig. 3.2.19 Final Results from Once-through Model -- Break Flowrates from Broken Tube

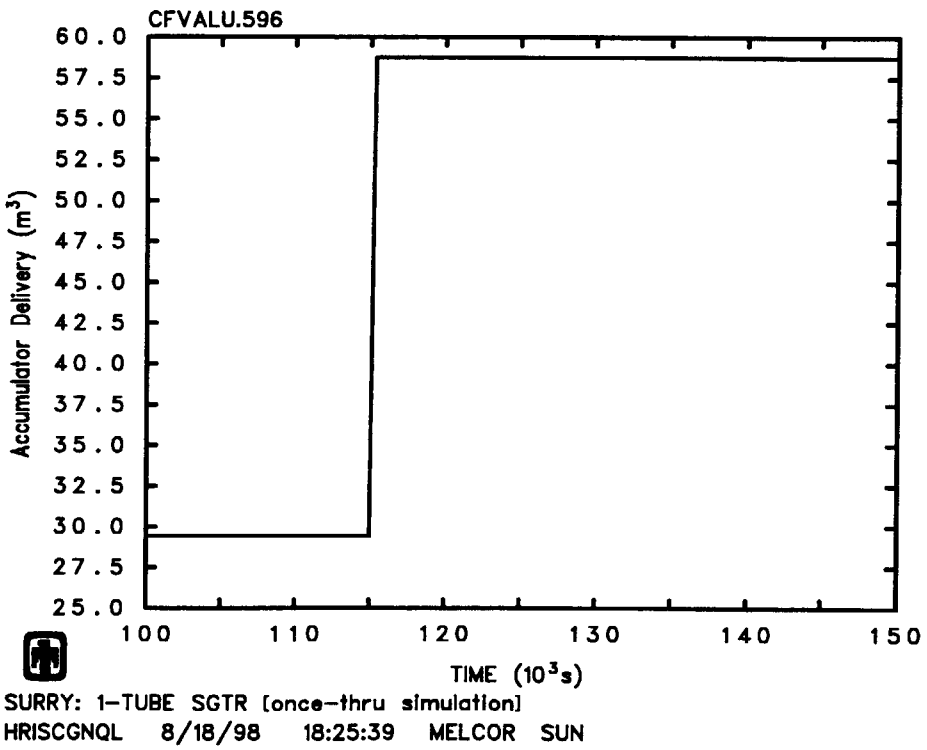

Fig. 3.2.20 Final Results from Once-through Model -- Accumulator Delivery

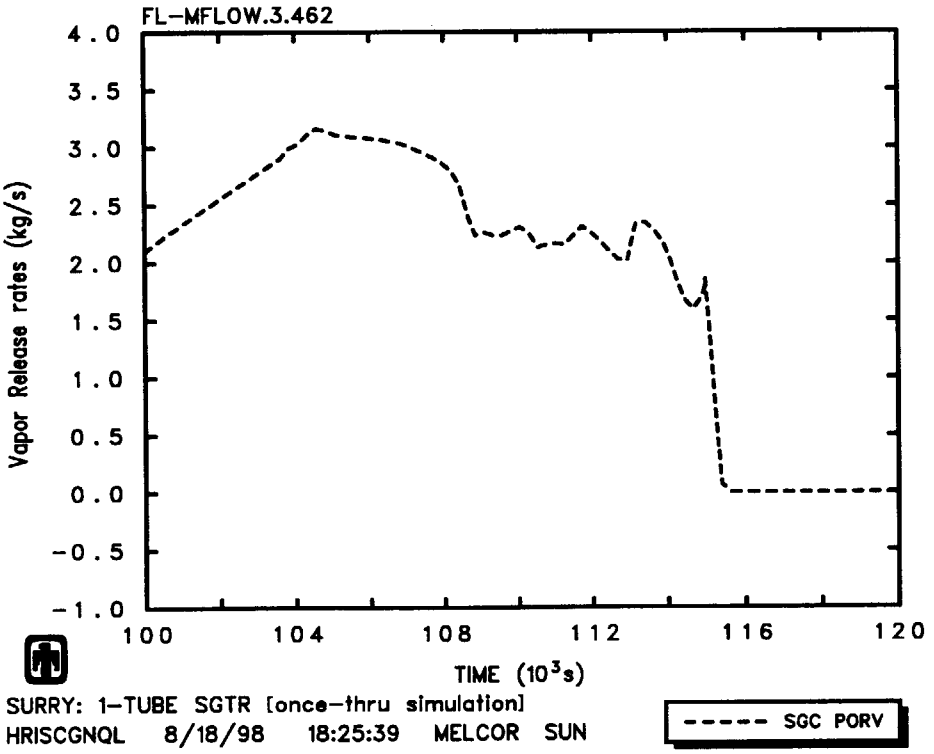

Fig. 3.2.21 Final Results from Once-through Model -- SG C PORV Vapor Release Rate

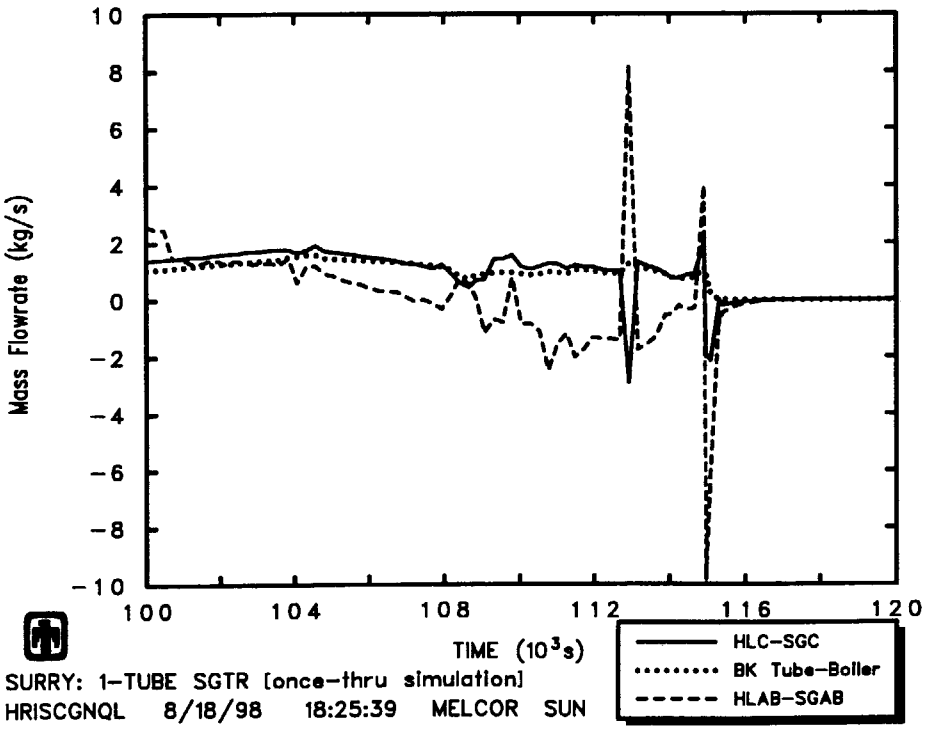

Fig. 3.2.22 Final Results from Once-through Model -- Mass Flowrates to SGs

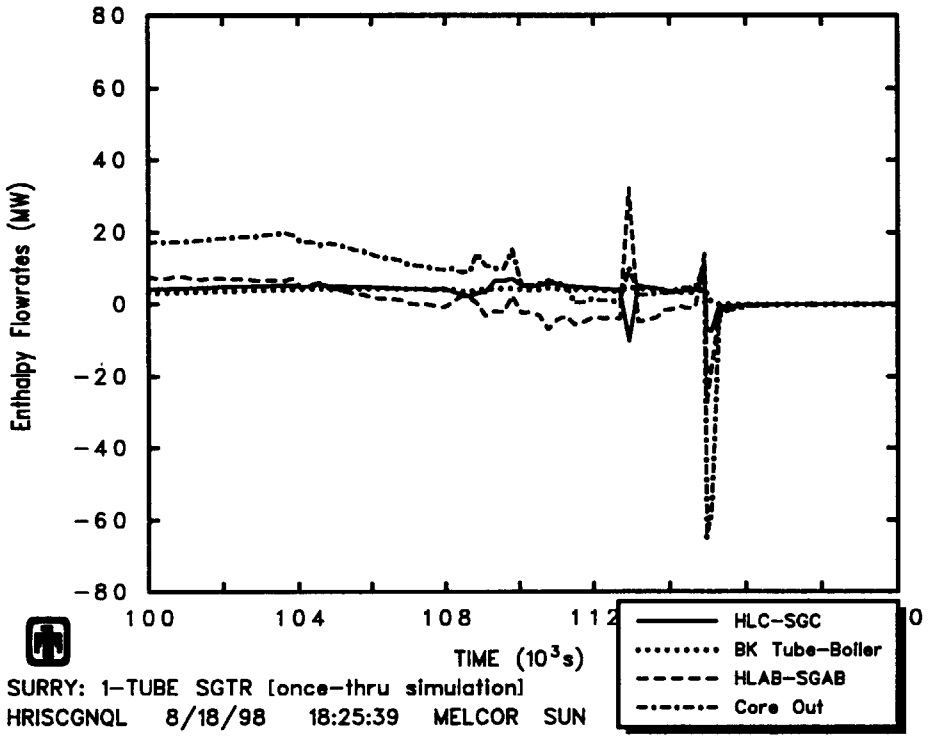

Fig. 3.2.23 Final Results from Once-through Model -- Enthalpy Flowrates from Core

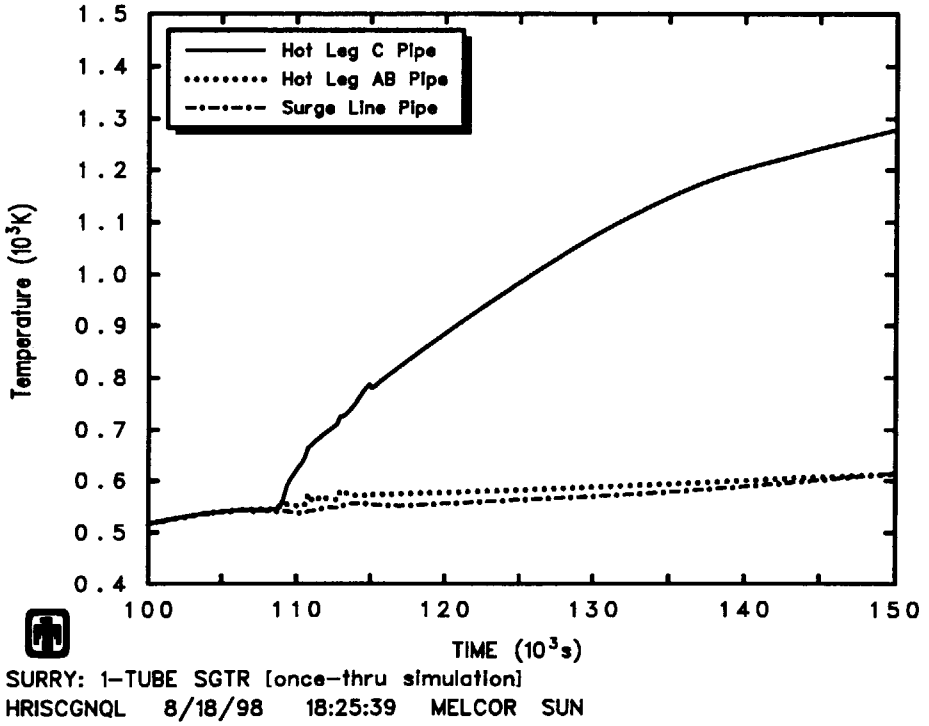

Fig. 3.2.24 Final Results from Once-through Model -- Hotleg & Surgeline Pipe Temperature

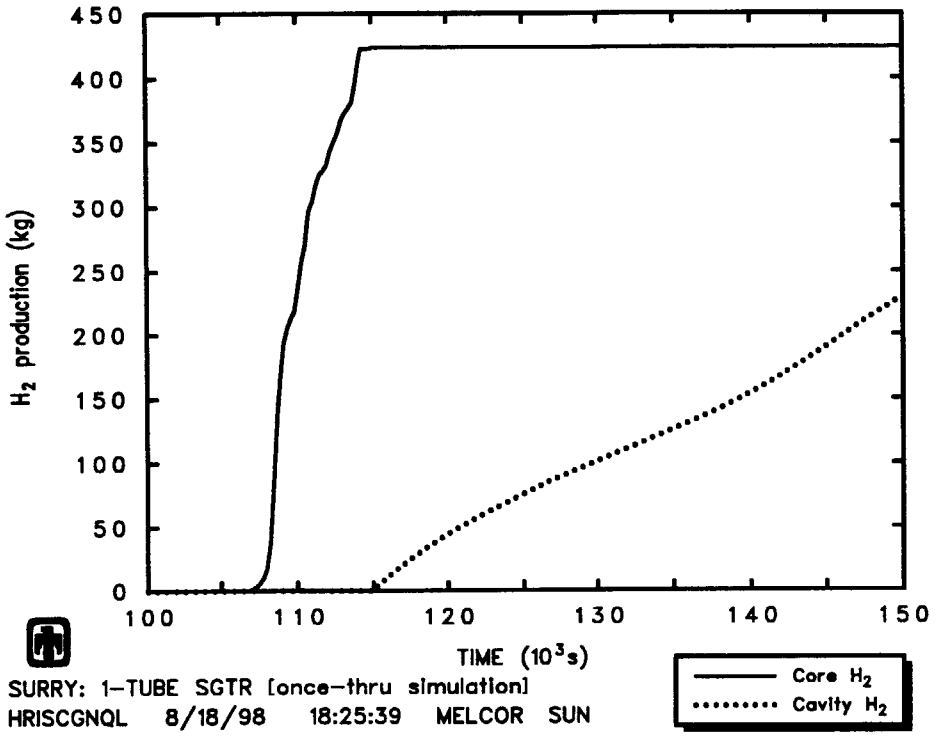

Fig. 3.2.25 Final Results from Once-through Model -- H_2 Production in Core and Cavity

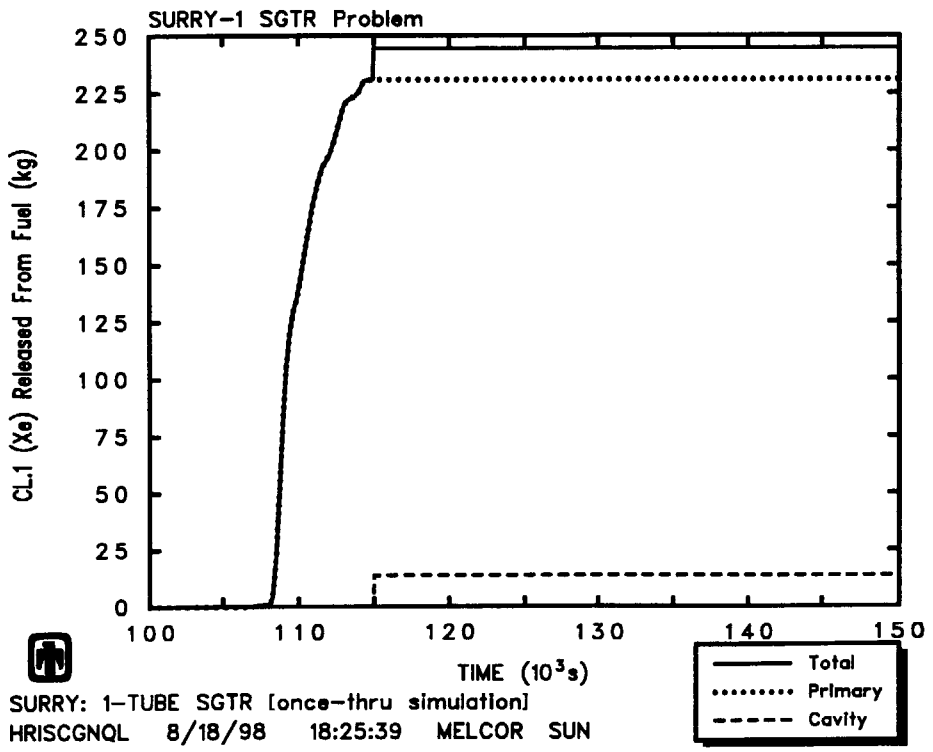

Fig. 3.2.26 Final Results from Once-through Model -- RN Released from Fuel (Xe)

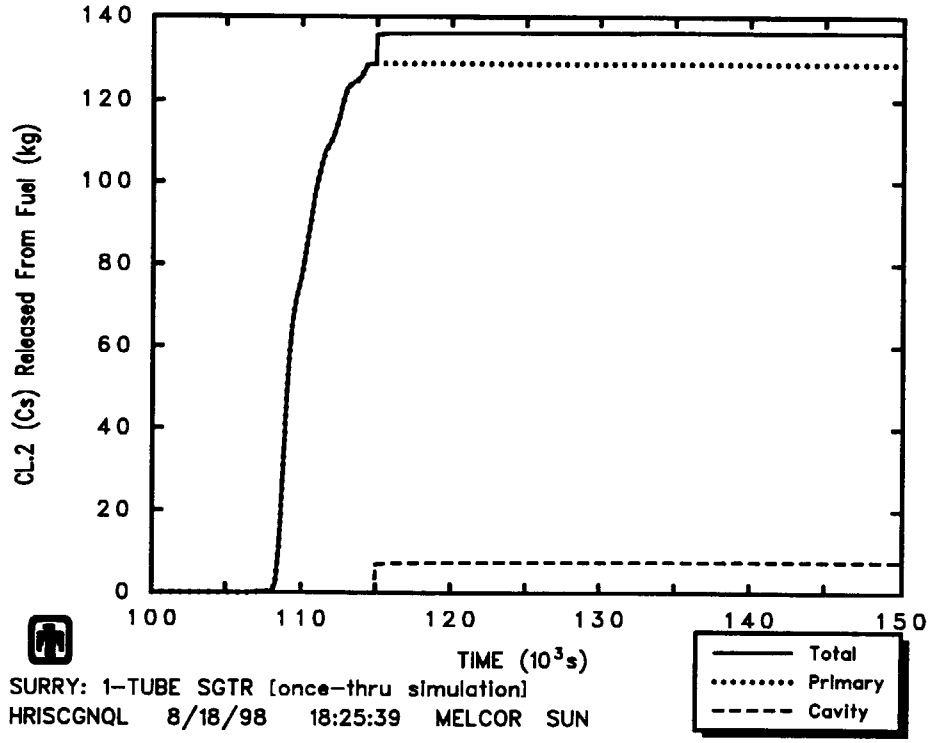

Fig. 3.2.27 Final Results from Once-through Model -- RN Released from Fuel (Cs)

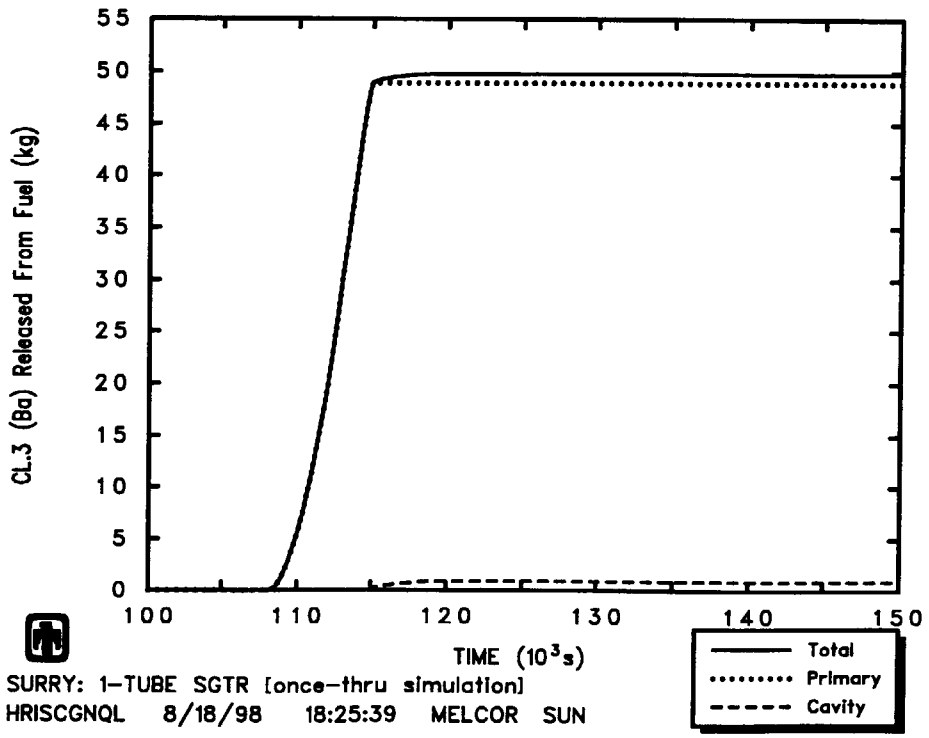

Fig. 3.2.28 Final Results from Once-through Model -- RN Released from Fuel (Ba)

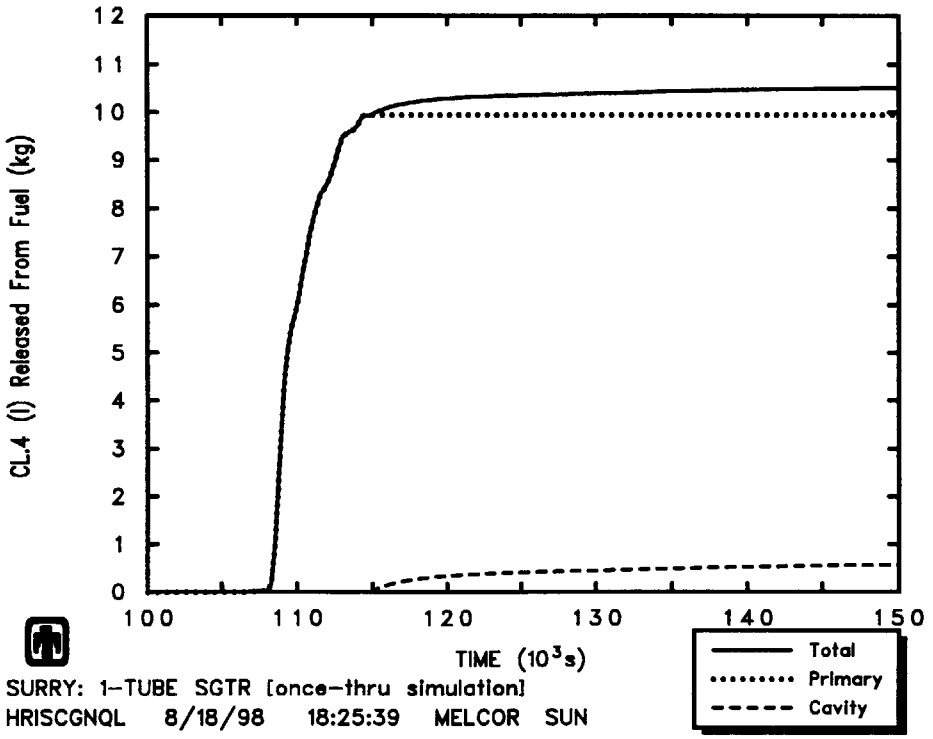

Fig. 3.2.29 Final Results from Once-through Model -- RN Released from Fuel (I)

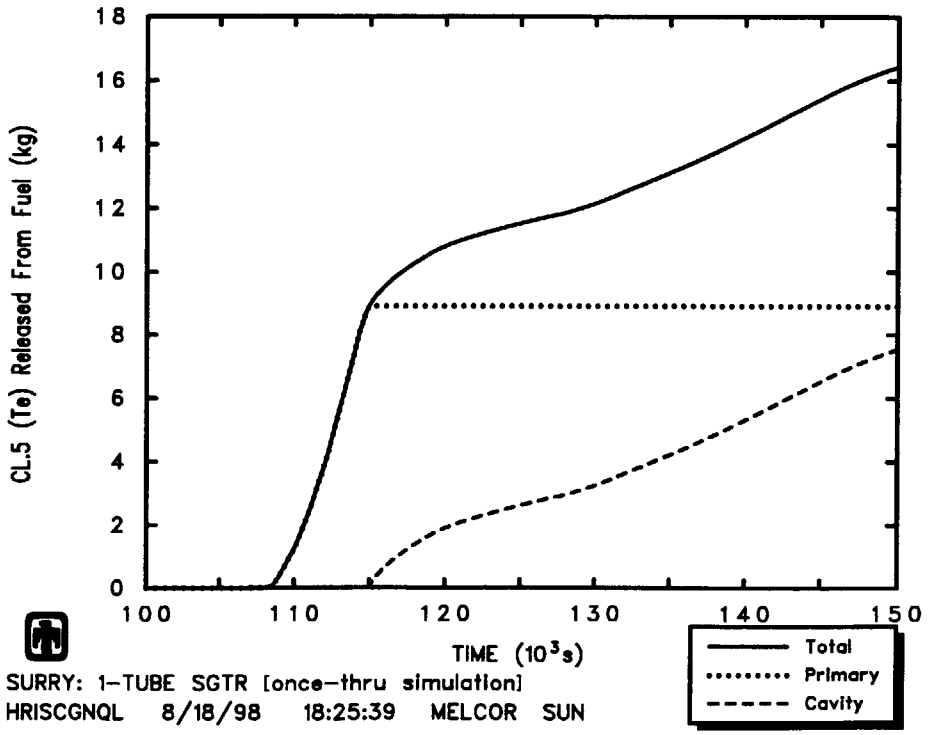

Fig. 3.2.30 Final Results from Once-through Model -- RN Released from Fuel (Te)

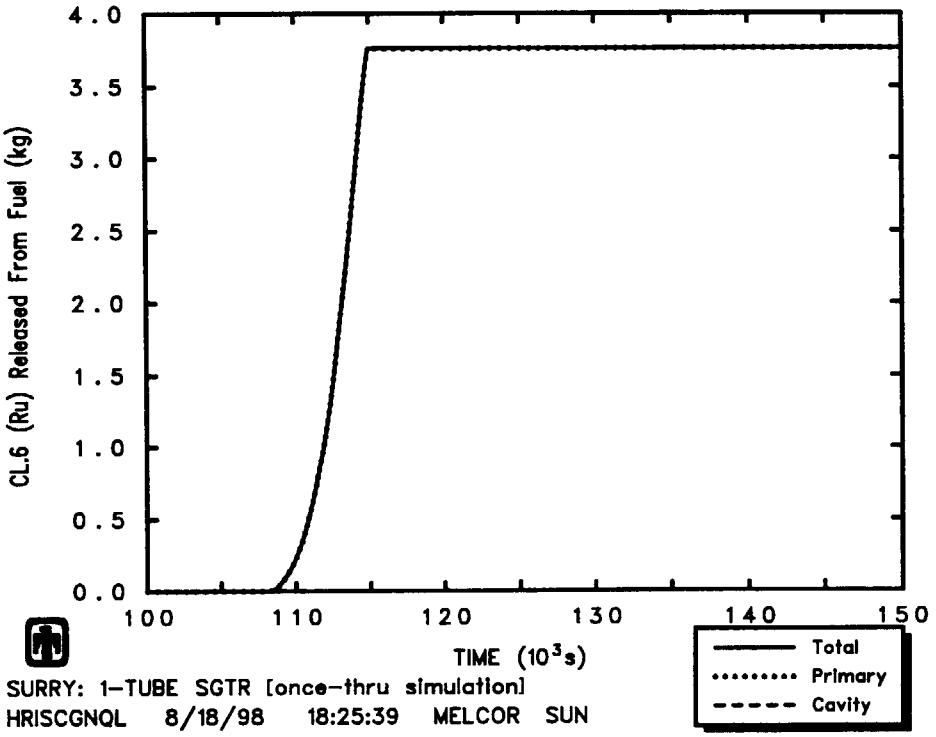

Fig. 3.2.31 Final Results from Once-through Model -- RN Released from Fuel (Ru)

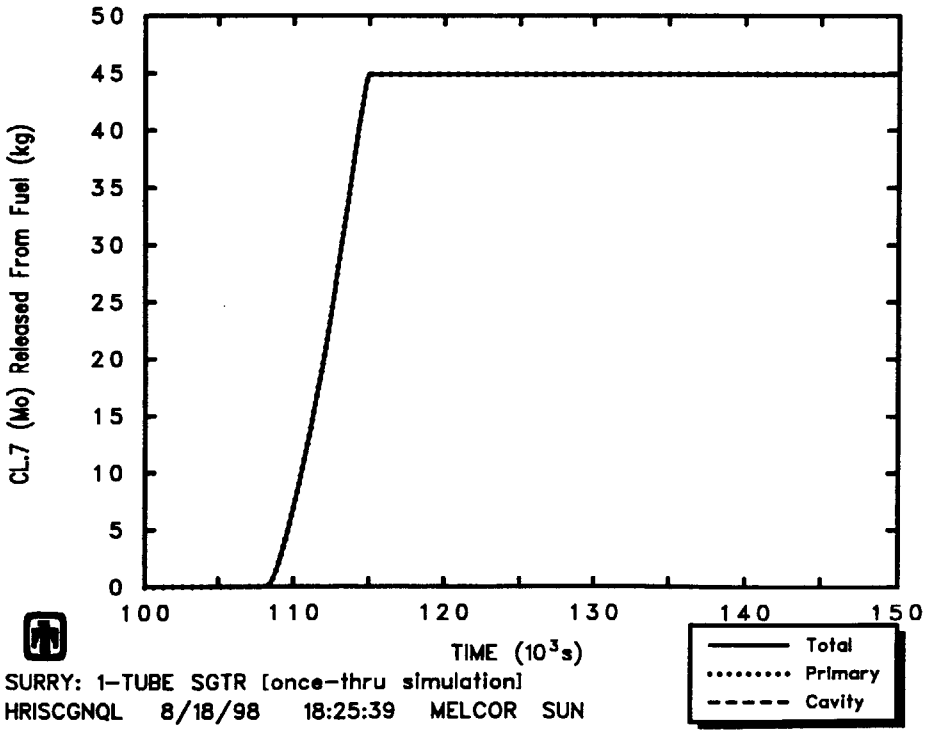

Fig. 3.2.32 Final Results from Once-through Model -- RN Released from Fuel (Mo)

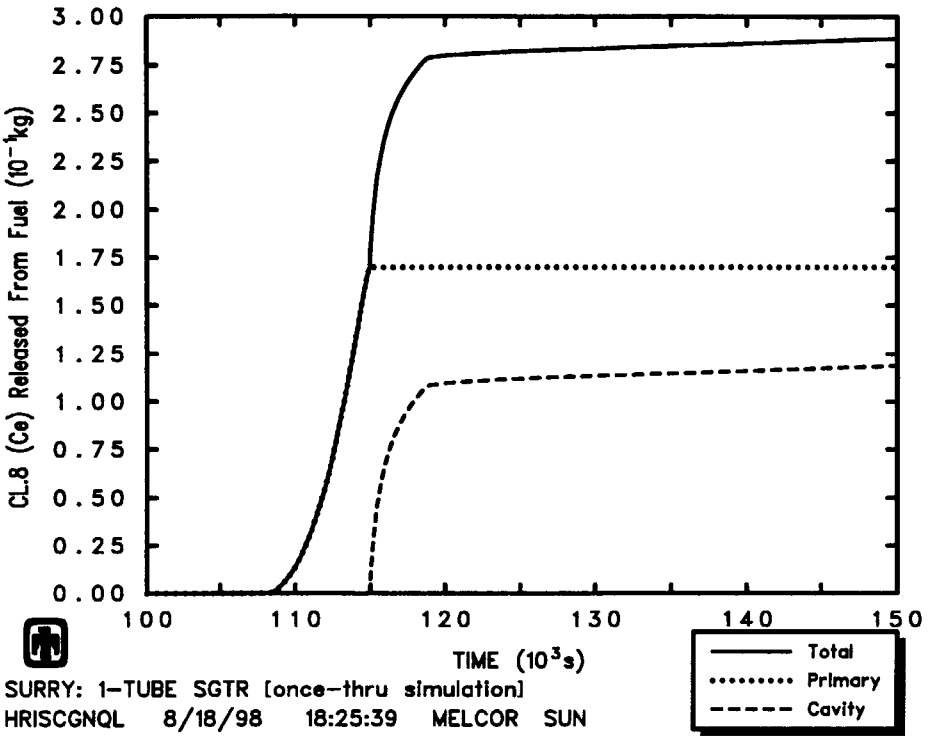

Fig. 3.2.33 Final Results from Once-through Model -- RN Released from Fuel (Ce)

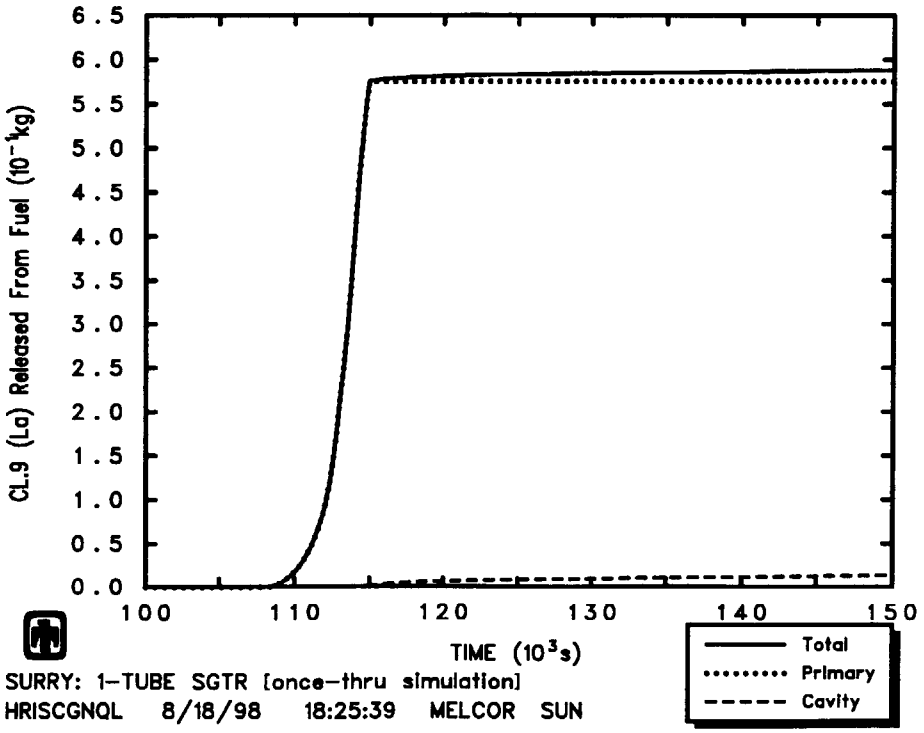

Fig. 3.2.34 Final Results from Once-through Model -- RN Released from Fuel (La)

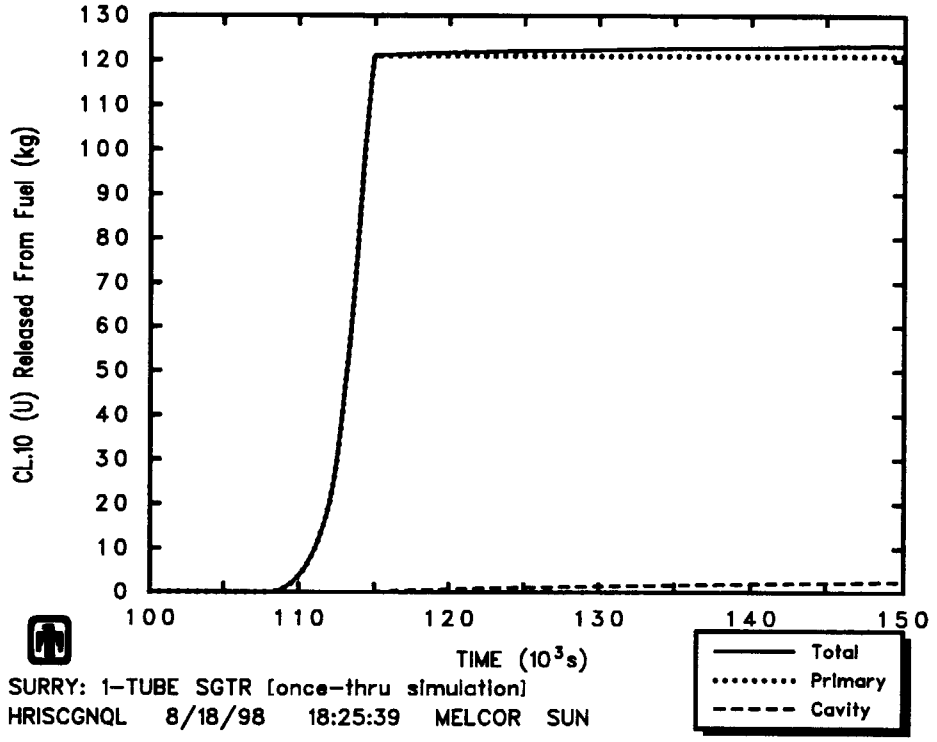

Fig. 3.2.35 Final Results from Once-through Model -- RN Released from Fuel (U)

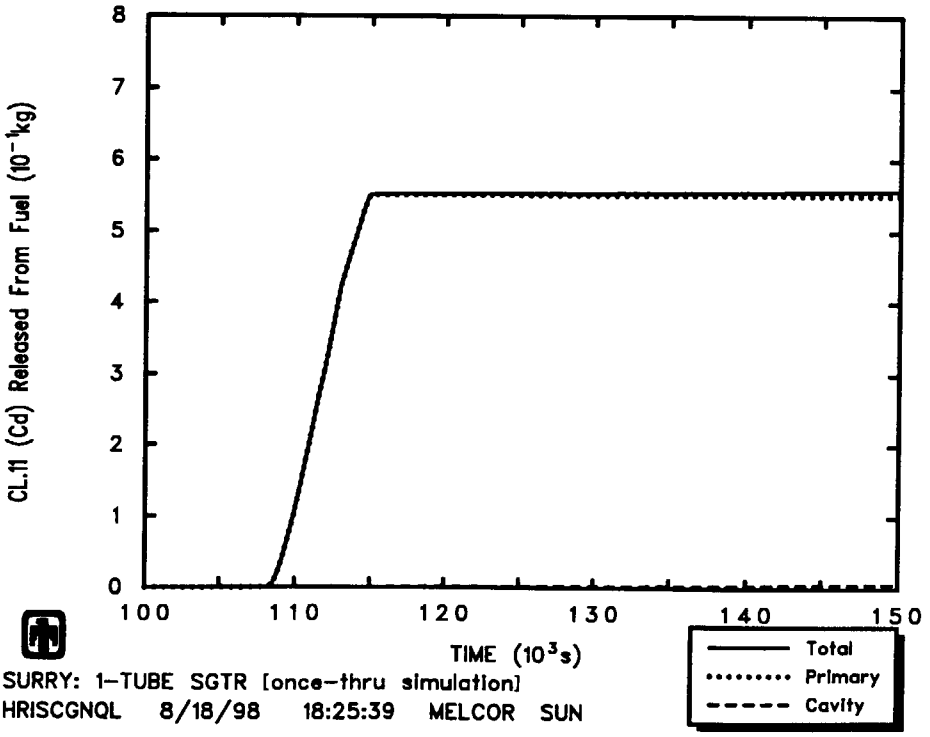

Fig. 3.2.36 Final Results from Once-through Model -- RN Released from Fuel (Cd)

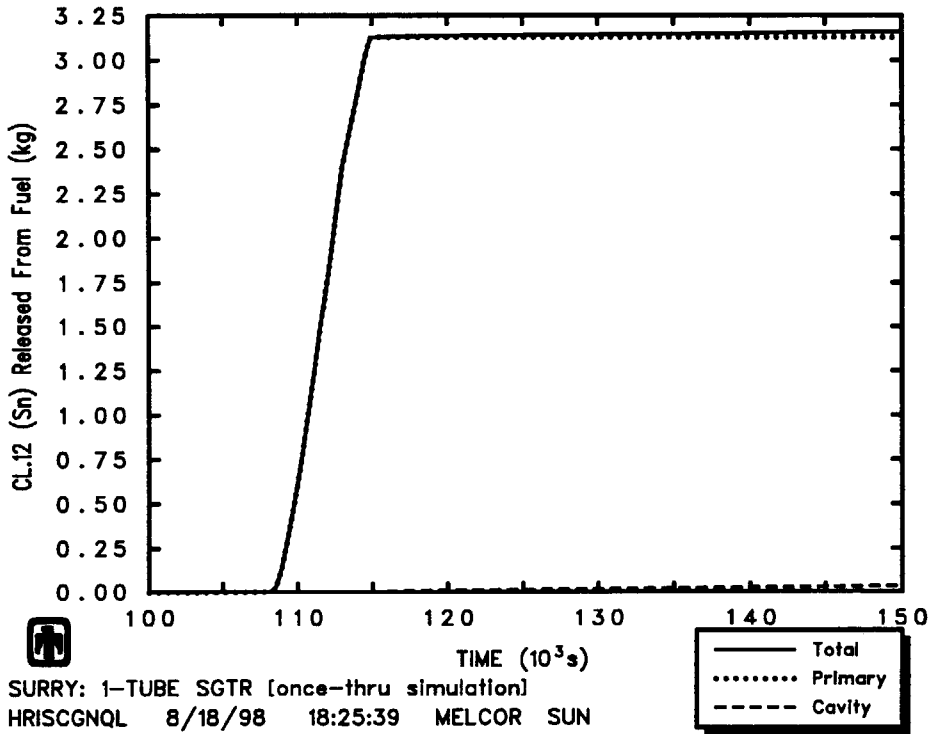

Fig. 3.2.37 Final Results from Once-through Model -- RN Released from Fuel (Sn)

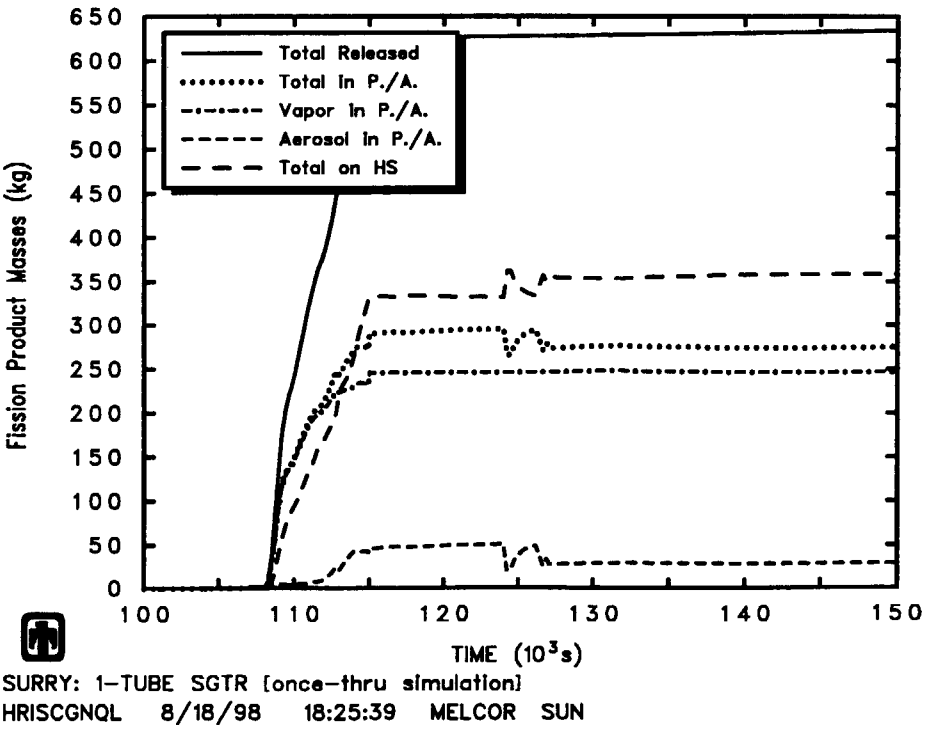

Fig. 3.2.38 Final Results from Once-through Model -- Fission Products Mass Distribution

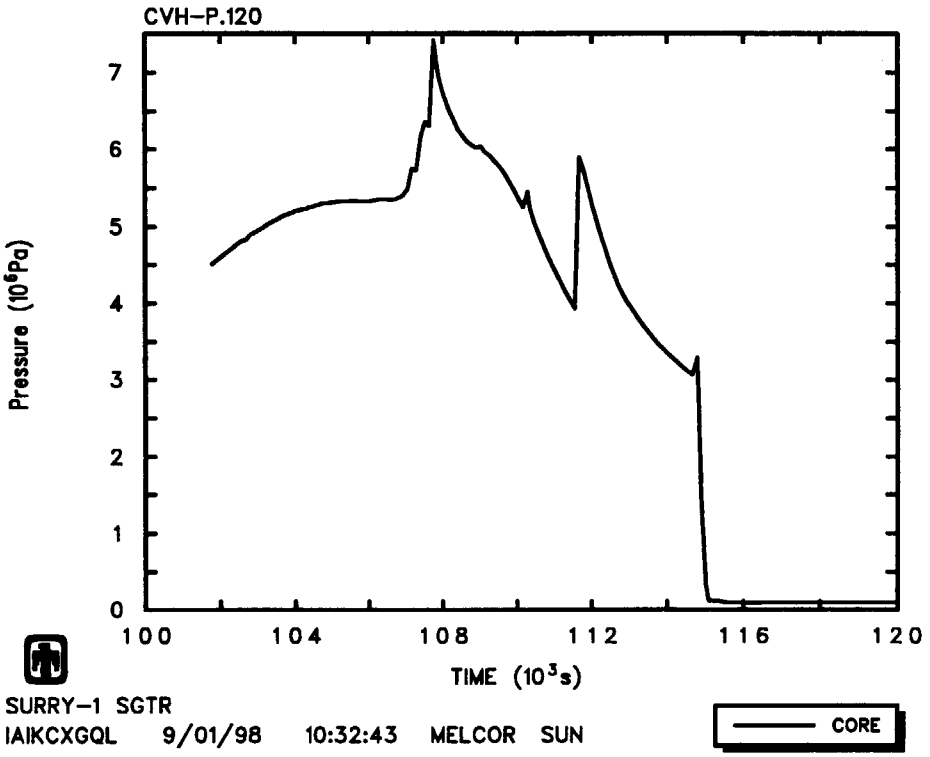

Fig. 3.3.1 Results from Natural Circulation Model -- Primary System Pressure

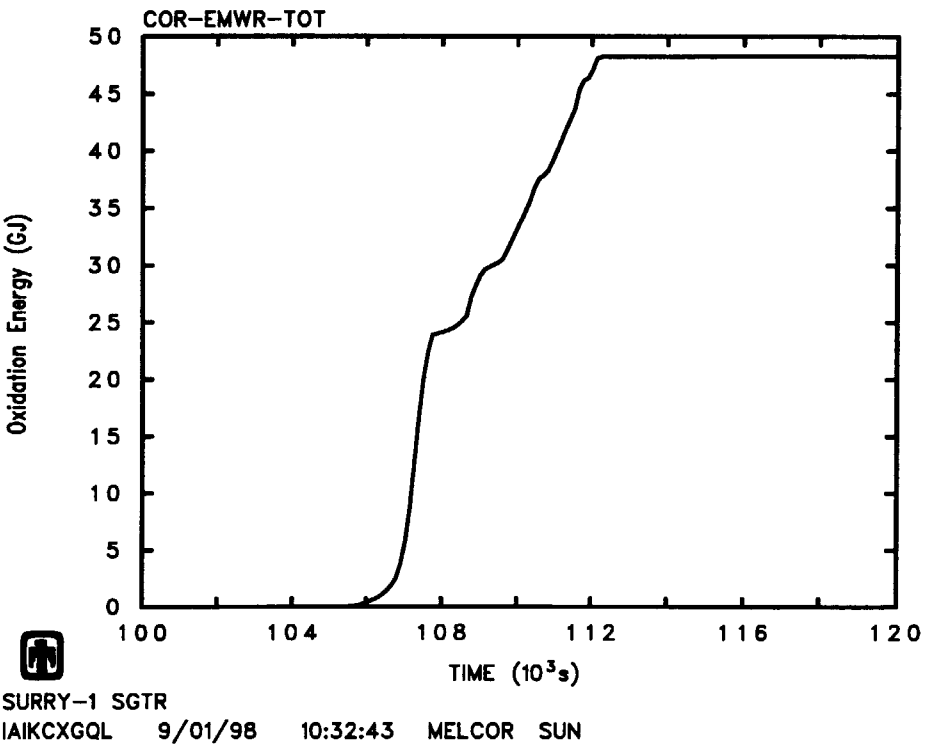

Fig. 3.3.2 Results from Natural Circulation Model -- Total Cumulative Oxidation Energy

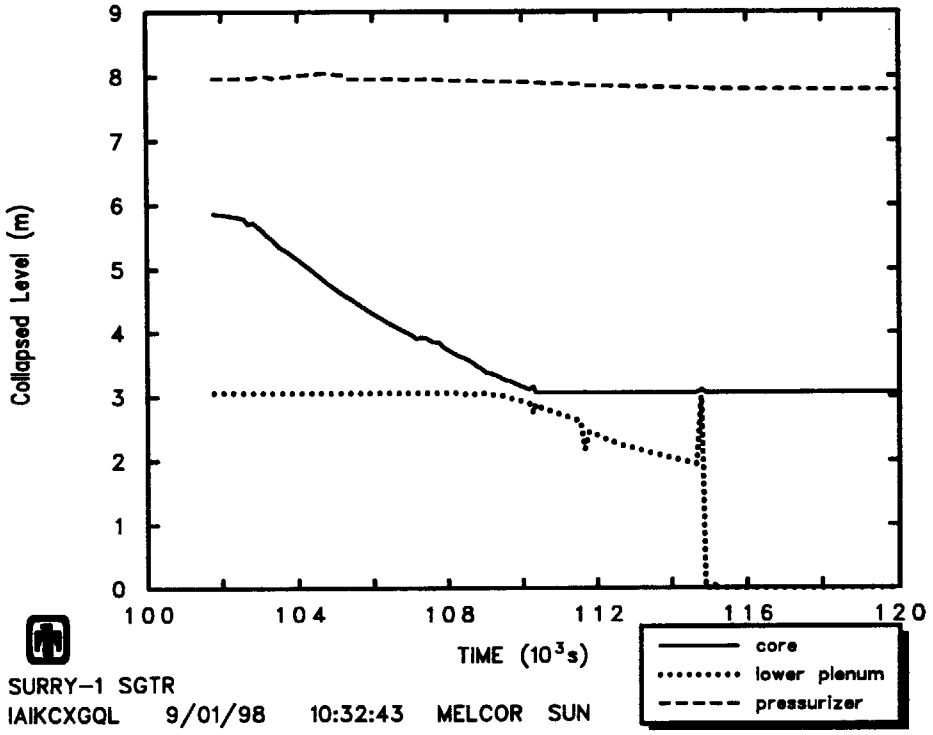

Fig. 3.3.3 Results from Natural Circulation Model -- Collapsed Level of Core, Lower Plenum and Pressurizer

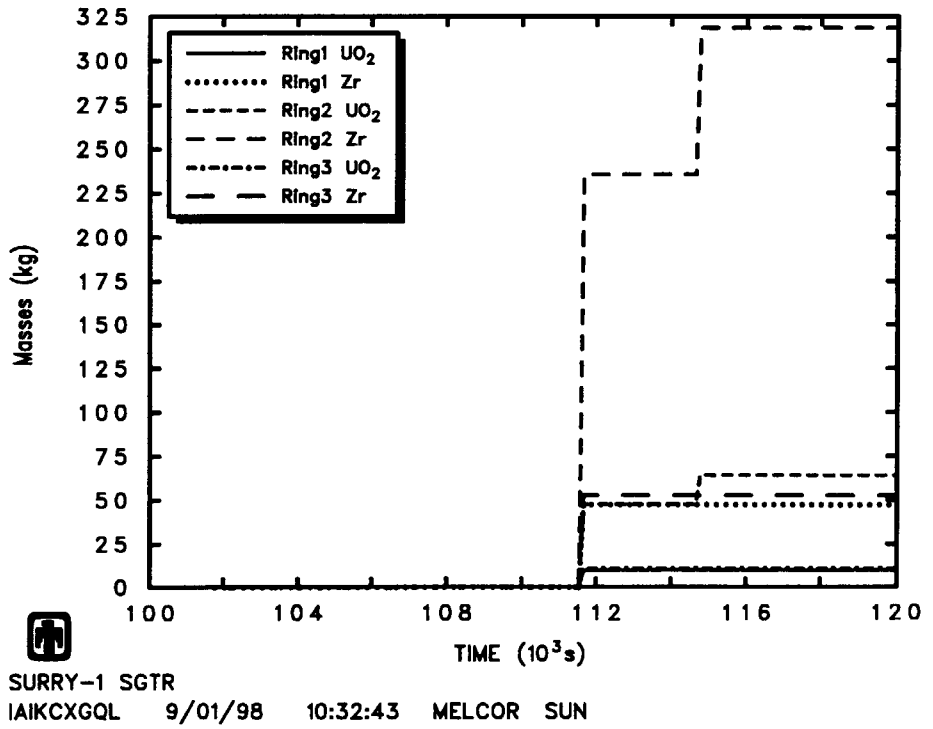

Fig. 3.3.4 Results from Natural Circulation Model -- the Masses of UO_2 and Zr at Level 3 Core Cell

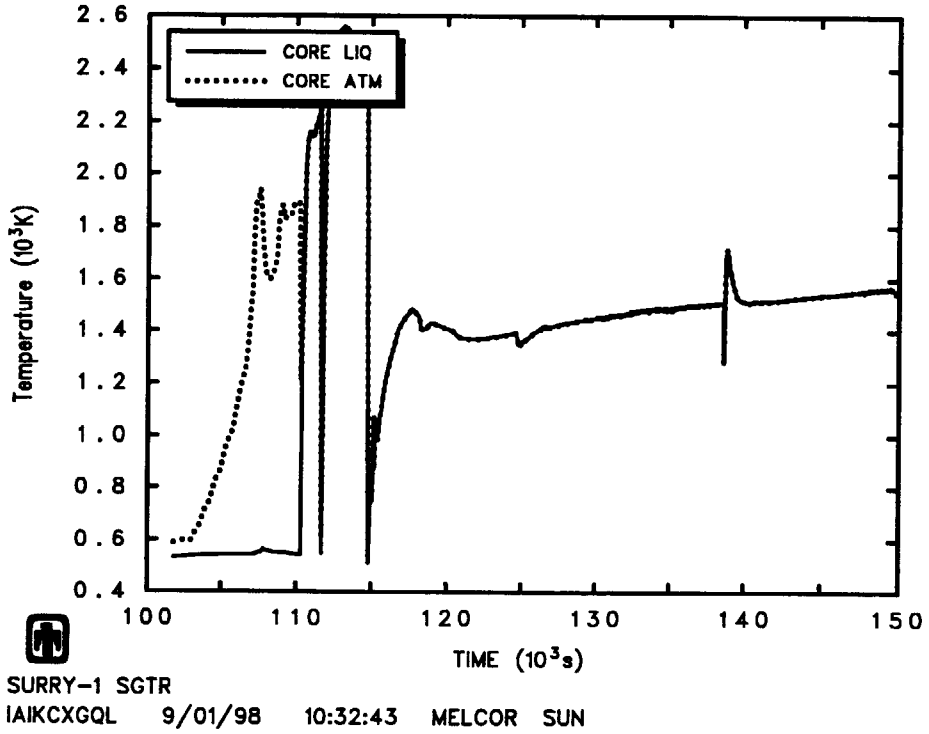

Fig. 3.3.5 Results from Natural Circulation Model -- Core Temperature

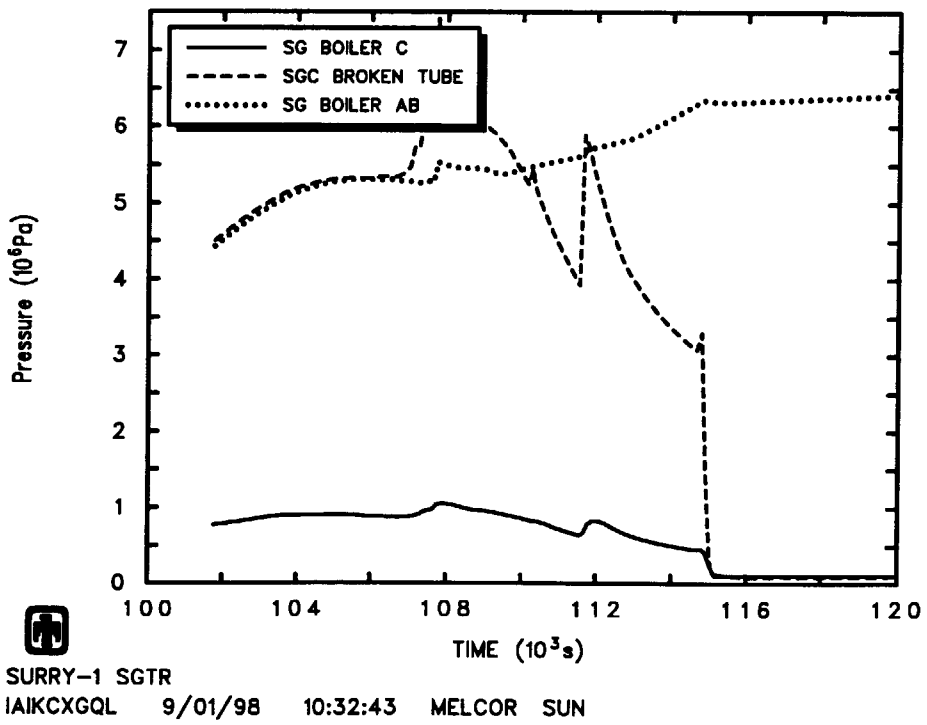

Fig. 3.3.6 Results from Natural Circulation Model -- Secondary System Pressure

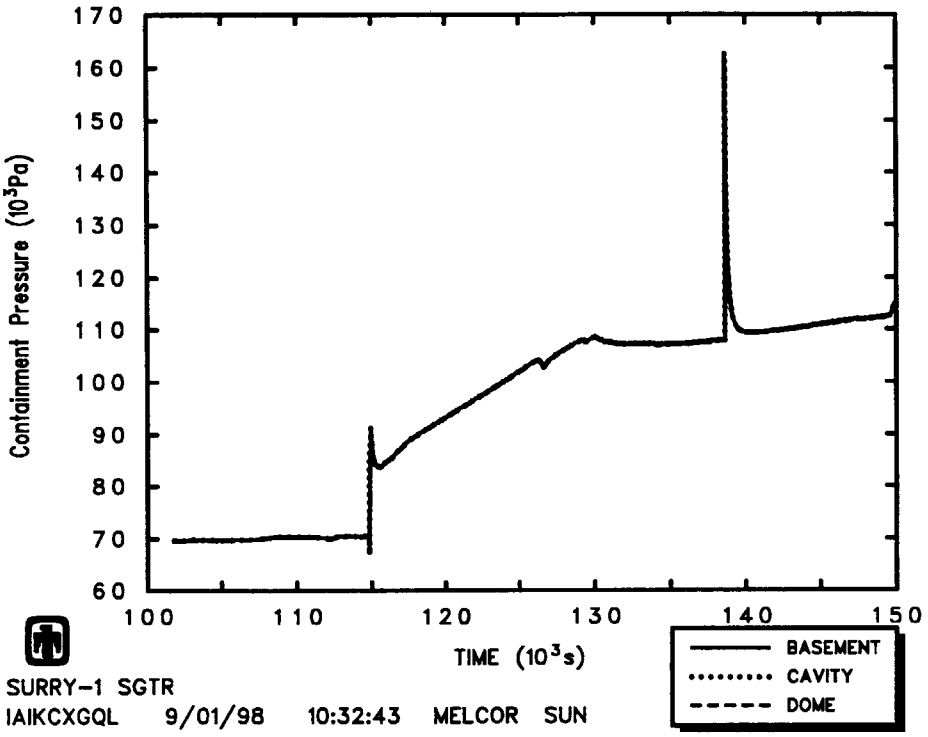

Fig. 3.3.7 Results from Natural Circulation Model -- Containment Pressure

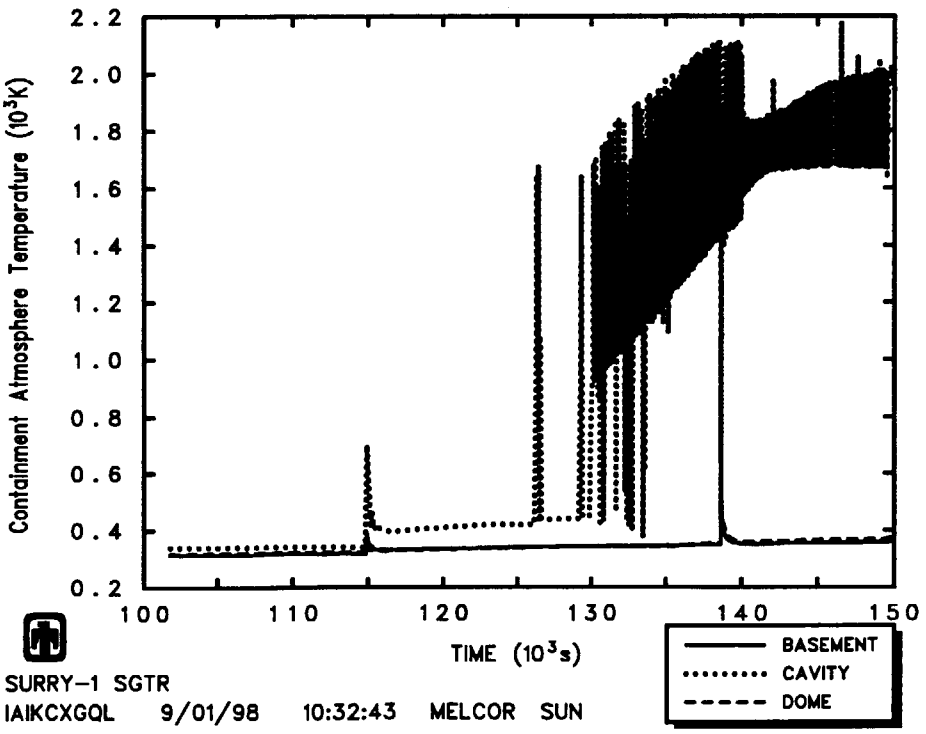

Fig. 3.3.8 Results from Natural Circulation Model -- Containment Atmosphere Temperature

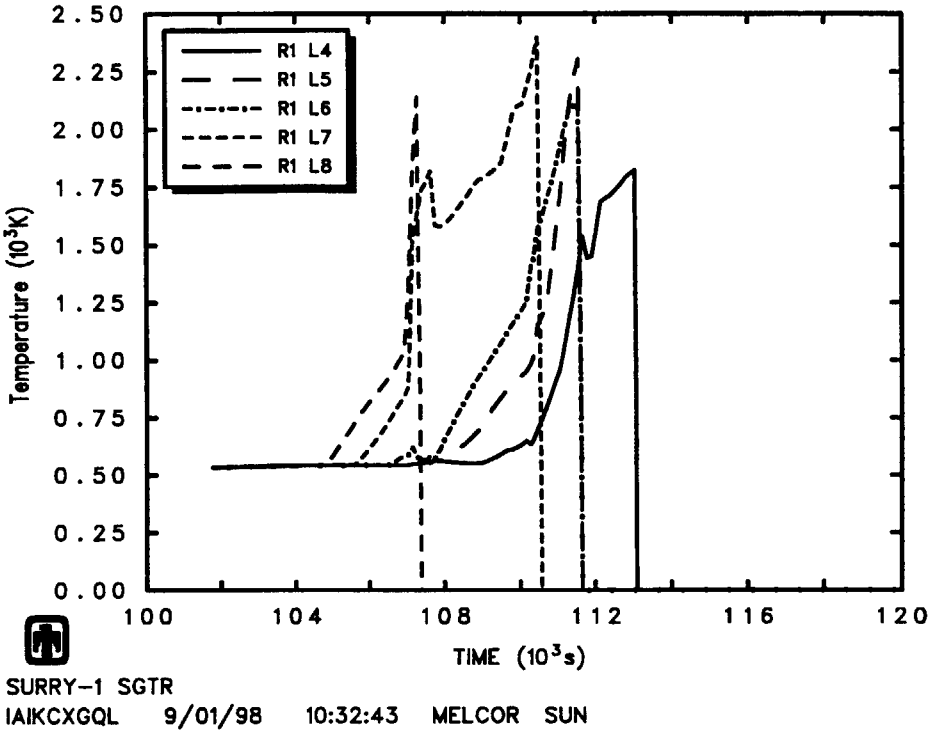

Fig. 3.3.9 Results from Natural Circulation Model --
Fuel Temperatures in Ring 1 Core Cells at Level 4 ~ Level 8

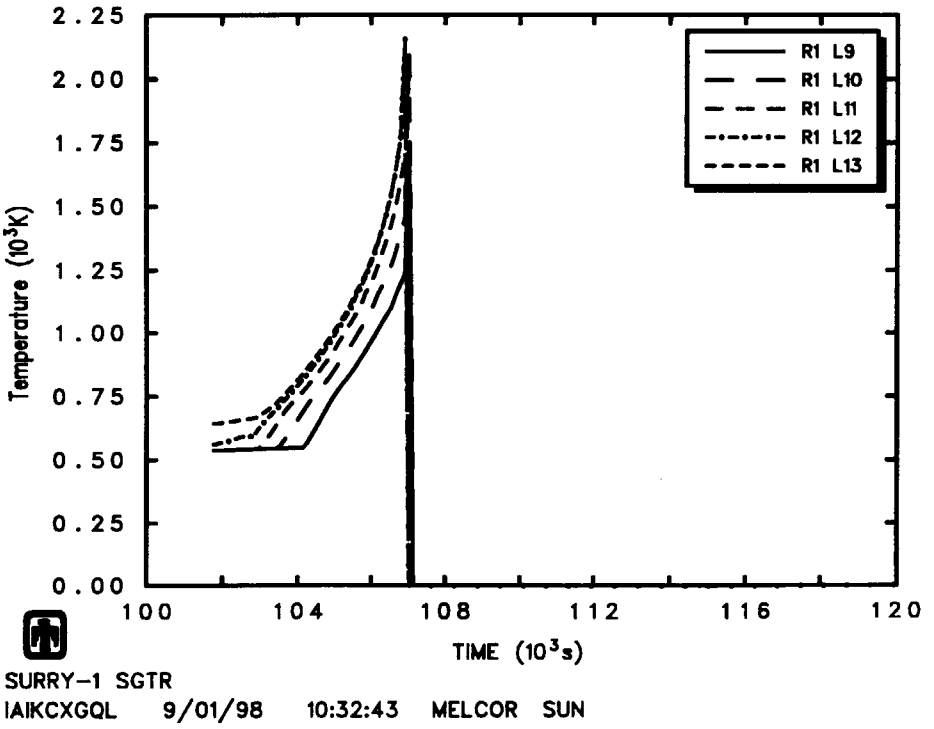

Fig. 3.3.10 Results from Natural Circulation Model --
Fuel Temperatures in Ring 1 Core Cells at Level 9 ~ Level 13

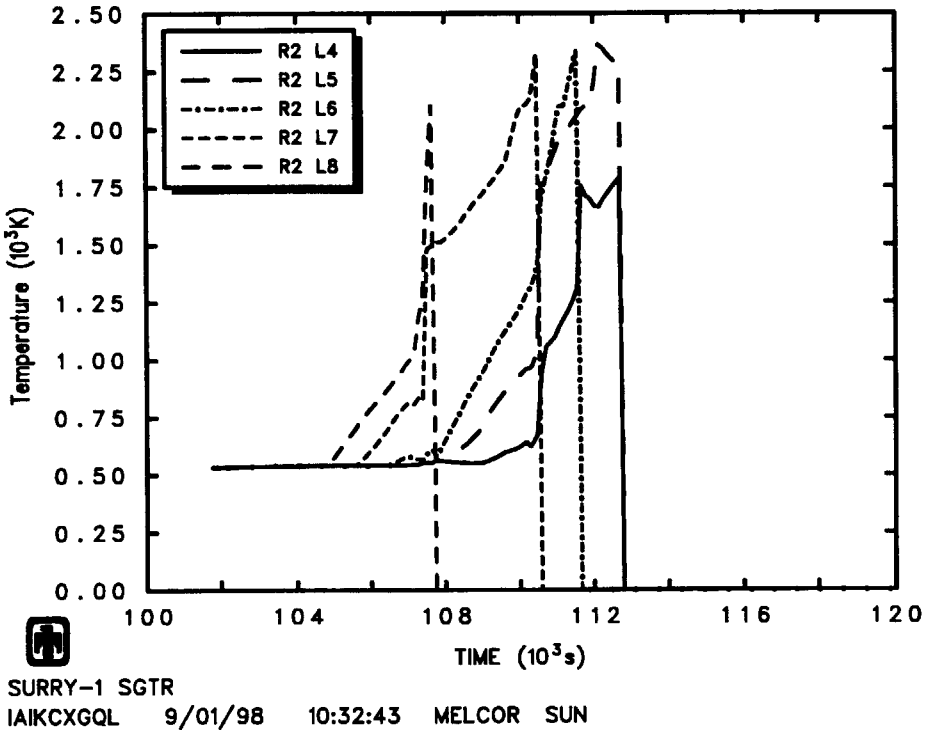

Fig. 3.3.11 Results from Natural Circulation Model --
Fuel Temperatures in Ring 2 Core Cells at Level 4 ~ Level 8

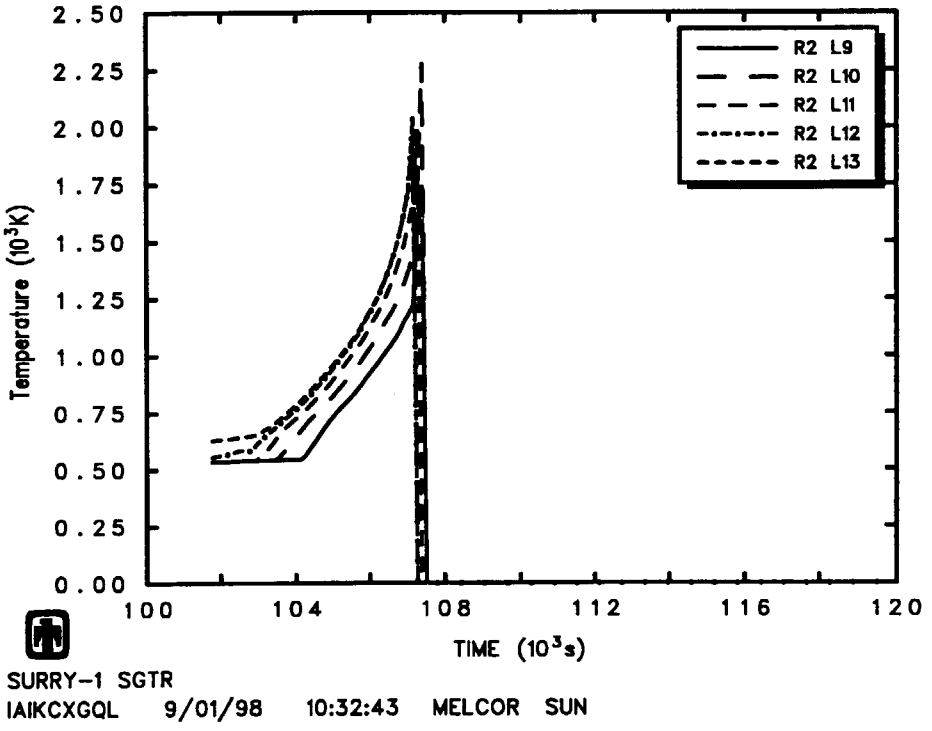

Fig. 3.3.12 Results from Natural Circulation Model --
Fuel Temperatures in Ring 2 Core Cells at Level 9 ~ Level 13

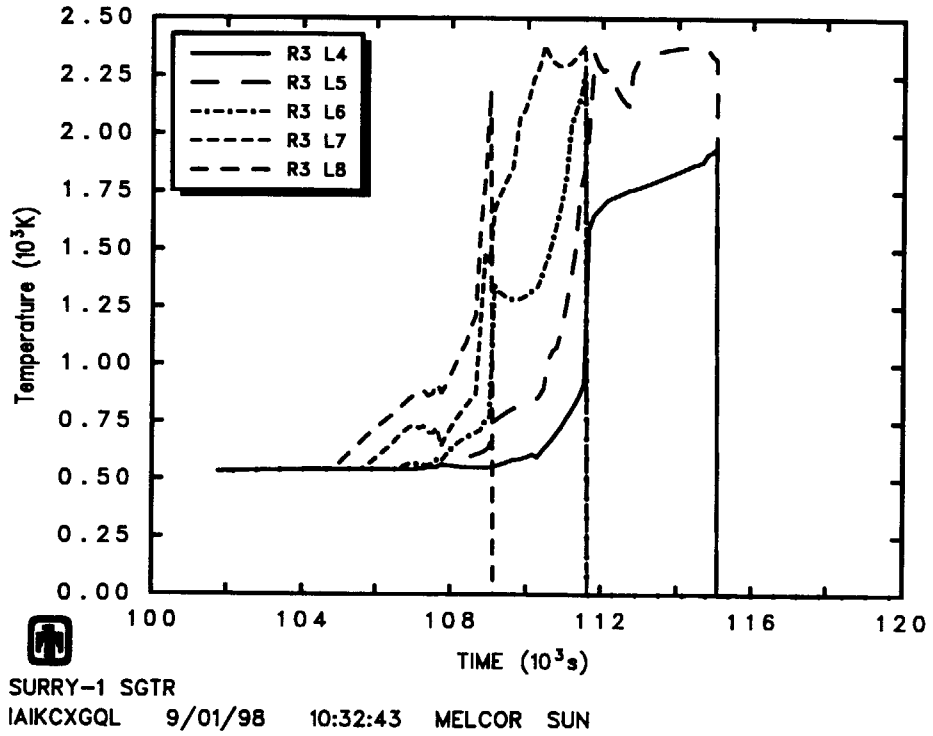

Fig. 3.3.13 Results from Natural Circulation Model --
Fuel Temperatures in Ring 3 Core Cells at Level 4 ~ Level 8

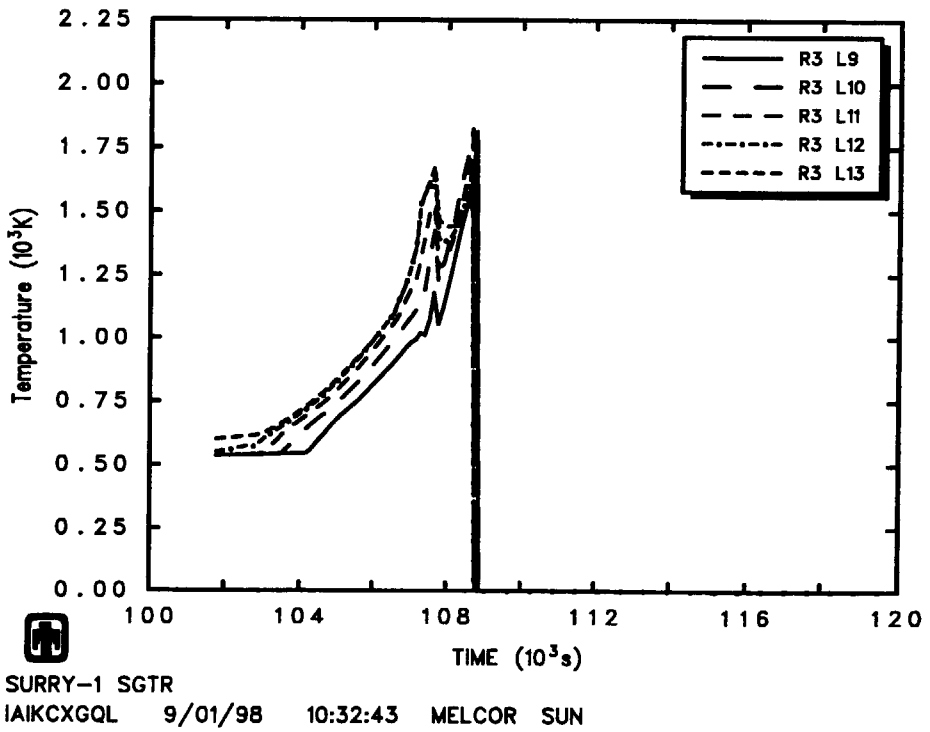

Fig. 3.3.14 Results from Natural Circulation Model --
Fuel Temperatures in Ring 3 Core Cells at Level 9 ~ Level 13

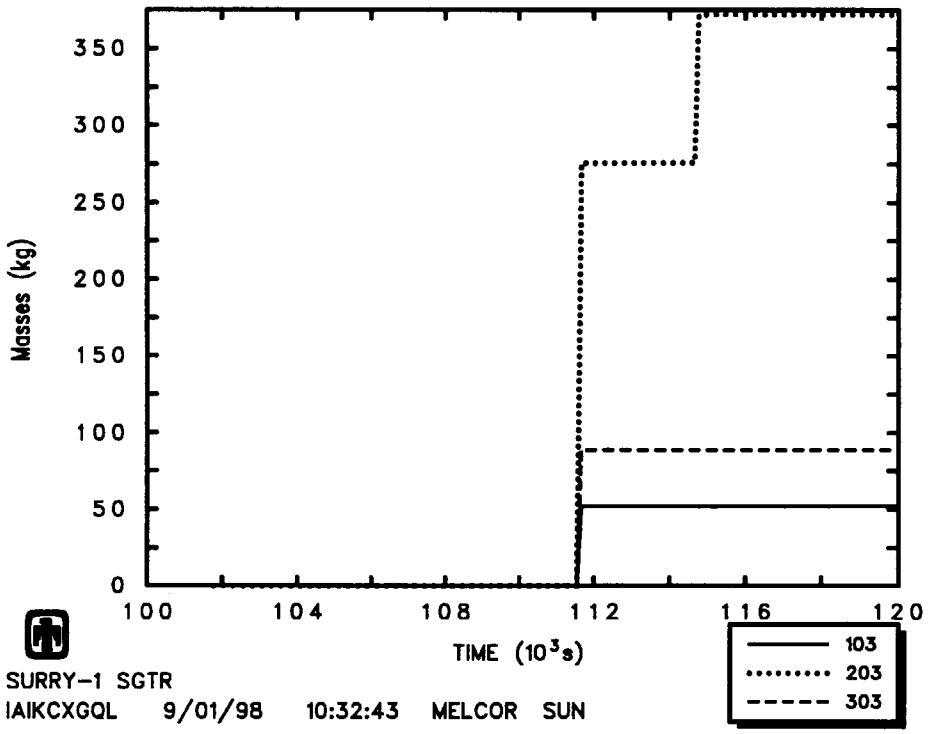

Fig. 3.3.15 Results from Natural Circulation Model -- ZrO_2 Masses at Level 3 Core Cells

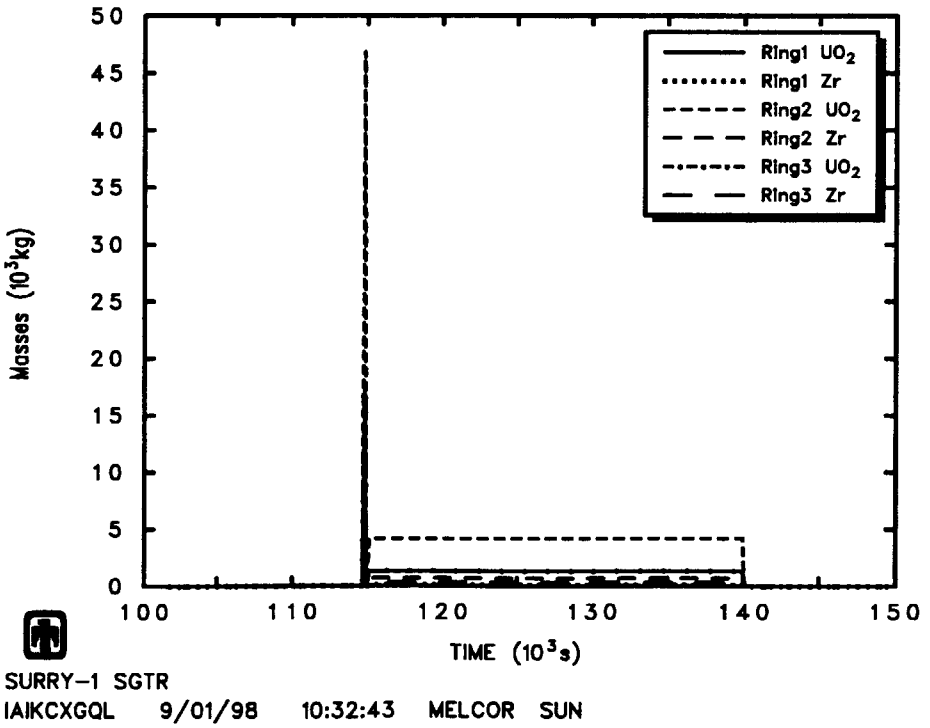

Fig. 3.3.16 Results from Natural Circulation Model -- UO_2 & Zr Masses at Level 1 Core Cells

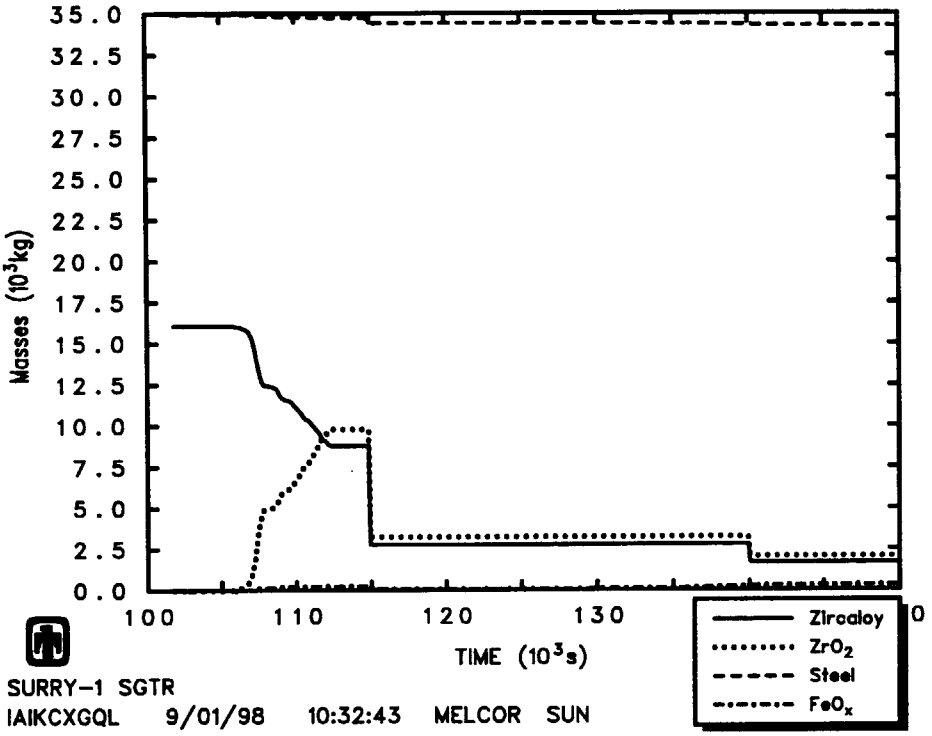

Fig. 3.3.17 Results from Natural Circulation Model -- Total Metal Material Masses in Core

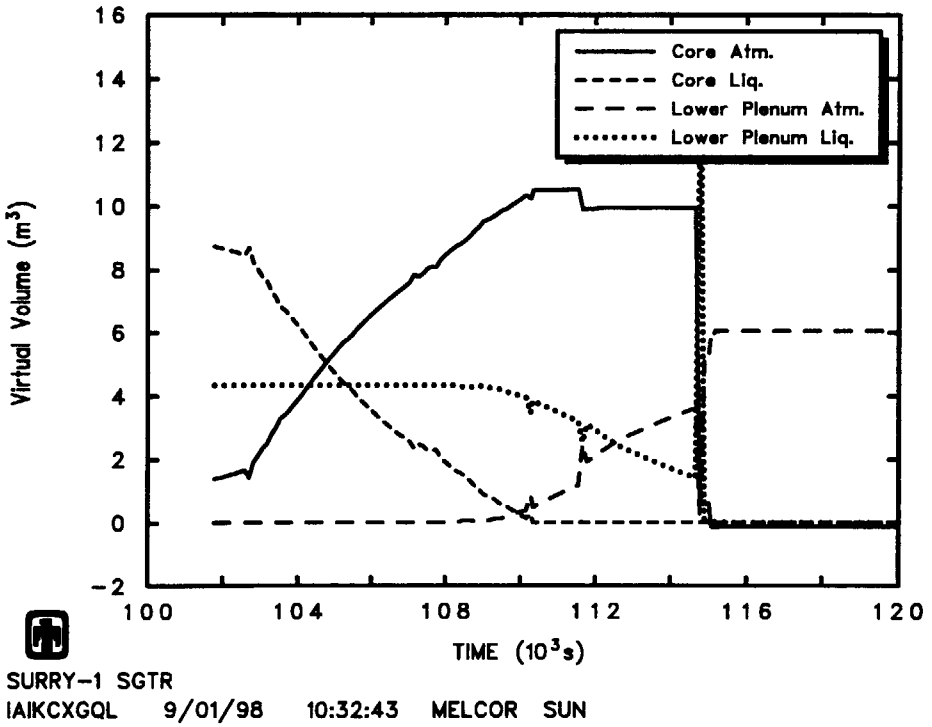

Fig. 3.3.18 Results from Natural Circulation Model -- the Core and Lower Plenum Virtual Volume

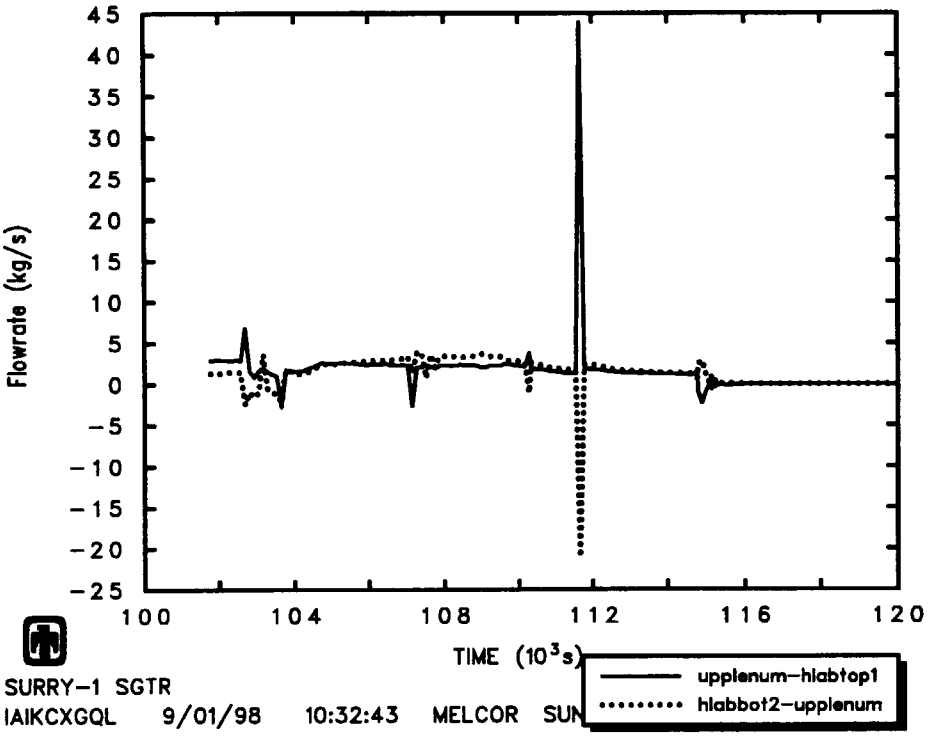

Fig. 3.3.19 Results from Natural Circulation Model --
Natural Circulation Flowrates between Upper Plenum and Hot Leg in Loop AB

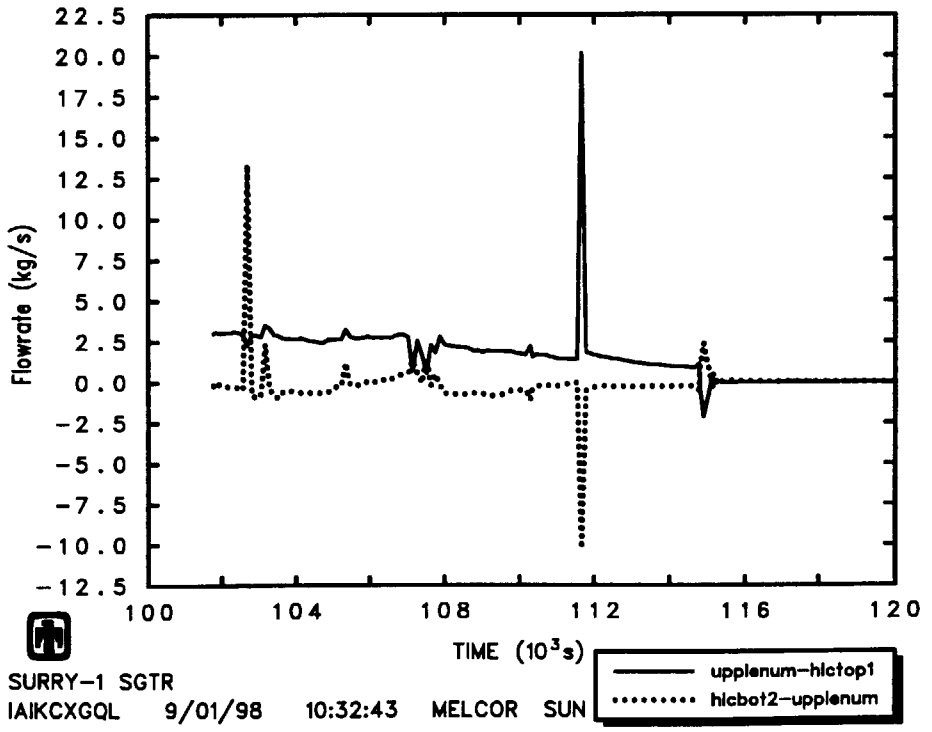

Fig. 3.3.20 Results from Natural Circulation Model --
Natural Circulation Flowrates between Upper Plenum and Hot Leg in Loop C

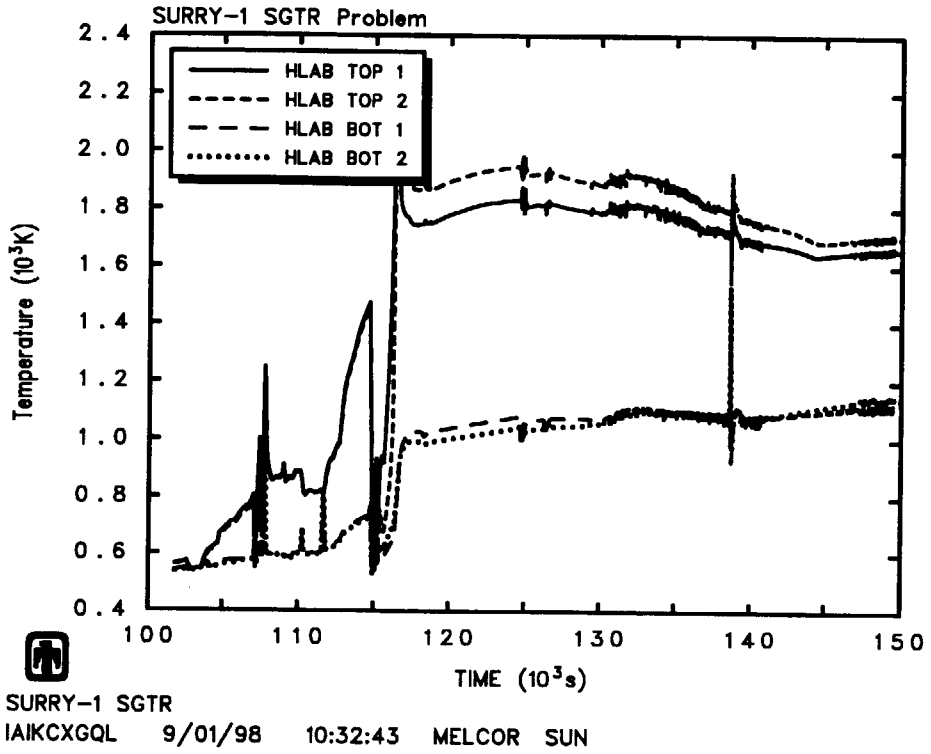

Fig. 3.3.21 Results from Natural Circulation Model -- Atmosphere Temperatures in Control Volumes of Hot Leg in Loop AB

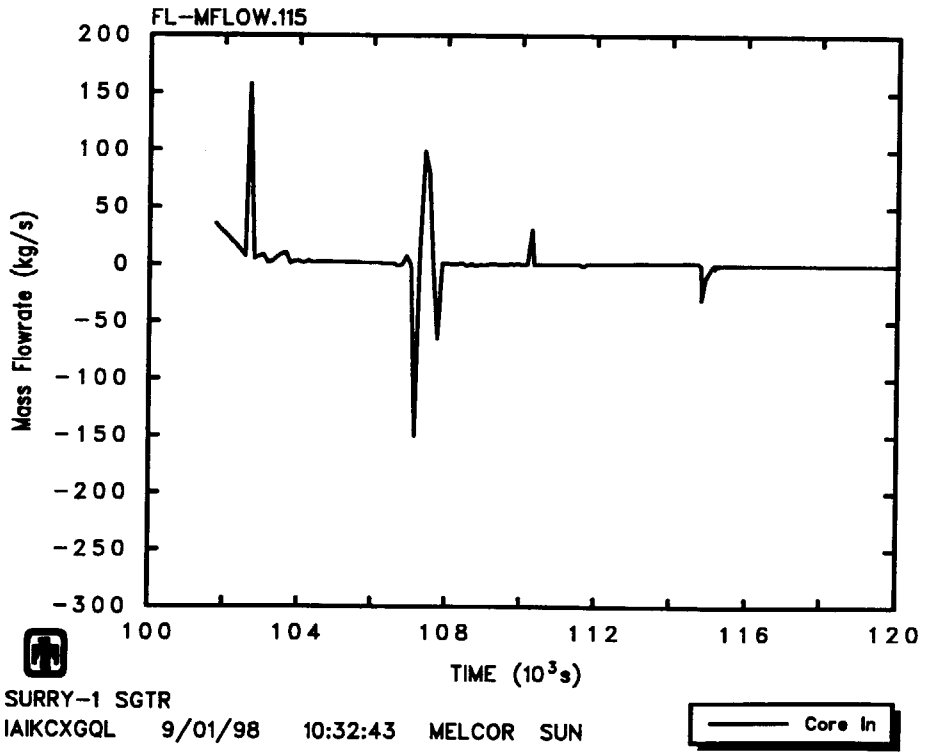

Fig. 3.3.22 Results from Natural Circulation Model -- Inlet Core Mass Flowrate

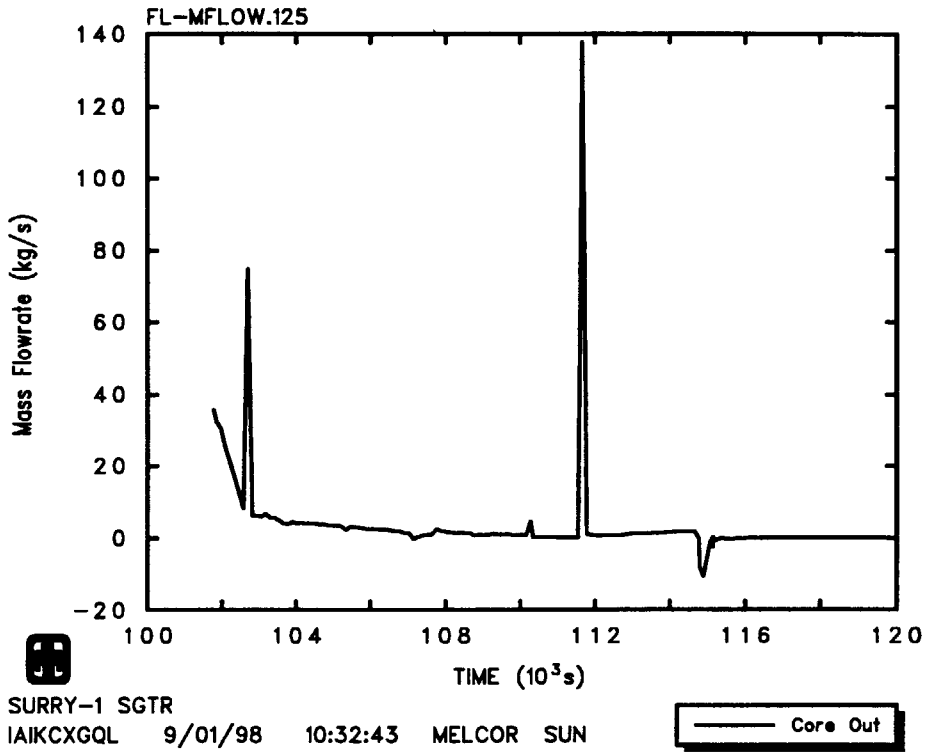

Fig. 3.3.23 Results from Natural Circulation Model -- Outlet Core Mass Flowrate

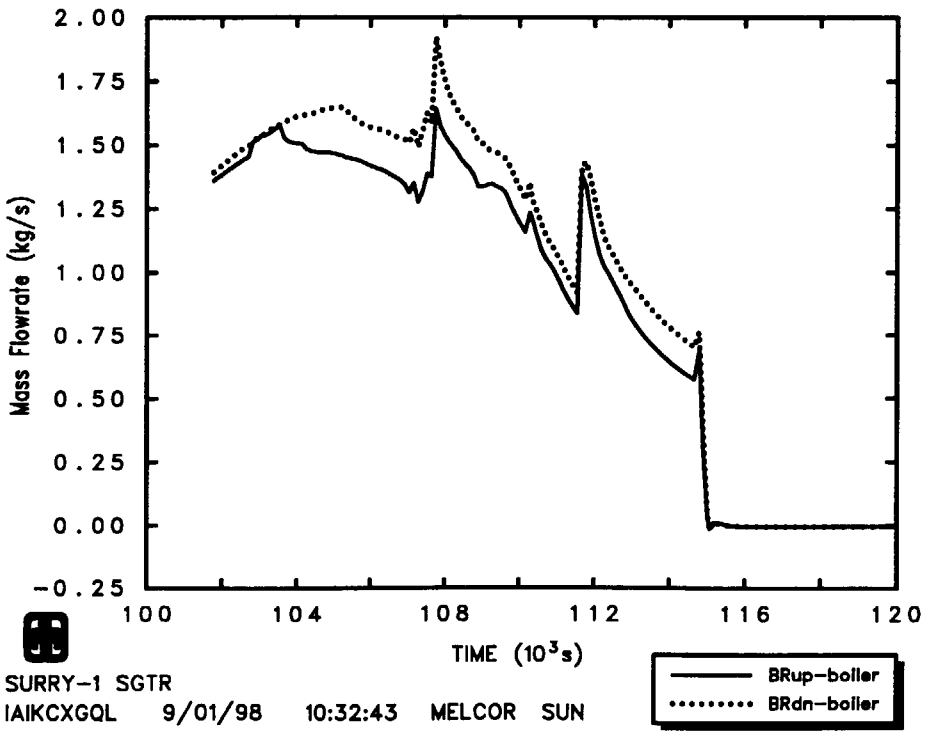

Fig. 3.3.24 Results from Natural Circulation Model -- Break Flowrates from Broken Tube

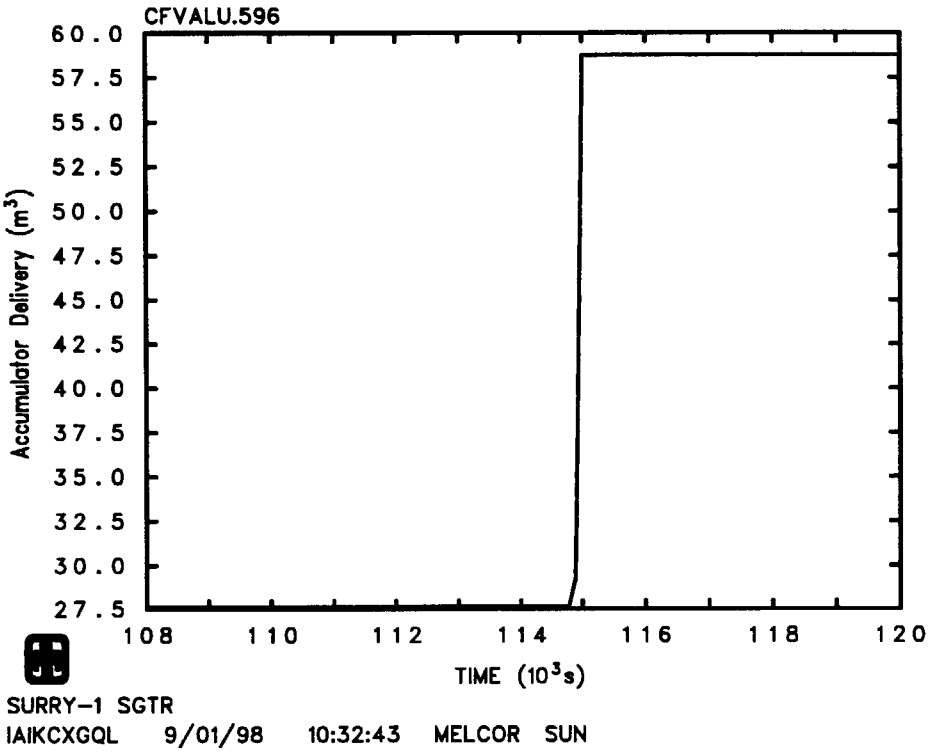

Fig. 3.3.25 Results from Natural Circulation Model -- Accumulator Delivery

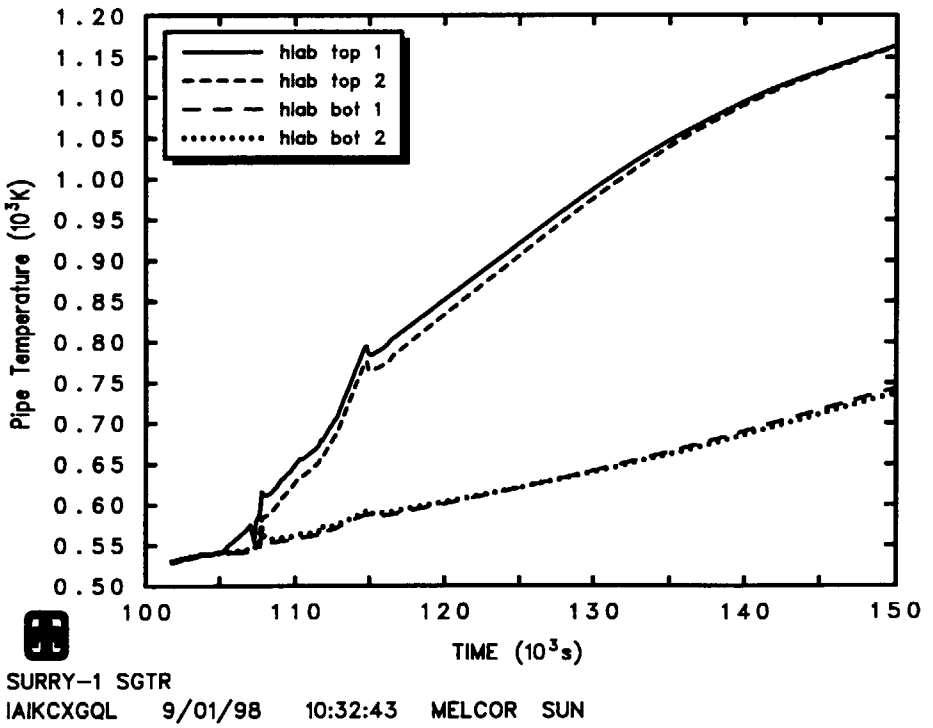

Fig. 3.3.26 Results from Natural Circulation Model -- Hot Leg Pipe Temperatures in Loop AB

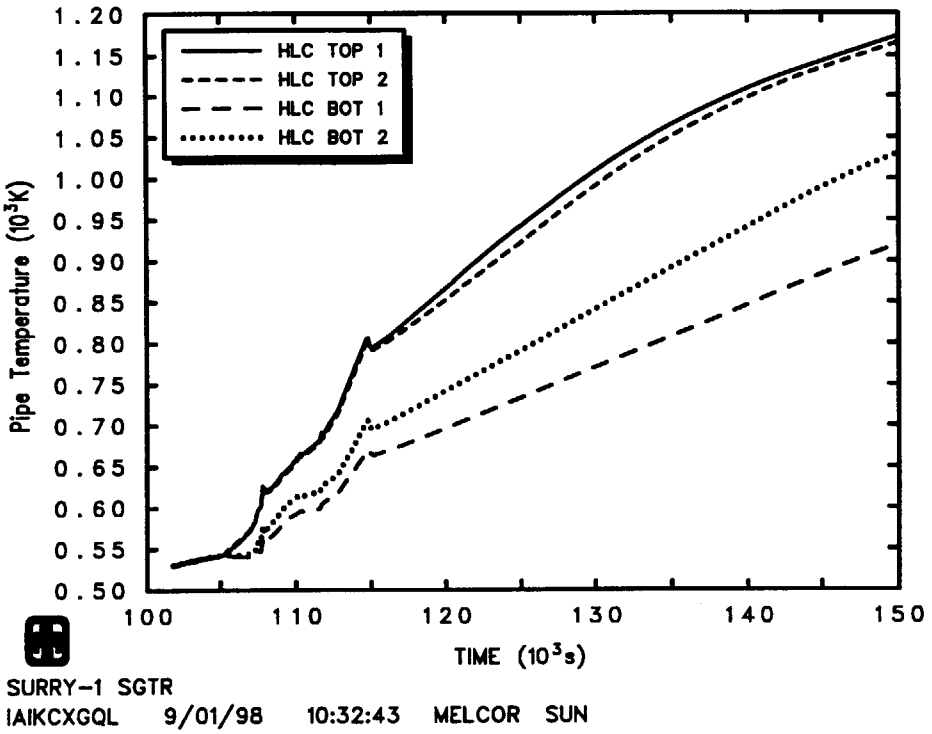

Fig. 3.3.27 Results from Natural Circulation Model -- Hot Leg Pipe Temperatures in Loop C

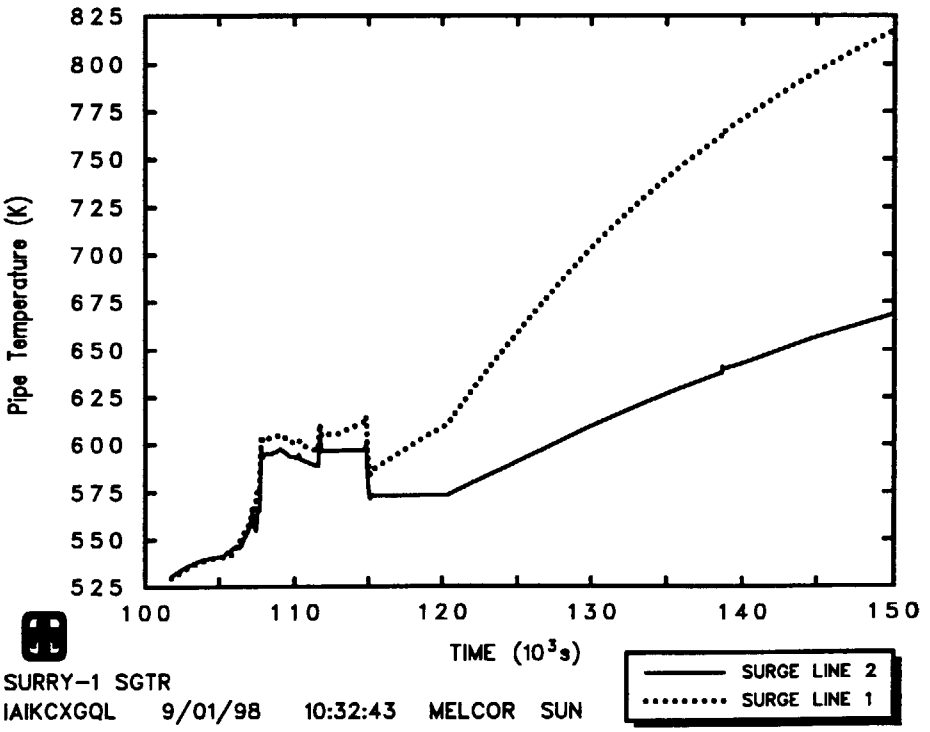

Fig. 3.3.28 Results from Natural Circulation Model -- Surge Line Pipe Temperature

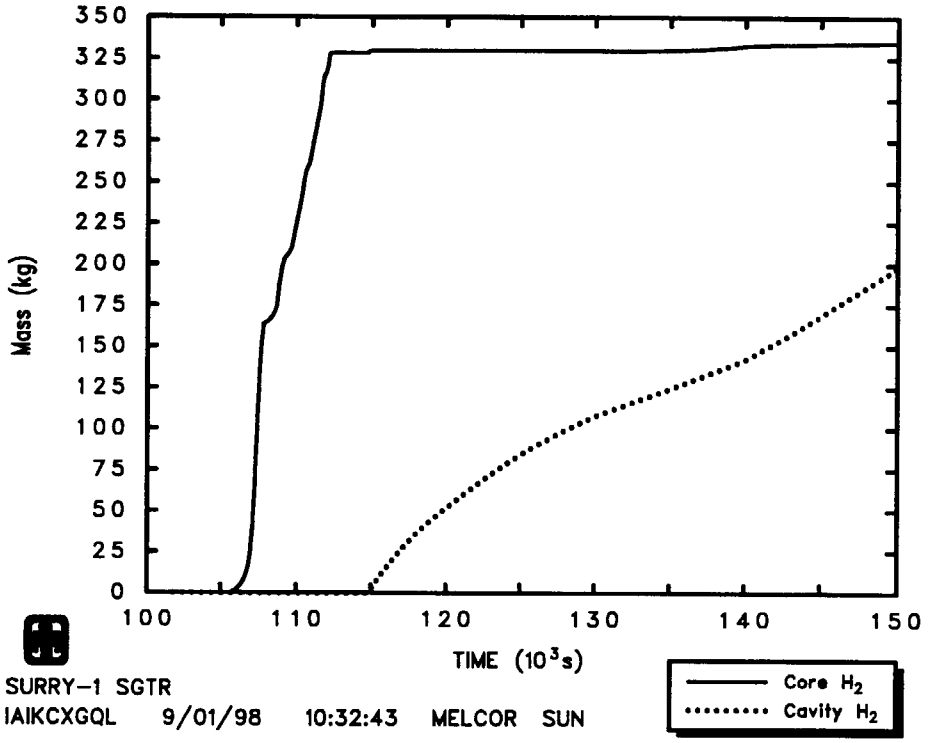

Fig. 3.3.29 Results from Natural Circulation Model -- H_2 Production in Core and Cavity

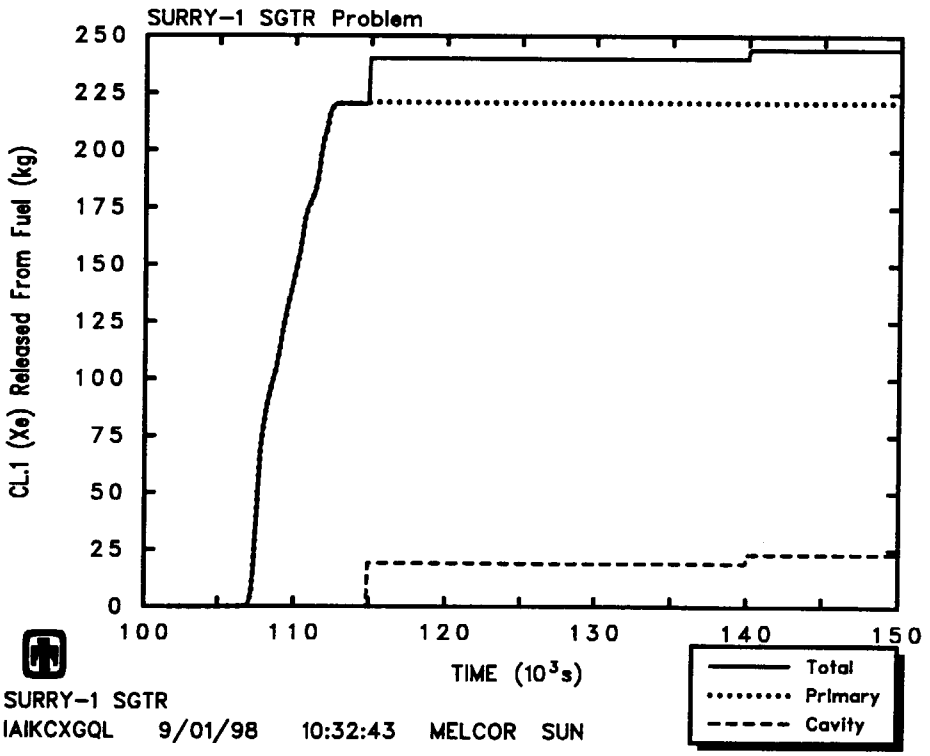

Fig. 3.3.30 Results from Natural Circulation Model -- RN Released from Fuel (Xe)

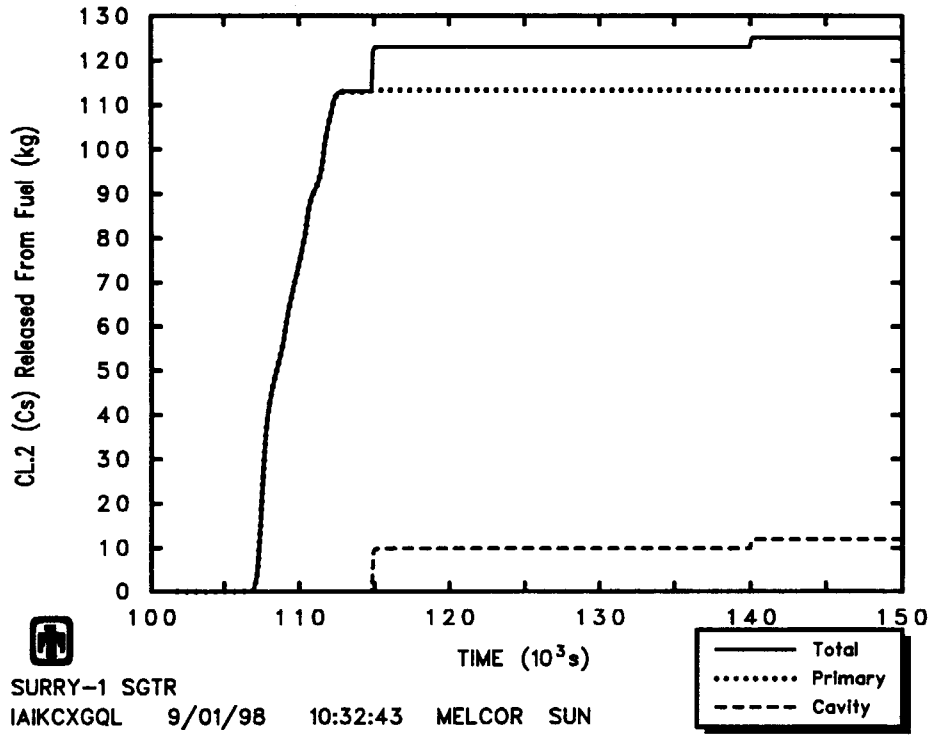

Fig. 3.3.31 Results from Natural Circulation Model -- RN Released from Fuel (Cs)

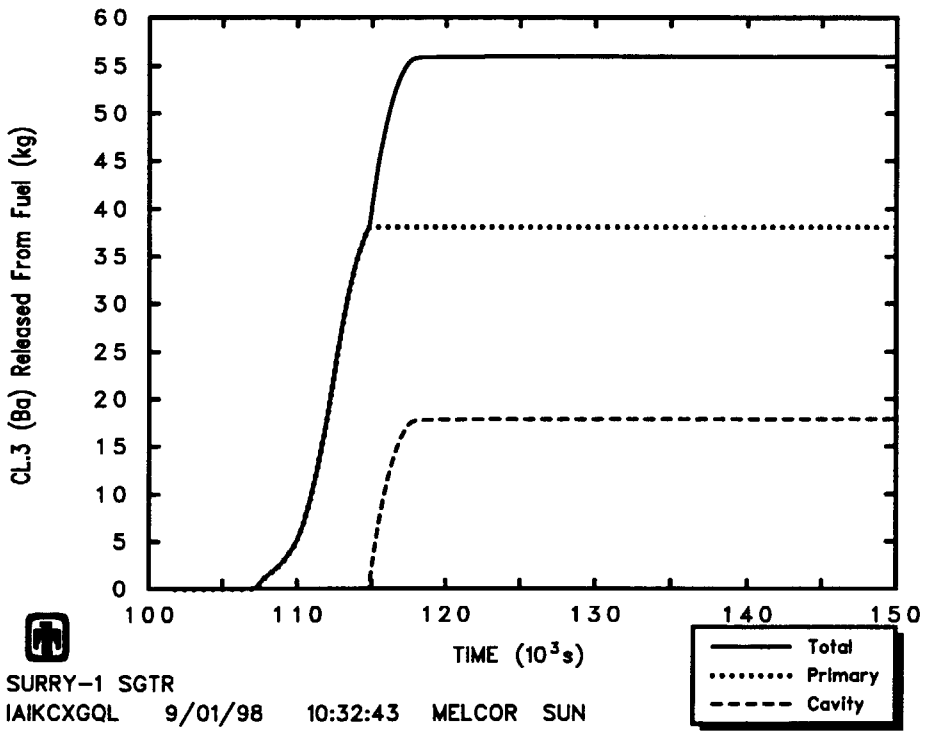

Fig. 3.3.32 Results from Natural Circulation Model -- RN Released from Fuel (Ba)

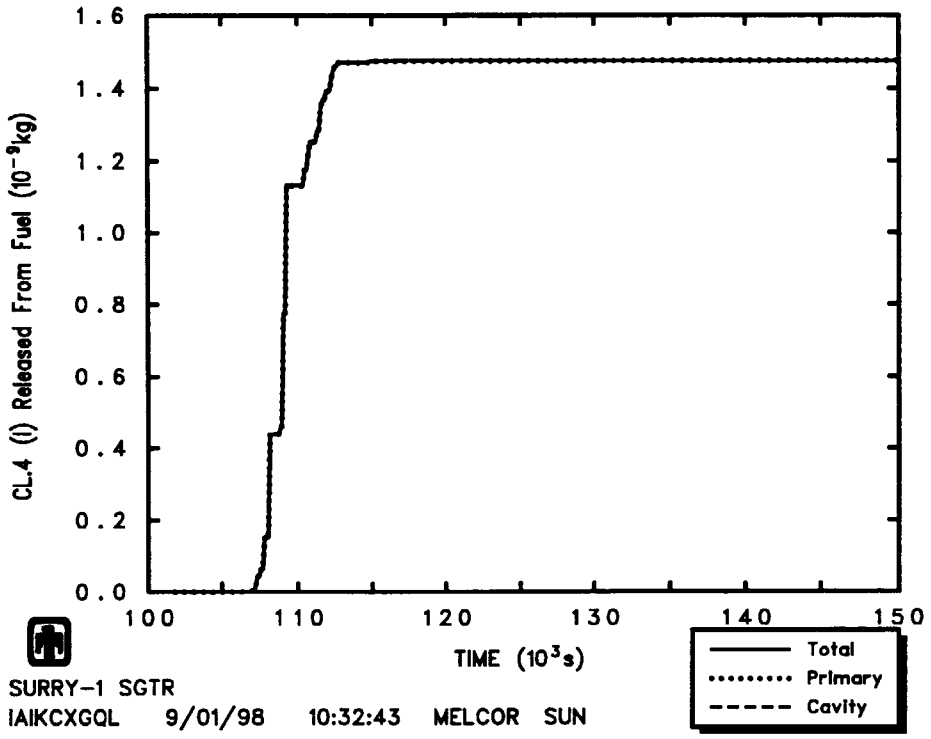

Fig. 3.3.33 Results from Natural Circulation Model -- RN Released from Fuel (I)

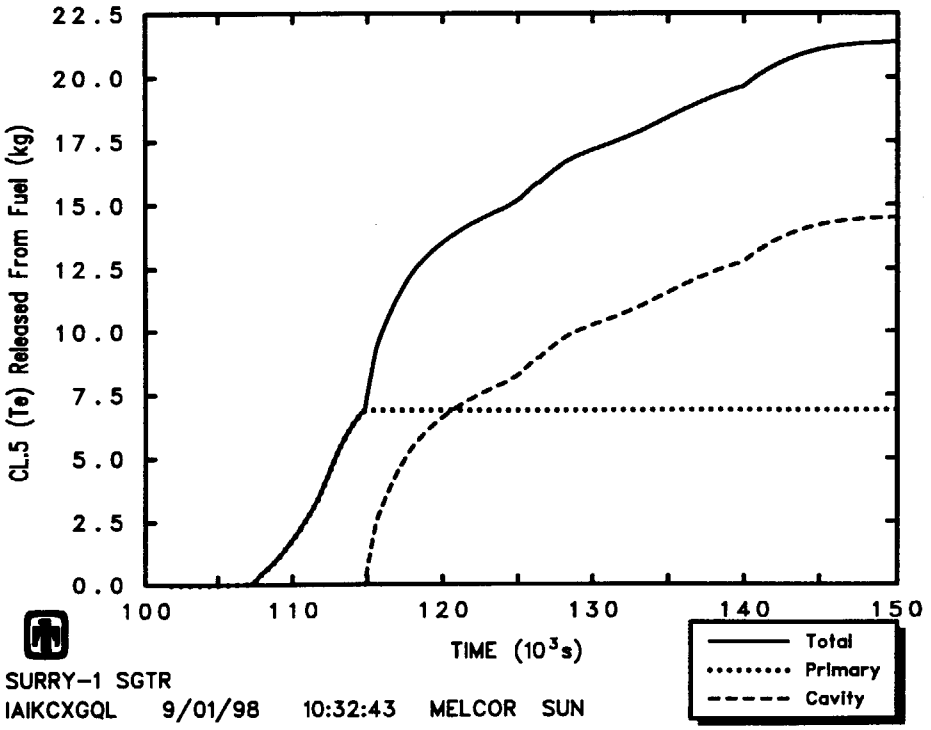

Fig. 3.3.34 Results from Natural Circulation Model -- RN Released from Fuel (Te)

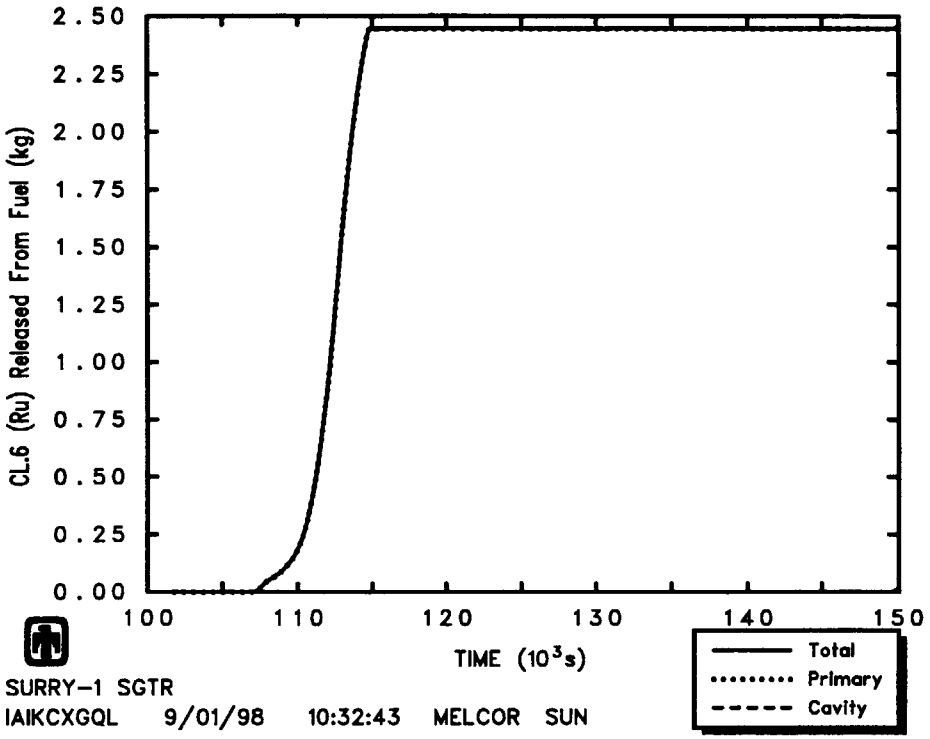

Fig. 3.3.35 Results from Natural Circulation Model -- RN Released from Fuel (Ru)

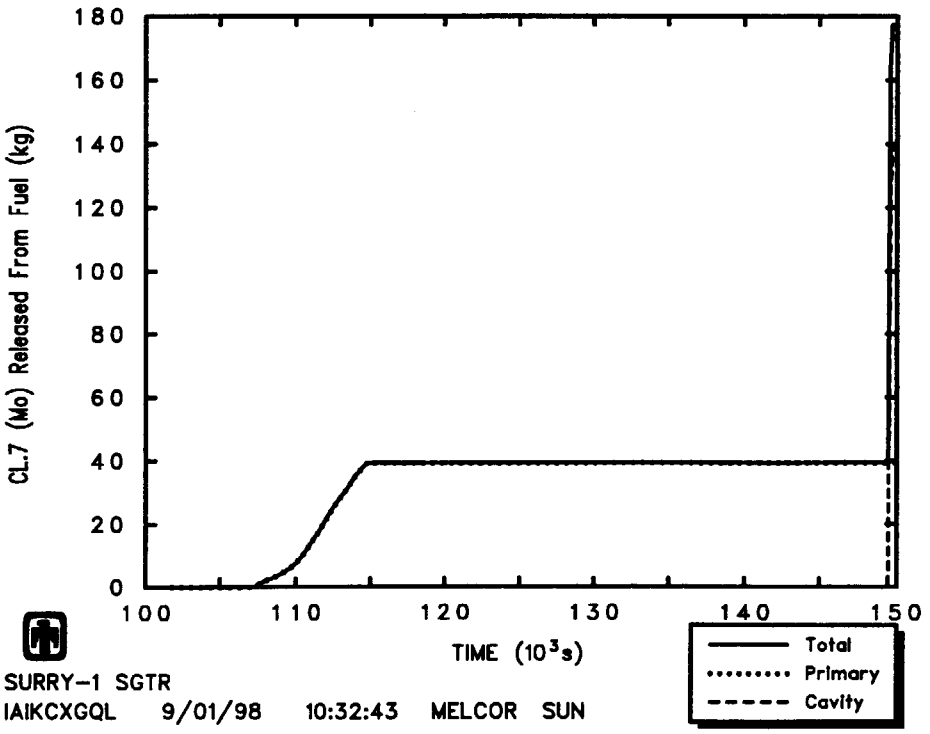

Fig. 3.3.36 Results from Natural Circulation Model -- RN Released from Fuel (Mo)

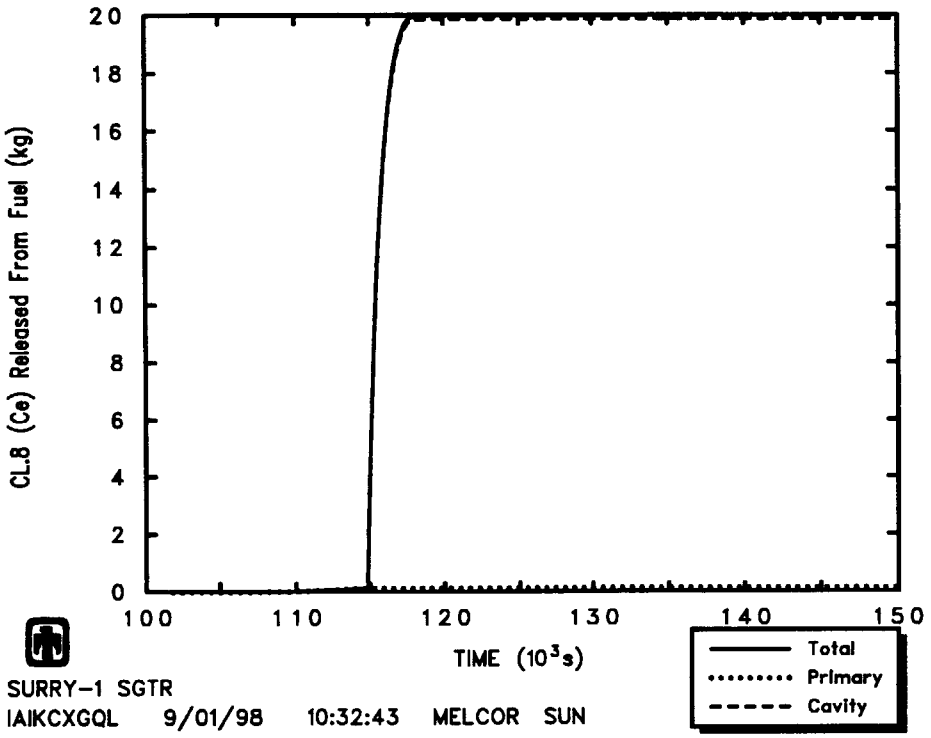

Fig. 3.3.37 Results from Natural Circulation Model -- RN Released from Fuel (Ce)

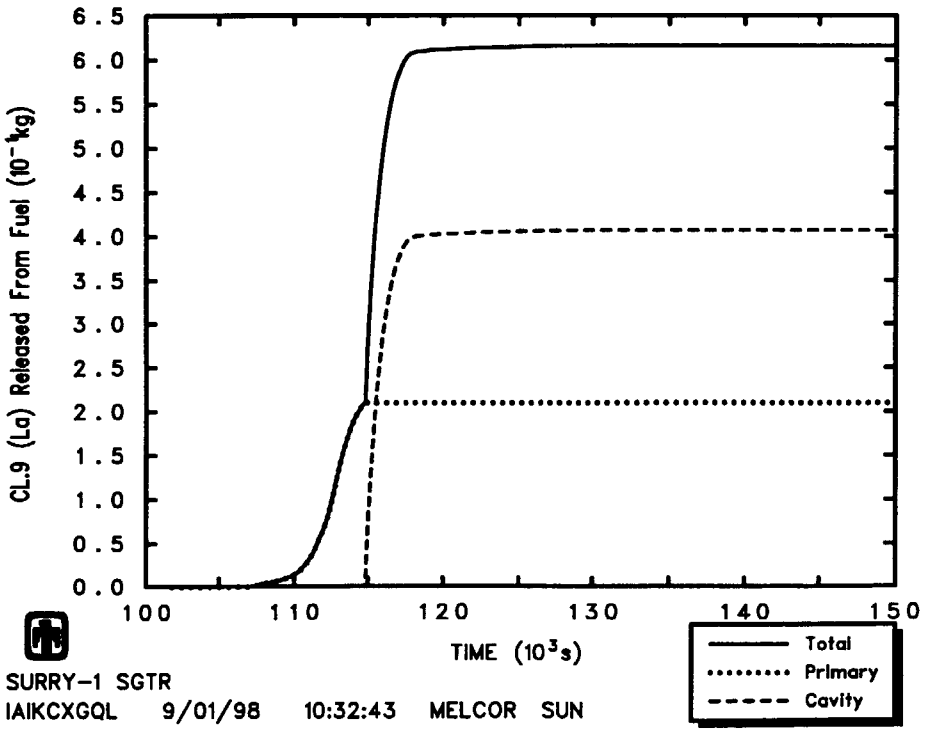

Fig. 3.3.38 Results from Natural Circulation Model -- RN Released from Fuel (La)

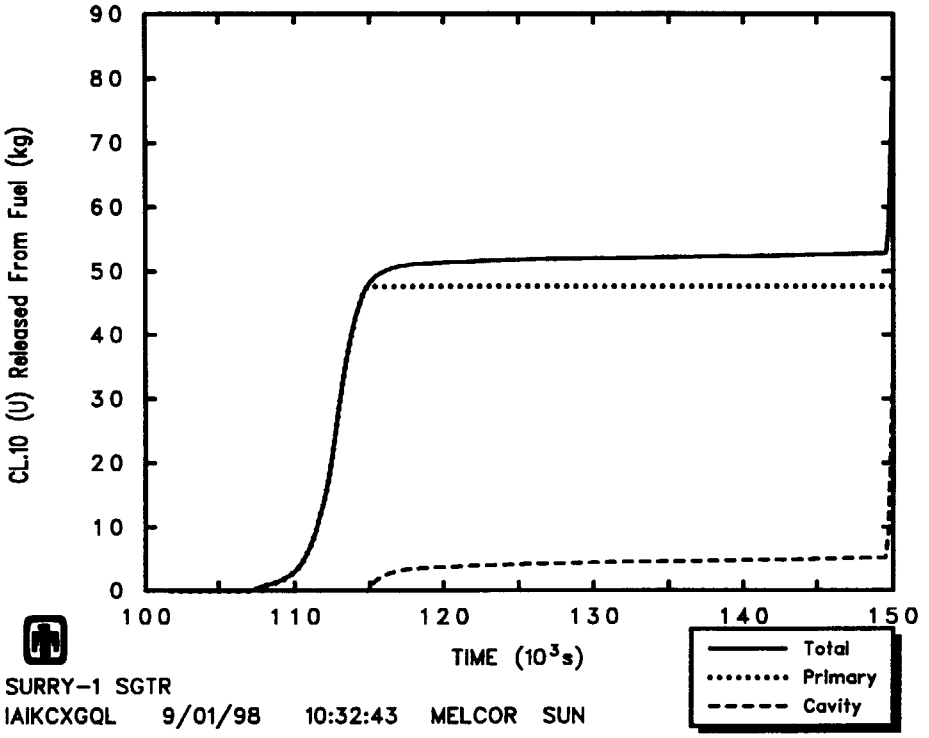

Fig. 3.3.39 Results from Natural Circulation Model -- RN Released from Fuel (U)

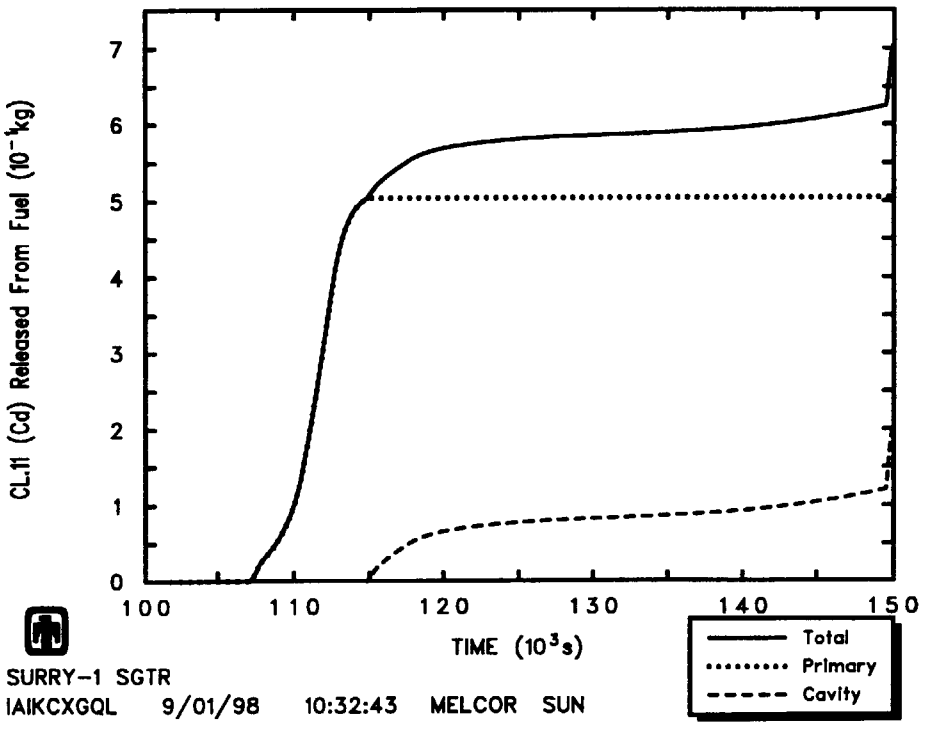

Fig. 3.3.40 Results from Natural Circulation Model -- RN Released from Fuel (Cd)

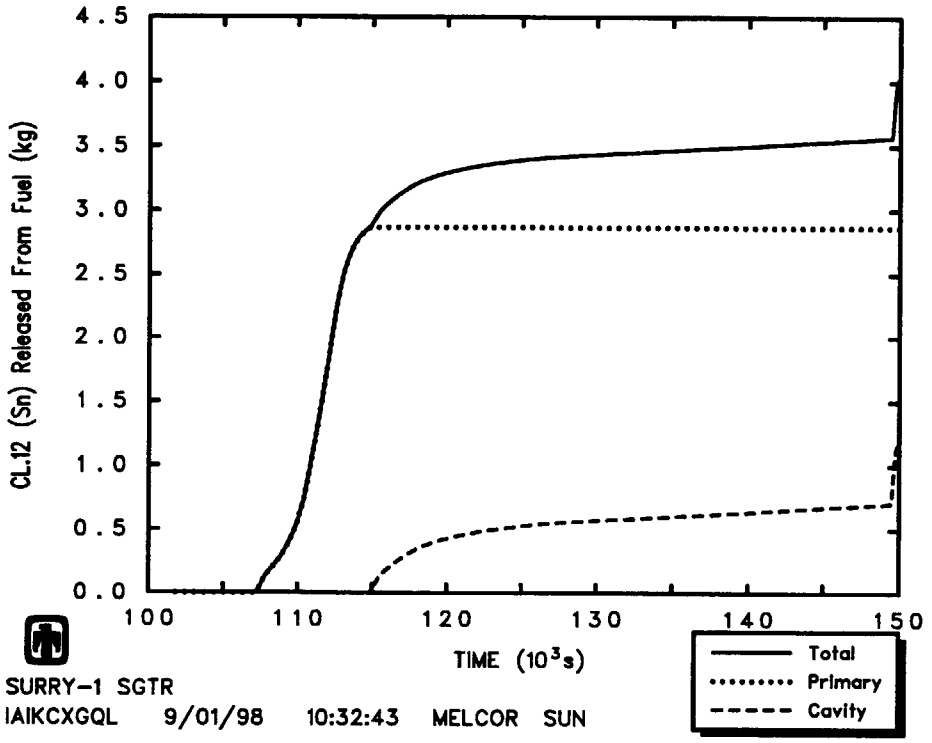

Fig. 3.3.41 Results from Natural Circulation Model -- RN Released from Fuel (Sn)

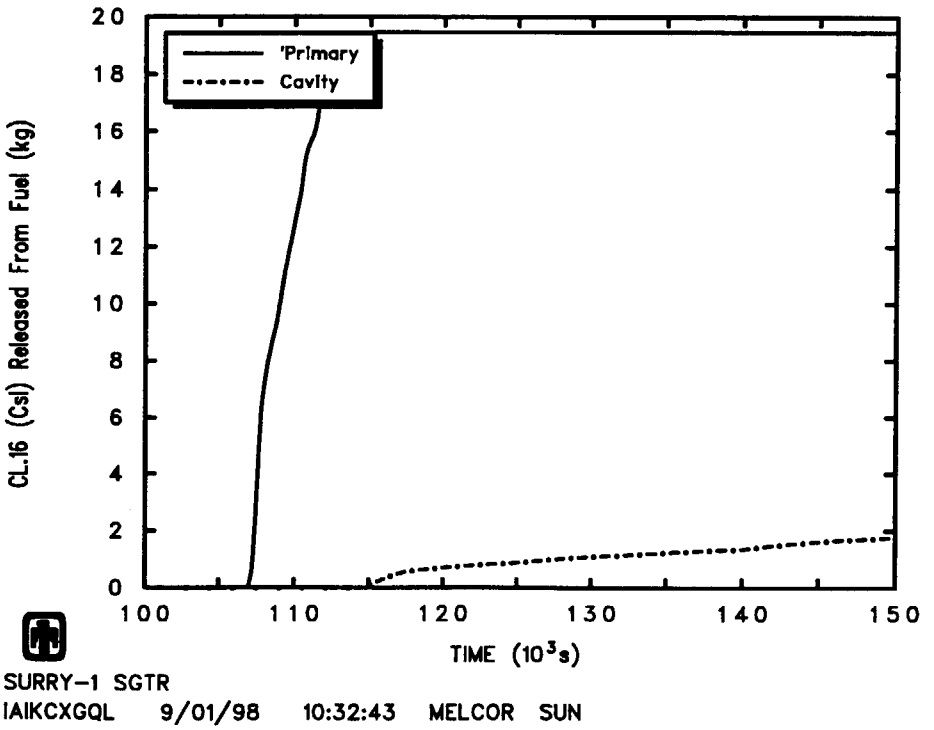

Fig. 3.3.42 Results from Natural Circulation Model -- RN Released from Fuel (CsI)

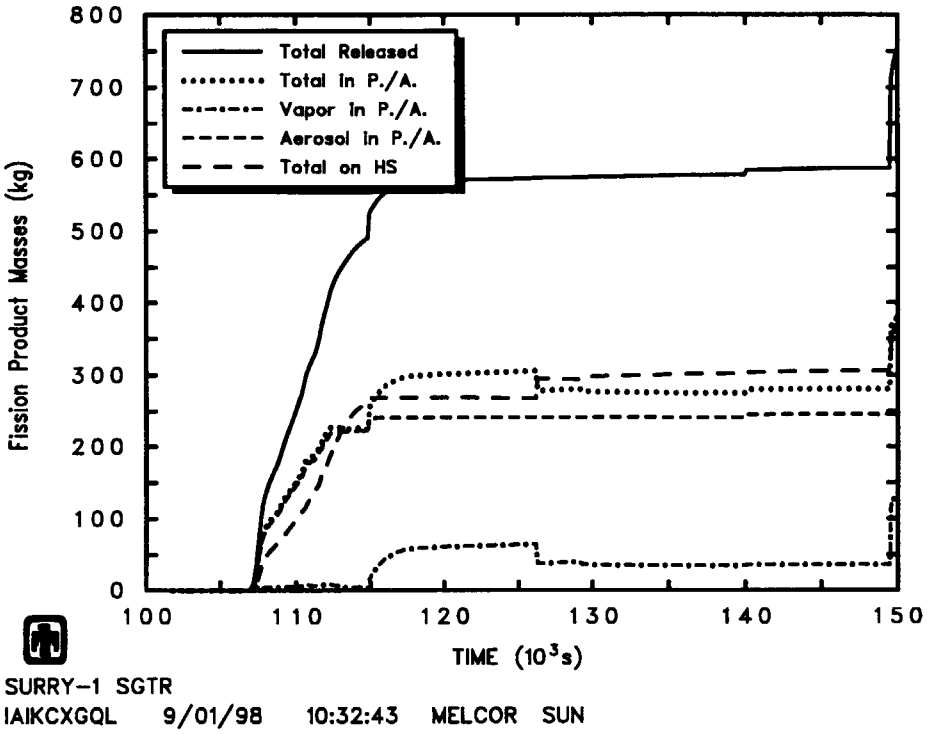

Fig. 3.3.43 Results from Natural Circulation Model -- Fission Products Mass Distribution

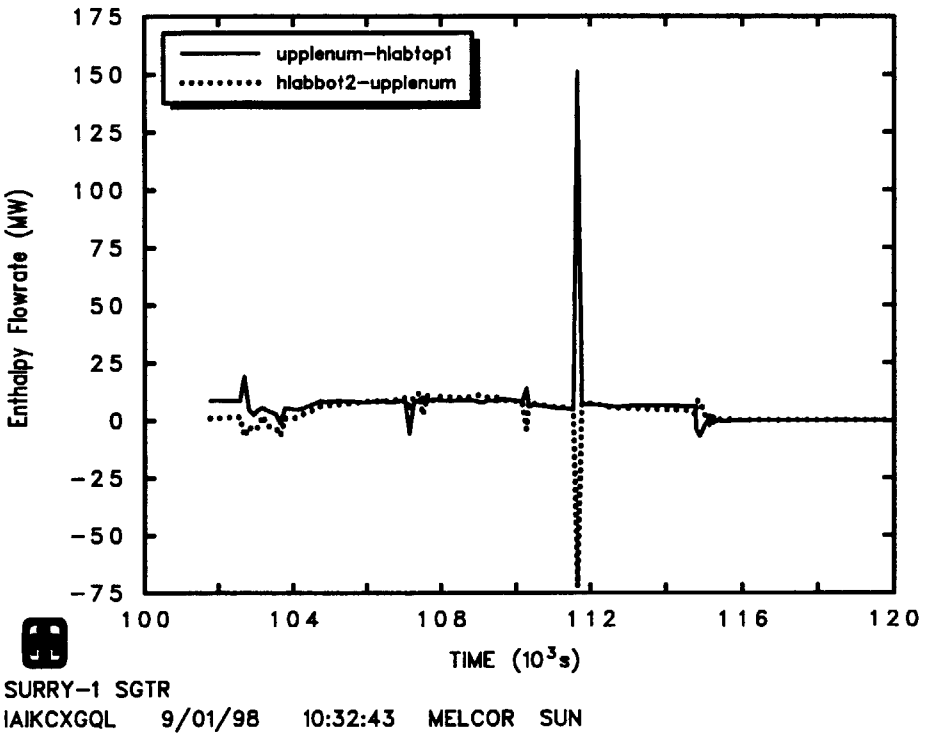

Fig. 3.4.1 Natural Circulation Enthalpy Flowrate Difference between Upper Plenum and Hot Leg AB

This is a blank page.

国際単位系 (SI) と換算表

表 1　SI 基本単位および補助単位

量	名称	記号
長さ	メートル	m
質量	キログラム	kg
時間	秒	s
電流	アンペア	A
熱力学温度	ケルビン	K
物質量	モル	mol
光度	カンデラ	cd
平面角	ラジアン	rad
立体角	ステラジアン	sr

表 2　SI と併用される単位

名称	記号
分，時，日	min，h，d
度，分，秒	°，′，″
リットル	l，L
トン	t
電子ボルト	eV
原子質量単位	u

1 eV = 1.60218 × 10^{-19} J

1 u = 1.66054 × 10^{-27} kg

表 5　SI 接頭語

倍数	接頭語	記号
10^{18}	エクサ	E
10^{15}	ペタ	P
10^{12}	テラ	T
10^{9}	ギガ	G
10^{6}	メガ	M
10^{3}	キロ	k
10^{2}	ヘクト	h
10^{1}	デカ	da
10^{-1}	デシ	d
10^{-2}	センチ	c
10^{-3}	ミリ	m
10^{-6}	マイクロ	μ
10^{-9}	ナノ	n
10^{-12}	ピコ	p
10^{-15}	フェムト	f
10^{-18}	アト	a

表 3　固有の名称をもつ SI 組立単位

量	名称	記号	他の SI 単位による表現
周波数	ヘルツ	Hz	s^{-1}
力	ニュートン	N	m·kg/s^2
圧力，応力	パスカル	Pa	N/m^2
エネルギー，仕事，熱量	ジュール	J	N·m
工率，放射束	ワット	W	J/s
電気量，電荷	クーロン	C	A·s
電位，電圧，起電力	ボルト	V	W/A
静電容量	ファラド	F	C/V
電気抵抗	オーム	Ω	V/A
コンダクタンス	ジーメンス	S	A/V
磁束	ウェーバ	Wb	V·s
磁束密度	テスラ	T	Wb/m^2
インダクタンス	ヘンリー	H	Wb/A
セルシウス温度	セルシウス度	℃	
光束	ルーメン	lm	cd·sr
照度	ルクス	lx	lm/m^2
放射能	ベクレル	Bq	s^{-1}
吸収線量	グレイ	Gy	J/kg
線量当量	シーベルト	Sv	J/kg

表 4　SI と共に暫定的に維持される単位

名称	記号
オングストローム	Å
バーン	b
バール	bar
ガル	Gal
キュリー	Ci
レントゲン	R
ラド	rad
レム	rem

1 Å = 0.1 nm = 10^{-10} m

1 b = 100 fm^2 = 10^{-28} m^2

1 bar = 0.1 MPa = 10^5 Pa

1 Gal = 1 cm/s^2 = 10^{-2} m/s^2

1 Ci = 3.7 × 10^{10} Bq

1 R = 2.58 × 10^{-4} C/kg

1 rad = 1 cGy = 10^{-2} Gy

1 rem = 1 cSv = 10^{-2} Sv

（注）

1. 表 1－5 は「国際単位系」第 5 版，国際度量衡局 1985 年刊行による。ただし，1 eV および 1 u の値は CODATA の 1986 年推奨値によった。
2. 表 4 には海里，ノット，アール，ヘクタールも含まれているが日常の単位なのでここでは省略した。
3. bar は，JIS では流体の圧力を表わす場合に限り表 2 のカテゴリーに分類されている。
4. EC 閣僚理事会指令では bar，barn および「血圧の単位」mmHg を表 2 のカテゴリーに入れている。

換　算　表

力	N(=10^5 dyn)	kgf	lbf
	1	0.101972	0.224809
	9.80665	1	2.20462
	4.44822	0.453592	1

粘度　1 Pa·s(N·s/m^2) = 10 P(ポアズ)(g/(cm·s))

動粘度　1 m^2/s = 10^4 St(ストークス)(cm^2/s)

圧力	MPa(=10 bar)	kgf/cm^2	atm	mmHg(Torr)	lbf/in^2(psi)
	1	10.1972	9.86923	7.50062 × 10^3	145.038
	0.0980665	1	0.967841	735.559	14.2233
	0.101325	1.03323	1	760	14.6959
	1.33322 × 10^{-4}	1.35951 × 10^{-3}	1.31579 × 10^{-3}	1	1.93368 × 10^{-2}
	6.89476 × 10^{-3}	7.03070 × 10^{-2}	6.80460 × 10^{-2}	51.7149	1

エネルギー・仕事・熱量	J(=10^7 erg)	kgf·m	kW·h	cal(計量法)	Btu	ft·lbf	eV
	1	0.101972	2.77778 × 10^{-7}	0.238889	9.47813 × 10^{-4}	0.737562	6.24150 × 10^{18}
	9.80665	1	2.72407 × 10^{-6}	2.34270	9.29487 × 10^{-3}	7.23301	6.12082 × 10^{19}
	3.6 × 10^6	3.67098 × 10^5	1	8.59999 × 10^5	3412.13	2.65522 × 10^6	2.24694 × 10^{25}
	4.18605	0.426858	1.16279 × 10^{-6}	1	3.96759 × 10^{-3}	3.08747	2.61272 × 10^{19}
	1055.06	107.586	2.93072 × 10^{-4}	252.042	1	778.172	6.58515 × 10^{21}
	1.35582	0.138255	3.76616 × 10^{-7}	0.323890	1.28506 × 10^{-3}	1	8.46233 × 10^{18}
	1.60218 × 10^{-19}	1.63377 × 10^{-20}	4.45050 × 10^{-26}	3.82743 × 10^{-20}	1.51857 × 10^{-22}	1.18171 × 10^{-19}	1

1 cal = 4.18605 J (計量法)

= 4.184 J　(熱化学)

= 4.1855 J　(15 °C)

= 4.1868 J (国際蒸気表)

仕事率　1 PS (仏馬力)

= 75 kgf·m/s

= 735.499 W

放射能	Bq	Ci
	1	2.70270 × 10^{-11}
	3.7 × 10^{10}	1

吸収線量	Gy	rad
	1	100
	0.01	1

照射線量	C/kg	R
	1	3876
	2.58 × 10^{-4}	1

線量当量	Sv	rem
	1	100
	0.01	1

(86 年 12 月 26 日現在)